13:48:08 OCA PAD INITIATION - PROJECT HEADER INFORMATION 04/11/89

Active

Project #: E-25-M77 Cost share #: E-25-351 Rev #: 0
Center # : R6705-0A0 Center shr #: F6705-0A0 OCA file #:
Work type : RES
Contract#: H928622 Mod #: Document : PO
Prime #: Contract entity: GTRC

Subprojects ? : N
Main project #:

Project unit: ME Unit code: 02.010.126
Project director(s):
MCDOWELL D L ME (404)894-5128

Sponsor/division names: GENERAL MOTORS CORP /
Sponsor/division codes: 206 / 012

Award period: 881101 to 891031 (performance) 891031 (reports)

Sponsor amount	New this change	Total to date
Contract value	45,000.00	45,000.00
Funded	45,000.00	45,000.00
Cost sharing amount		5,500.00

Does subcontracting plan apply ?: N

Title: DAMAGE RATE APPROACHES FOR THERMOMECHANICAL FATIGUE OF SUPERALLOYS...

PROJECT ADMINISTRATION DATA

OCA contact: E. Faith Gleason 894-4820

Sponsor technical contact

DR. BILL SCHNEIDER, T-10
(317)230-5638
ALLISON GAS TURBINE OPERATIONS
P.O. BOX 420
INDIANAPOLIS, IN 46206-0420

Sponsor issuing office

ROXANNE ELEY
(317)230-3777
GENERAL MOTORS CORP, ALLISON GAS
TURBINE OPERATIONS, P.O. BOX 420
INDIANAPOLIS, IN 46206-0420

Security class (U,C,S,TS) :
Defense priority rating :
Equipment title vests with: Sponsor GIT
NONE AUTHORIZED

ONR resident rep. is ACO (Y/N): N
supplemental sheet

Administrative comments -
INITIATION. 3RD YEAR/12 MONTH CONTRACT OF ANTICIPATED 4 YEAR PROGRAM, STARTED UNDER PROJECT #E-25-M13

GEORGIA INSTITUTE OF TECHNOLOGY
OFFICE OF CONTRACT ADMINISTRATION

NOTICE OF PROJECT CLOSEOUT

Closeout Notice Date 12/19/89
Original Closeout Started ********

Project No. E-25-M77 Center No. R6705-0A0

Project Director MCDOWELL D L School/Lab ME

Sponsor GENERAL MOTORS CORP/

Contract/Grant No. H928622 Contract Entity GTRC

Prime Contract No.

Title DAMAGE RATE APPROACHES FOR THERMOMECHANICAL FATIGUE OF SUPERALLOYS...

Effective Completion Date 891031 (Performance) 891031 (Reports)

Closeout Actions Required:	Y/N	Date Submitted
Final Invoice or Copy of Final Invoice	Y	
Final Report of Inventions and/or Subcontracts	N	
Government Property Inventory & Related Certificate	N	
Classified Material Certificate	N	
Release and Assignment	N	
Other	N	

Subproject Under Main Project No.

Continues Project No. E-25-M13

Distribution Required:

Project Director	Y
Administrative Network Representative	Y
GTRI Accounting/Grants and Contracts	Y
Procurement/Supply Services	Y
Research Property Managment	Y
Research Security Services	N
Reports Coordinator (OCA)	Y
GTRC	Y
Project File	Y
OCA/CSD	N
Other	N
	N

LETTER REPORT

"DAMAGE RATE APPROACHES FOR THERMOMECHANICAL FATIGUE OF SUPERALLOYS"

By David L. McDowell
Principal Investigator

R.L.T. Oehmke
Research Engineer

Project # E-25-M77

June 1989

Submitted to Allison Gas Turbine Operations, General Motors Corporation

Sponsor Technical Contact:

Dr. Bill Schneider,T-10
Allison Gas Turbine Operations
P.O. Box 420
Indianapolis, IN 46206-0420
(317) 230-5638

Sponsor Administration and Contractual Matters:

Roxanne Eley
General Motors Corp.
Allison Gas Turbine Operations
P.O. Box 420
Indianapolis, IN 46206-0420
(317) 230-3777

Georgia Tech

THE GEORGE W. WOODRUFF SCHOOL OF
MECHANICAL ENGINEERING

Georgia Institute of Technology
Atlanta, Georgia 30332-0405

June 20, 1989

Dr. Bill Schneider, T-10
Allison Gas Turbine Operations
P.O. Box 420
Indianapolis, IN 46206-0420

Dear Dr. Schneider:

This report summarizes the activities of our effort on GM PO#H928622, "Damage Rate Approaches for Thermomechanical Fatigue of Superalloys" for the period November 1, 1988 to June 15, 1989.

We have completed all completely reversed tests in laboratory air on as-cast MAR M 246 at both 650°C and 900°C. In addition, we have completed fast-slow and slow-fast (ramp waveform with strain rates of 10^{-2} and 10^{-4}) experiments at 900°C as well as tests at a strain rate of 10^{-4} and tensile hold times of 10 sec and 1000 sec per cycle. The tensile hold times are beneficial rather than detrimental, as found for other Ni-base alloys, probably due to the compressive mean stresses set up. Both fast-slow and slow-fast tests are more damaging than constant strain rate tests at either the fast or slow rate in terms of number of reversals to failure. See Figures 1-5 for plots of stress, total strain and inelastic strain amplitude versus life (time or reversals to failure) the for 900°C tests.

We have also completed a step-stress creep history (Figure 6) at 900°C with the sequence 300-360-420 repeated twice until creep rupture occurred at an engineering strain of about 3.6%. This history will be useful for assessing the viability of the creep properties as determined by earlier static stress studies for the case when the load is varied.

The purpose of conducting 650°C tests was to get some idea of the fatigue properties of the material at a temperature representative of the low end of a TMF cycle. It was not viewed as imperative to determine the fatigue properties with same level of confidence as at 900°C although more tests may be run at 650°C if this is desired. At 650°C, diffusion-assisted processes (oxidation and creep) are retarded tremendously compared to the 900°C case. As seen in Figure 7, the 10^{-2} strain rate experiments do not reveal substantially different fatigue behavior than at 900°C. In contrast the slow 10^{-4} tests reveal that the lives at 900°C are substantially degraded compared to the 650°C tests. This result is expected since the lower strain rate experiments are more sensitive to both creep and oxidation processes which prevail at 900°C. This also suggests that the use of a "universal" relationship for cyclic strain-based fatigue damage (if augmented by separate creep and oxidation damage rate equations) will suffice for this material.

Figures 8-9 show results of tensile tests at 650°C conducted at strain rates of 10^{-2} and 10^{-4}.

Table I gives a listing of experimental results obtained to date.

We are in the process of running 10 and 1000 sec compressive hold time tests in air at 900°C. Preliminary results suggest that these histories will be detrimental. Additionally, we will run additional 650°C tests at strain rates of 10^{-2} and 10^{-4} for a life of approximately 1000 reversals to establish more confidence in the 650°C strain life curves.

We have had some frustrating problems with the pumps on our vacuum system and with the air conditioning system in the room which houses it. This has delayed us in conducting vacuum experiments, but this system appears to be operating fine now and we are scheduled to conduct a set of six completely reversed experiments at strain rates of 10^{-2} and 10^{-4} at 900°C to judge the influence of environment.

Matthew P. Miller, an M.S. student at Georgia Tech, is currently involved in the program. He has conducted the 650°C experiments and will focus his efforts on scanning electron microscopy evaluation of failure surfaces, oxide formation and secondary cracking as well as creep-fatigue-environment damage rate models. By the end of this year's contract, we hope to have developed a damage rate framework applicable to this class of alloys along with specific constants for MAR M 246. Then, we may conduct some nonisothermal experiments next year to confirm the model. In Appendix 1, please find a copy of a recent paper supported by this work which will be presented at a Post SMiRT conference at UC-Santa Barbara in August.

Sincerely

David L. McDowell
Principal Investigator

DLM:cn

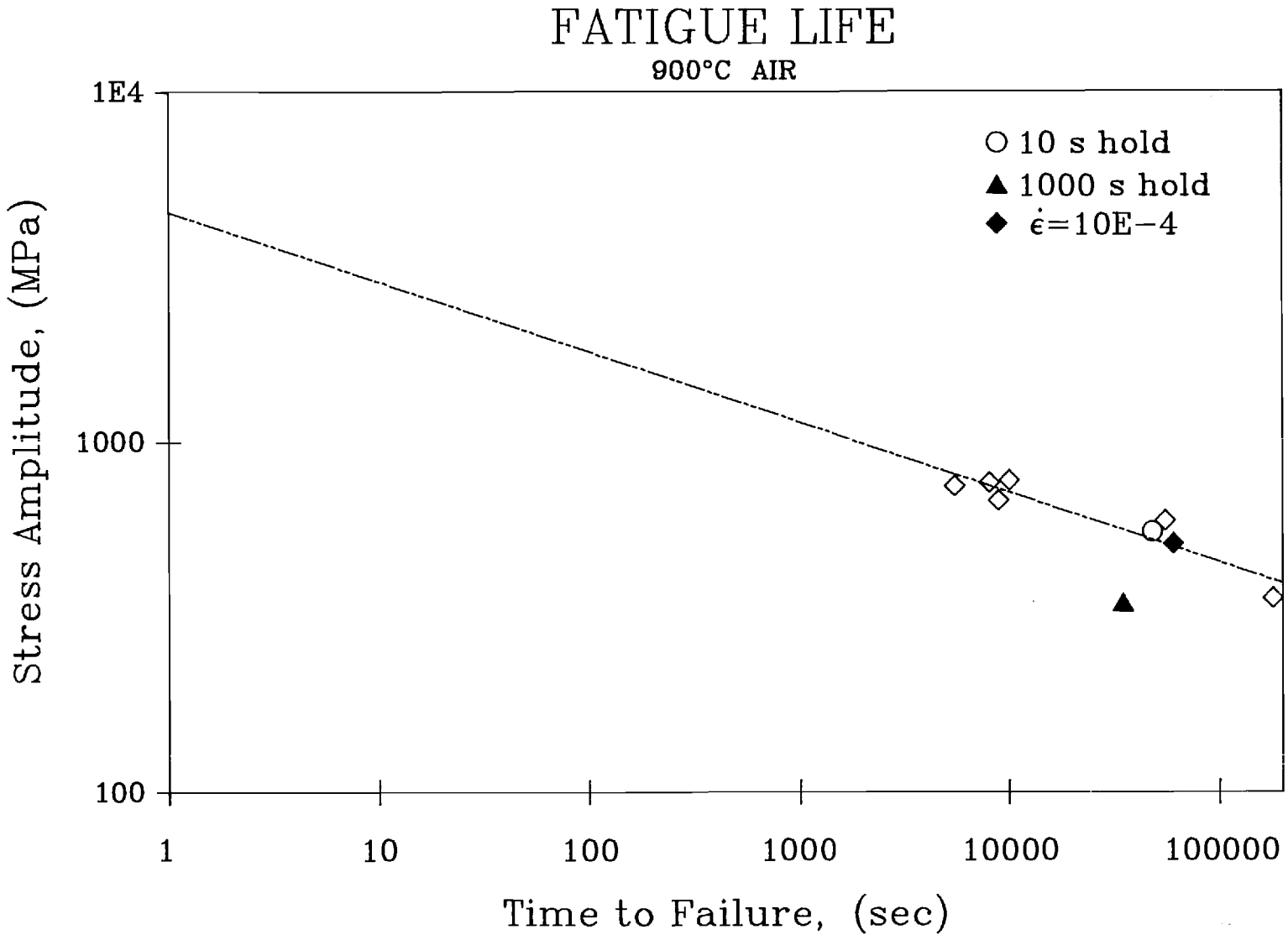
FATIGUE LIFE
900°C AIR
1E4
1000
100
Stress Amplitude, (MPa)
10 s hold
1000 s hold
ε̇=10E−4
1
10
100
1000
10000
100000
Time to Failure, (sec)

Figure 1

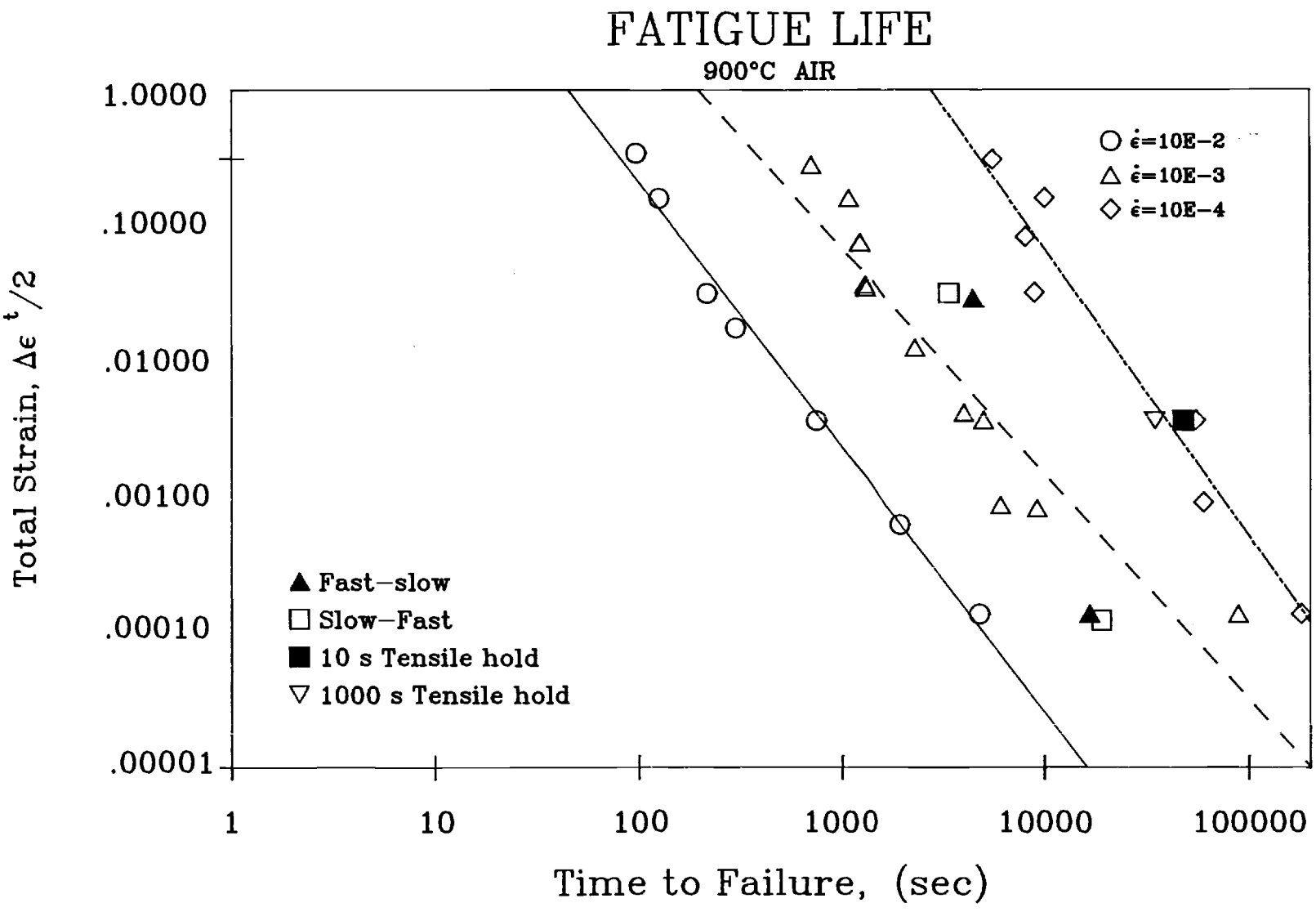
FATIGUE LIFE
900°C AIR
1.0000
.10000
.01000
.00100
.00010
.00001
Total Strain, Δε t /2
1
10
100
1000
10000
100000
Time to Failure, (sec)
ε̇=10E−2
ε̇=10E−3
ε̇=10E−4
Fast−slow
Slow−Fast
10 s Tensile hold
1000 s Tensile hold

Figure 2

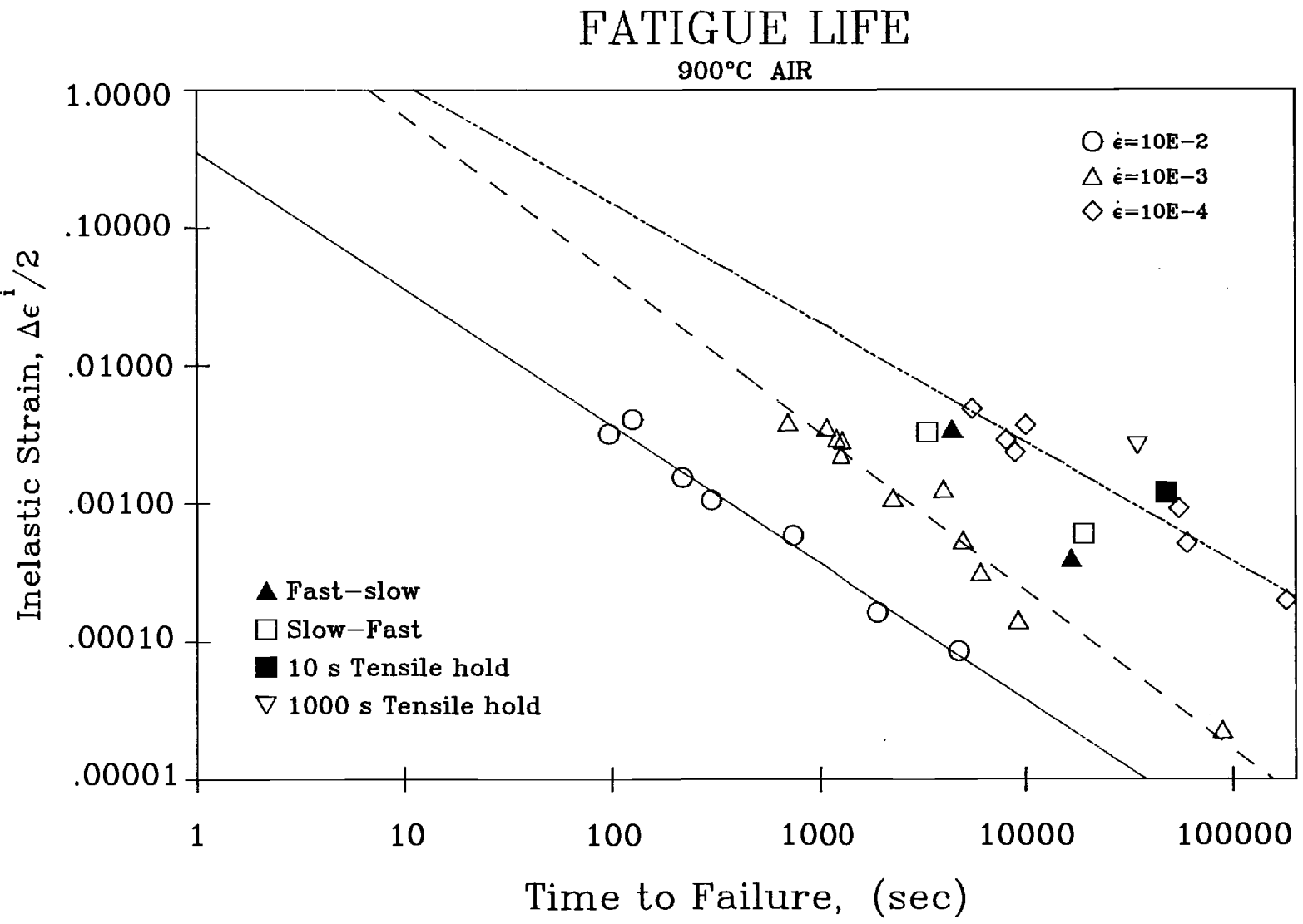
FATIGUE LIFE
900°C AIR
1.0000
.10000
.01000
.00100
.00010
.00001
Inelastic Strain, $\Delta\epsilon^i/2$
1
10
100
1000
10000
100000
Time to Failure, (sec)
○ ε̇=10E-2
△ ε̇=10E-3
◇ ε̇=10E-4
▲ Fast-slow
□ Slow-Fast
■ 10 s Tensile hold
▽ 1000 s Tensile hold

Figure 3

Figure 4

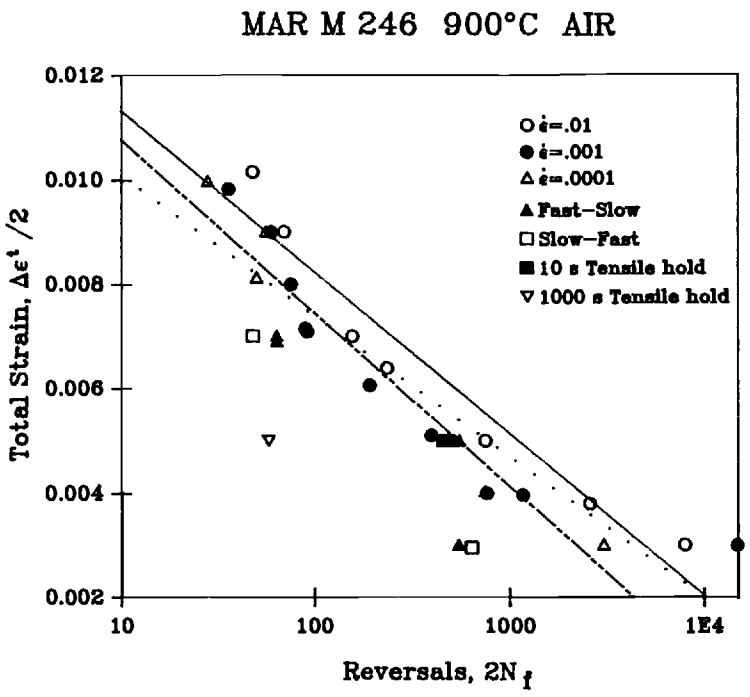
MAR M 246 900°C AIR
Total Strain, Δε^t /2
0.012
0.010
0.008
0.006
0.004
0.002
10
100
1000
1E4
Reversals, 2N_f
ε̇=.01
ε̇=.001
ε̇=.0001
Fast–Slow
Slow–Fast
10 s Tensile hold
1000 s Tensile hold

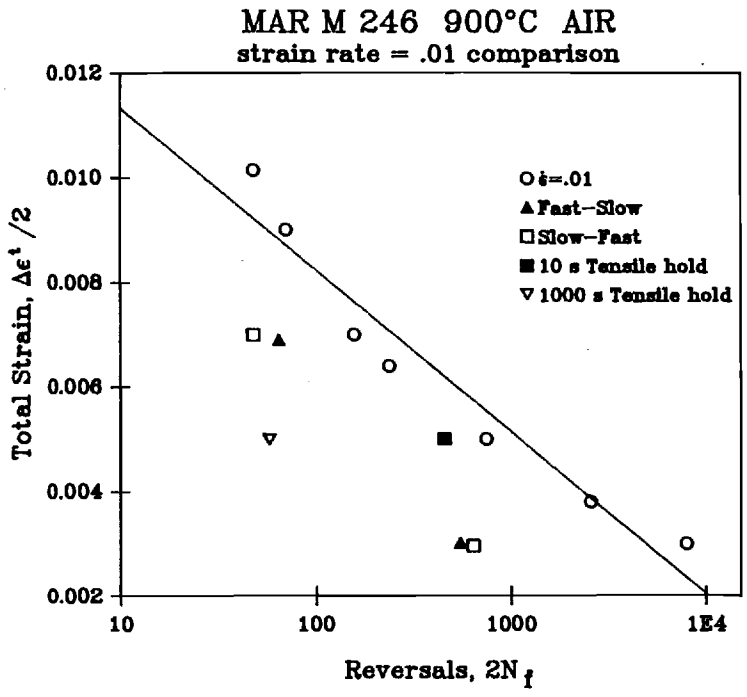
MAR M 246 900°C AIR
strain rate = .01 comparison
Total Strain, Δε^t /2
0.012
0.010
0.008
0.006
0.004
0.002
10
100
1000
1E4
Reversals, 2N_f
ε̇=.01
Fast–Slow
Slow–Fast
10 s Tensile hold
1000 s Tensile hold

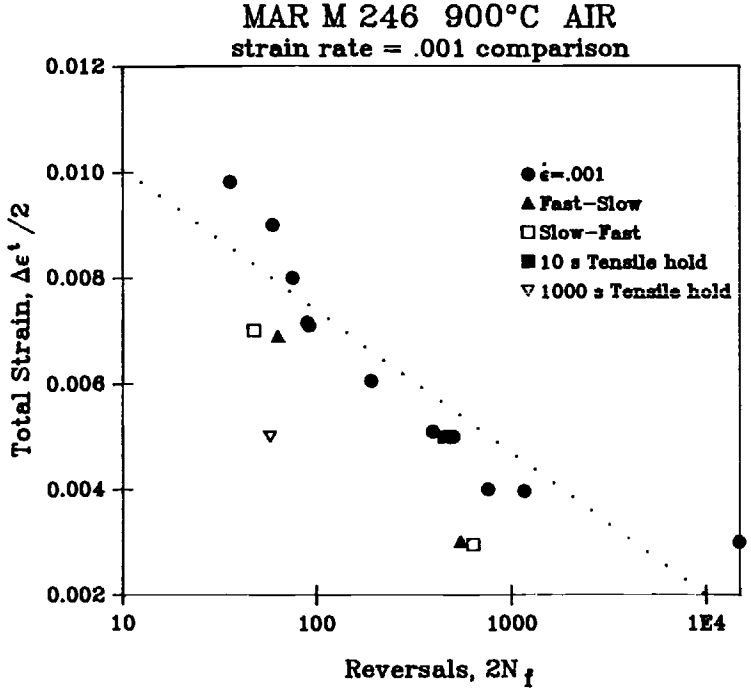
MAR M 246 900°C AIR
strain rate = .001 comparison
Total Strain, Δε^t /2
0.012
0.010
0.008
0.006
0.004
0.002
10
100
1000
1E4
Reversals, 2N_f
ε̇=.001
Fast–Slow
Slow–Fast
10 s Tensile hold
1000 s Tensile hold

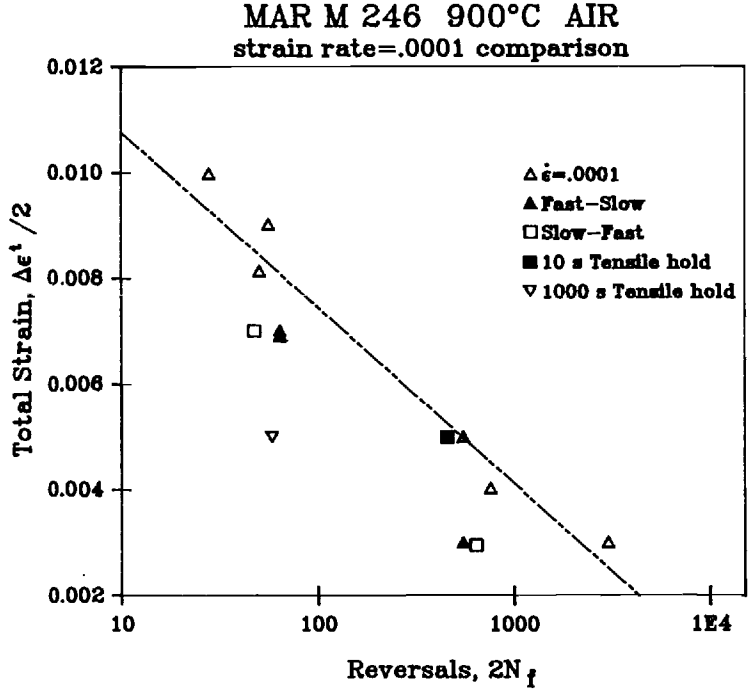
MAR M 246 900°C AIR
strain rate=.0001 comparison
Total Strain, Δε^t /2
0.012
0.010
0.008
0.006
0.004
0.002
10
100
1000
1E4
Reversals, 2N_f
ε̇=.0001
Fast–Slow
Slow–Fast
10 s Tensile hold
1000 s Tensile hold

Figure 5

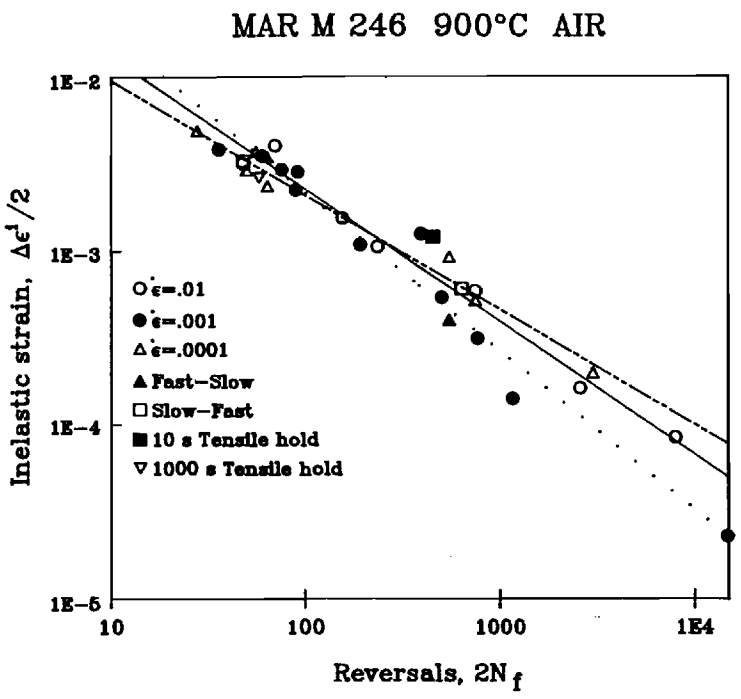
MAR M 246 900°C AIR
Inelastic strain, $\Delta\epsilon^i/2$
1E-2
1E-3
1E-4
1E-5
10
100
1000
1E4
Reversals, $2N_f$
○ $\dot{\epsilon}$=.01
● $\dot{\epsilon}$=.001
△ $\dot{\epsilon}$=.0001
▲ Fast–Slow
□ Slow–Fast
■ 10 s Tensile hold
▽ 1000 s Tensile hold

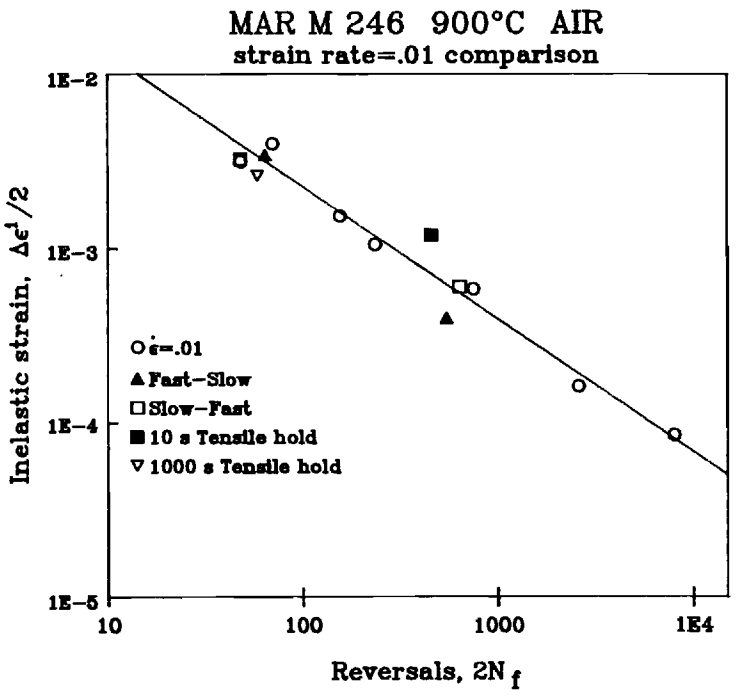
MAR M 246 900°C AIR
strain rate=.01 comparison
Inelastic strain, $\Delta\epsilon^i/2$
1E-2
1E-3
1E-4
1E-5
10
100
1000
1E4
Reversals, $2N_f$
○ $\dot{\epsilon}$=.01
▲ Fast–Slow
□ Slow–Fast
■ 10 s Tensile hold
▽ 1000 s Tensile hold

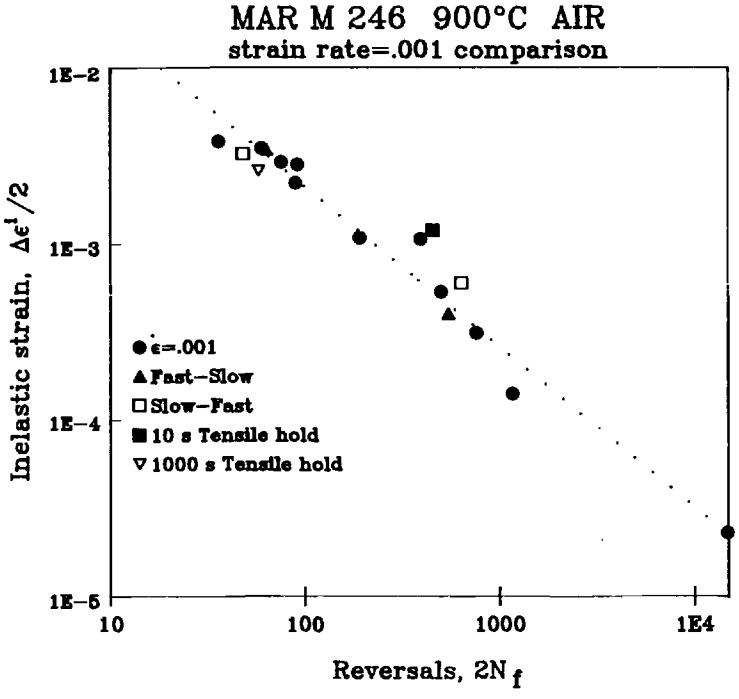
MAR M 246 900°C AIR
strain rate=.001 comparison
Inelastic strain, $\Delta\epsilon^i/2$
1E-2
1E-3
1E-4
1E-5
10
100
1000
1E4
Reversals, $2N_f$
● $\dot{\epsilon}$=.001
▲ Fast–Slow
□ Slow–Fast
■ 10 s Tensile hold
▽ 1000 s Tensile hold

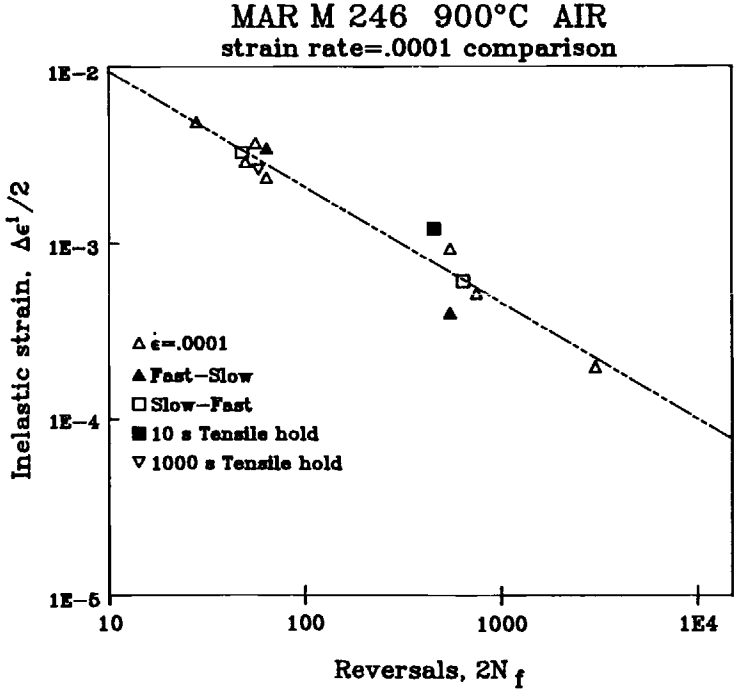
MAR M 246 900°C AIR
strain rate=.0001 comparison
Inelastic strain, $\Delta\epsilon^i/2$
1E-2
1E-3
1E-4
1E-5
10
100
1000
1E4
Reversals, $2N_f$
△ $\dot{\epsilon}$=.0001
▲ Fast–Slow
□ Slow–Fast
■ 10 s Tensile hold
▽ 1000 s Tensile hold

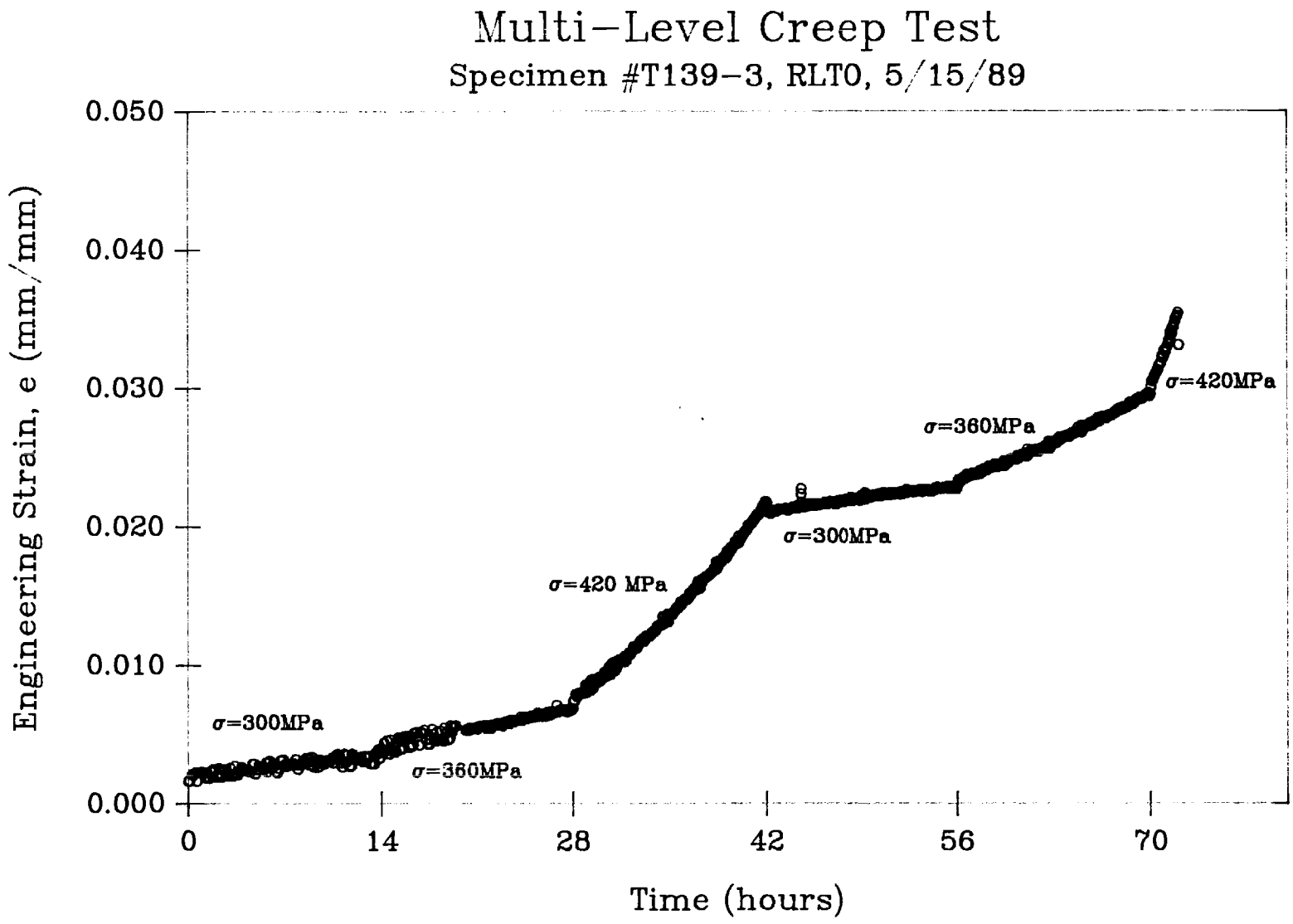
Multi–Level Creep Test
Specimen #T139–3, RLT0, 5/15/89
Engineering Strain, e (mm/mm)
0.050
0.040
0.030
0.020
0.010
0.000
0
14
28
42
56
70
Time (hours)
σ=300MPa
σ=360MPa
σ=420 MPa
σ=300MPa
σ=360MPa
σ=420MPa

Figure 6

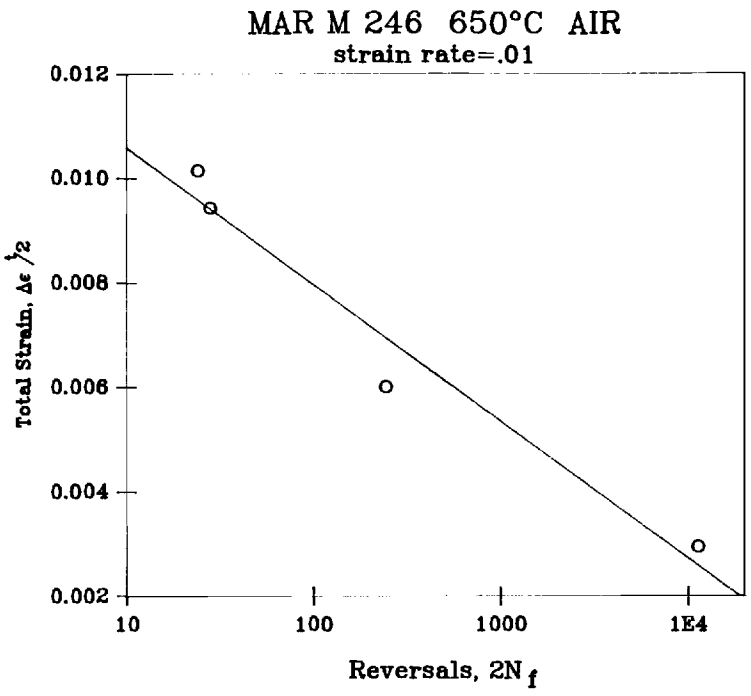
MAR M 246 650°C AIR
strain rate=.01
0.012
0.010
0.008
0.006
0.004
0.002
Total Strain, Δε t/2
10
100
1000
1E4
Reversals, 2N f

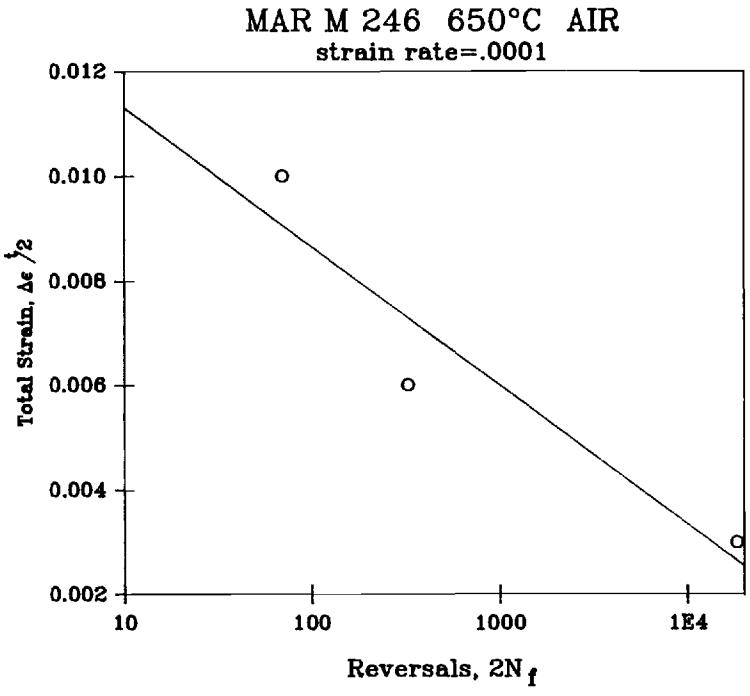
MAR M 246 650°C AIR
strain rate=.0001
0.012
0.010
0.008
0.006
0.004
0.002
Total Strain, Δε t/2
10
100
1000
1E4
Reversals, 2N f

Figure 7

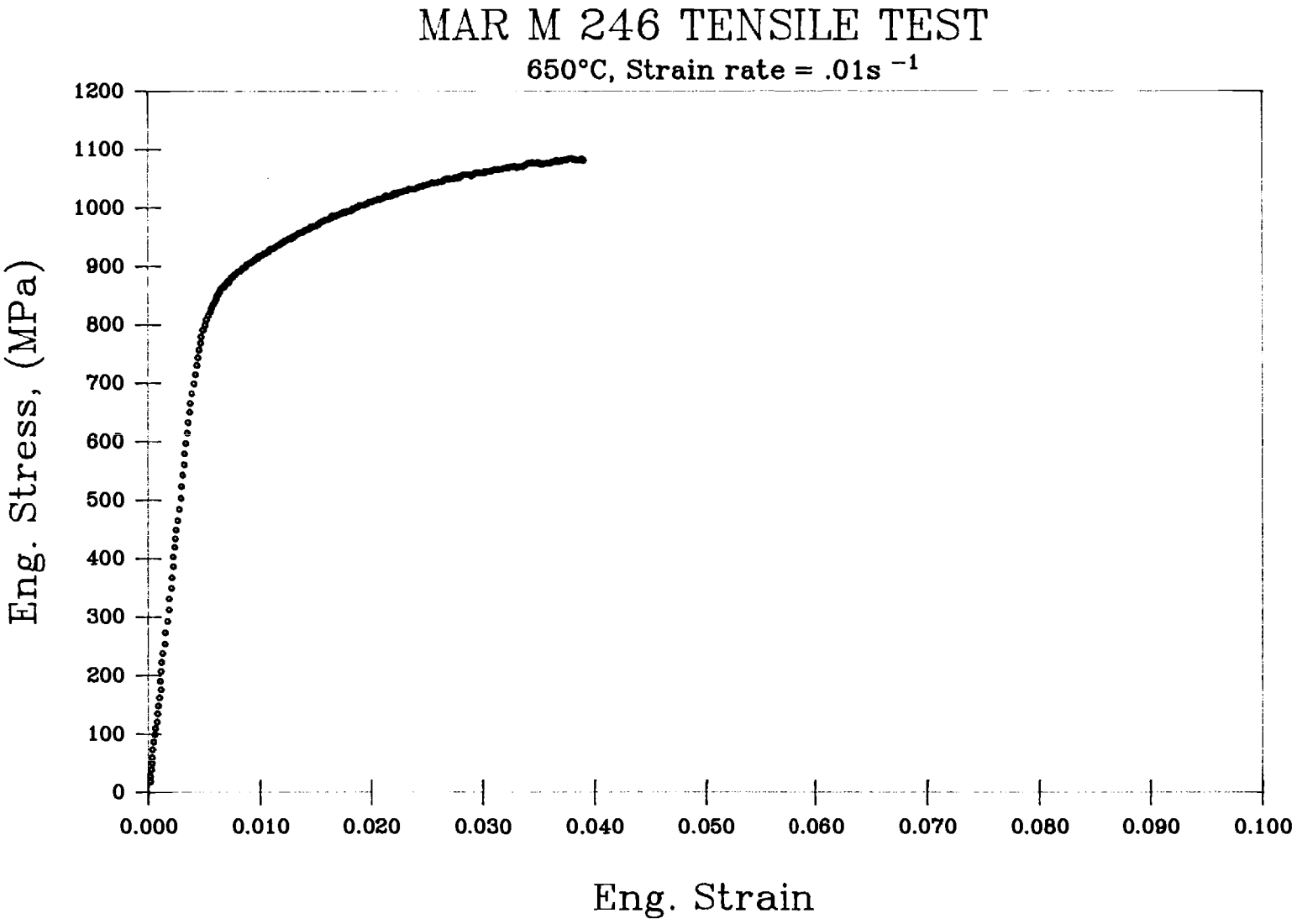
MAR M 246 TENSILE TEST
650°C, Strain rate = .01s $^{-1}$
Eng. Stress, (MPa)
1200
1100
1000
900
800
700
600
500
400
300
200
100
0
0.000
0.010
0.020
0.030
0.040
0.050
0.060
0.070
0.080
0.090
0.100
Eng. Strain

Figure 8

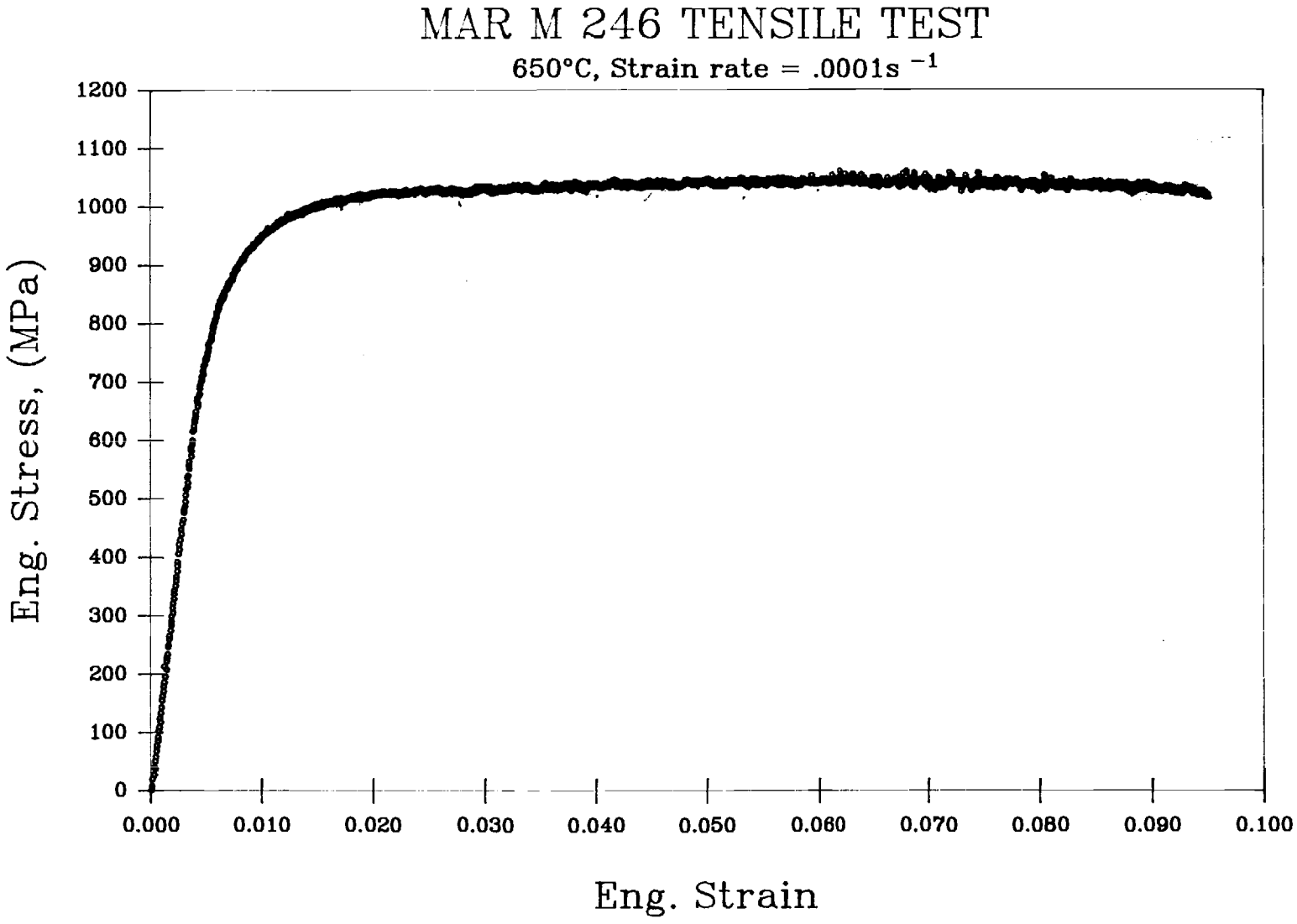
MAR M 246 TENSILE TEST
650°C, Strain rate = .0001s $^{-1}$
Eng. Stress, (MPa)
1200
1100
1000
900
800
700
600
500
400
300
200
100
0
0.000
0.010
0.020
0.030
0.040
0.050
0.060
0.070
0.080
0.090
0.100
Eng. Strain

Figure 9

TABLE I

MAR M 246, 900° AIR

COMPLETED TESTS

	SPEC ID	STRAIN RATE	LOAD AMP LBS	DIAMETER IN.	TOTAL STRAIN AMP	STRESS AMP MPA	ELASTIC STRAIN AMP	INELASTIC STRAIN AMP	REVERSALS TO FAILURE	TIME TO FAILURE SECONDS
900C test										
	G12	10E-2			0.010143	1015.25	0.006977	0.003166	48	97
	T010-2		5125	0.2491	0.009	725.06	0.004983	0.004017	70	126
	T001-5		5500	0.2465	0.007	794.62	0.005461	0.001539	156	218
	G5				0.006387	775.52	0.005330	0.001057	236	301
	T015-1		4500	0.248	0.005	642.30	0.004414	0.000586	748	748
	G22				0.003801	529.48	0.003639	0.000162	2576	1958
	T010-1		2975	0.24815	0.003	424.12	0.002915	0.000085	8000	4800
	G16	10E-3			0.009824	871.60	0.005990	0.003834	36	707
	S999-1		5540	0.247	0.009	797.16	0.005478	0.003522	60	1080
	T015-3		5100	0.2465	0.008	736.83	0.005064	0.002936	76	1216
	G18				0.007158	717.51	0.004931	0.002227	90	1288
	G6				0.006058	723.34	0.004971	0.001087	192	2326
	T015-5		4550	0.248	0.005	649.44	0.004463	0.000537	504	5040
	G7				0.003968	556.69	0.003826	0.000142	1166	9253
	T001-4		2385	0.2461	0.003	275.40	0.002376	0.000023	14842	89052
	G10	10E-4			0.009967	746.94	0.005133	0.004834	28	5582
	T010-4		5335	0.24575	0.009	775.49	0.005329	0.003671	56	10080
	G8				0.008121	763.79	0.005249	0.002872	50	8121
	T011-3		4745	0.24775	0.007	678.64	0.004664	0.002336	64	8960
	T016-1		4230	0.25	0.005	594.14	0.004083	0.000917	550	55000
	G4				0.004024	510.83	0.003511	0.000513	748	60199
	T011-2		2975	0.2485	0.003	356.97	0.002453	0.000197	3008	180480
FAST-SLO	T132-2		3493	0.2468	0.0069	503.43	0.003460	0.003440	64	4460
	T133-4	-2/-4	2723	0.2513	0.003	378.52	0.002601	0.000399	548	16604
SLO-FAST	T133-1	-4/-2	3883	0.2504	0.007	543.66	0.003736	0.003264	48	3396
	T133-5		2371	0.2468	0.00295	341.72	0.002348	0.000602	638	19009
	T132-4	10E-3	4263	0.2457	0.0071	619.92	0.004260	0.002840	92	1306
	T133-3	10E-3	3800	0.2385	0.0051	586.46	0.004030	0.001070	396	4039
	T138-1	10E-3	3740	0.2474	0.004	536.42	0.003686	0.000314	762	6096
tensile	hold tests									
10S HLD	T132-3	10E-4	3795	0.2455	0.005	552.76	0.003799	0.001201	456	47880
1000S HLD	T138-2	10E-4	2475	0.2505	0.005	346.25	0.002380	0.002620	58	34800

MAR M 246, 650° AIR
COMPLETED TESTS

SPEC ID	STRAIN RATE	LOAD AMP	DIAMETER	TOTAL STRAIN AMP	STRESS AMP	ELASTIC STRAIN AMP	INELASTIC STRAIN AMP	REVERSALS TO FAILURE	TIME TO FAILURE SECONDS
		LBS	IN.		MPA				
650C tests									
T138-4	10E-2	3634	0.246	0.00295	527.16	0.003083		11246	6748
T138-3	10E-2	5952	0.2473	0.006	854.37	0.004996	0.001004	244	293
T139-2	10E-2	7427	0.2494	0.009434	1048.21	0.006130	0.003304	28	56
T139-4	10E-2	7289	0.2464	0.010148	1053.94	0.006163	0.003985	24	48
T139-1	10E-4	3720	0.247	0.003	535.28	0.003130		18334	1100040
T138-5	10E-4	5993	0.2462	0.006	867.96	0.005076	0.000924	324	38880
T139-5	10E-4	7275	0.2464	0.01	1051.92	0.006152	0.003848	70	14000
650C tensile tests		ult.			ult.				
T133-2	10E-2	7193	0.239	0.039	1105.46	0.006465	0.032535		
T132-5	10E-4	7032	0.242	0.095	1054.09	0.006164	0.088836	terminated @ 9.5%	

APPENDIX

MECHANISTIC CONSIDERATIONS FOR TMF LIFE PREDICTION OF NICKEL-BASE SUPERALLOYS

D.L. McDowell, S.D. Antolovich and R.L.T. Oehmke

Mechanical Properties Research Laboratory
Georgia Institute of Technology
Atlanta, GA 30332-0405

To be Presented at the SMiRT-10 Post-Conference Seminar on
Inelastic Analysis, Fracture, and Life Prediction
August 21-22, 1989
University of California
Santa Barbara

ABSTRACT: Typical gas turbine and jet engine hot section components are subjected to severe environment along with variable thermal and mechanical loading histories. Nickel-base superalloys are often used in such applications because of their superior creep resistance and strength at high temperature. Most popular models for thermomechanical fatigue (TMF) life prediction are based on the creep-fatigue interactions exhibited by ductile metals and do not explicitly contain an environmental feature [1]. Such models may be viewed as parametric damage approaches, in which the environmental effect is assumed to be incorporated in the time-dependence of the formulation. In this paper, we briefly review some potential TMF life prediction models with special attention devoted to consideration of oxidation effects for nickel-base superalloys.

INTRODUCTION

The nickel-base superalloys are a technologically important class of materials for high temperature structural applications. They retain or develop strength at temperatures up to their maximum use temperature of approximately 1700°F due to the properties of the γ' precipitate. Above this temperature range, microstructural aging effects degrade performance.

In developing life prediction schemes for nickel-base gas turbine and jet engine components, the tendency has been to draw heavily from knowledge of creep-fatigue interactions typical of ductile high temperature materials such as the austenitic stainless steels, Cr-Mo steels, etc. Reference [1] provides a good comparative review of the performance of various models for creep-fatigue interaction for such materials. Nickel-base superalloys, however, exhibit a time-dependent cyclic damage response associated predominately with environment-fatigue interaction. The time-dependence is manifested by oxide penetration (diffusion) along grain boundaries and slip bands at high temperatures which then interacts detrimentally with cyclic slip processes at lower temperatures. Hence, thermomechanical fatigue is strongly path history-dependent in the sense of both thermal and mechanical loadings.

To place a perspective on the demands of a constitutive framework for life prediction of nickel-base superalloys, the following two features much be borne in mind [2-3]:

(i) Methods which accurately correlate creep-fatigue life of more ductile high temperature alloys do not necessarily extend to less ductile superalloys; the plastic strain range is typically small for superalloys in contrast to stainless or pressure vessel steels. Consequently, mean stress effects associated with creep-fatigue interaction (e.g. cycling with hold times) are more pronounced than for more ductile alloys.

(ii) The interaction of fatigue and time-dependent damage for superalloys is quite different from the interaction of cavities and fatigue microcracks exhibited by more ductile high temperature alloys. The role of environmental attack is pronounced relative to that of creep cavitation.

The purpose of this paper is to discuss the basis of several contemporary approaches to thermomechanical fatigue with special emphasis on the nickel-base superalloys. Although neither the list of approaches or applications/results are

exhaustively reviewed, some fundamental aspects related to applicability to nickel-base superalloys are discussed.

SOME PROPOSED APPROACHES

Here, we consider several different classes of approaches. The first class we may label as "parametric" damage approaches characterized by a somewhat indirect link between the damage parameter(s) and physical damage mechanisms. Damage parameters are then introduced to model evolution and interaction of creep damage, fatigue damage, etc. The second set of methods may be viewed as modified stress- or strain-life relationships; time-dependence of damage is implicitly embedded in such theories. The third class of theories considered are the "micromechanical" theories which explicitly include time-dependent damage mechanisms. Finally, the so-called "damage rate" approaches, which are characterized by more specific relation of state variables to physical quantities which either comprise or abet damage, are considered. It should be stated at the outset that some theories, such as damage parameter approaches, may belong to several classes depending on the degree of specificity of the definition of the damage variable(s).

Parametric Damage Approaches

Here we present several theories representative of the parametric approach which have met with significant industrial application to high temperature components such as turbine blades, disks, rotors, power plant components, etc.

The continuum damage approach attempts to relate local stress-strain behavior to evolution of damage. This approach has been widely used in various forms for creep fracture and other bulk-distributed damage problems [4-5]. Here, we consider a class of continuum damage approaches applied to isothermal and anisothermal creep-fatigue interaction by Chaboche and Lemaitre [6-9]. Other damage parameter approaches are similar (c.f. [10-13]). For simplicity, the uniaxial case with isotropic damage will be considered although more general anisotropic forms have also been introduced.

The starting point for this theory is the definition of effective stress

$$\tilde{\sigma} = \frac{\sigma}{1-D} \tag{1}$$

where D is the scalar damage parameter. For undamaged material, D = 0. At failure, D = D_c with D_c = 1 typically. D can be associated with the normalized loss of cross sectional area due to void or crack formation [6] and may be measured by loss of elastic stiffness. For example, for load-controlled pure fatigue cycling,

$$D = 1 - (\Delta\epsilon_p^{ss}/\Delta\epsilon_p)^{n'} \tag{2}$$

where $\Delta\epsilon_p^{ss}$ is the cyclically stable plastic strain range (without damage effect), n' is the cyclic strain hardening exponent and $\Delta\epsilon_p$ is the subsequent increased plastic strain range associated with damage accumulation. Likewise, for a constant stress creep test we may derive

$$D = 1 - \left(\dot{\epsilon}_c^{ss}/\dot{\epsilon}_c\right)^{1/n} \tag{3}$$

where $\dot{\epsilon}_c^{ss}$ is the secondary creep rate at a given stress, n is the creep exponent and $\dot{\epsilon}_c$ is the actual creep rate. Power law plasticity and creep are assumed in equations (2)-(3), respectively. Lemaitre [9] has also written the continuum damage equations in terms of strain, the more usual control condition at notches. On this basis, D may be identified for completely reversed, strain-controlled fatigue with the decrease in stress range relative to the cyclically stable case, $\Delta\sigma^{ss}$, i.e. D = $(1 - \Delta\sigma/\Delta\sigma^{ss})$.

A great advantage of the continuum damage approach is its evolutionary framework which in principle introduces the various physical damage mechanisms along with interactions, i.e.

$$dD_p = f_p(\phi, \varsigma, D_p, D_t, D_f, T)d\sigma \quad (4)$$

$$dD_t = f_t(\phi, \varsigma, D_p, D_t, D_f, T)dt \quad (5)$$

$$dD_f = f_f(\phi, \varsigma, D_p, D_t, D_f, T)dN \quad (6)$$

where ϕ denotes forcing variables, ς represents internal variables and T is absolute temperature. D_p represents damage associated with time- and rate-independent plastic deformation (e.g. ductile hole growth), D_t represents time-dependent damage and D_f represents cycle-dependent fatigue damage. In the general format of equations (4)-(6), this approach is very appealing, particularly if D_p, D_t and D_f each have specific physical correspondence. If this is the case, we may consider the continuum damage theory as a damage rate approach rather than a parametric damage approach using the terminology defined in the introduction.

To introduce interactions, however, between the several damage parameters, the assumption of additivity is often made. For example, for creep-fatigue interaction, assuming $D_t = D_c$, the damage parameter has been defined as $D = (D_c + D_f)$ [6-7] with the evolution of D_c and and D_f given by

$$dD_c = f_c(\phi, \varsigma, D, T)dt \quad (7)$$

$$dD_f = f_f(\phi, \varsigma, D, T)dN \quad (8)$$

Chaboche and co-workers have successfully applied specific forms of (7)-(8) to problems of creep-fatigue interaction under isothermal and thermomechanical loading, an example of which is the set of equations [7-8]

$$\frac{\delta D_F}{\delta N} = \left[1 - [1 - D]^{\upsilon+1}\right]^{\alpha[\sigma_M,\sigma_m]} \left[\frac{\sigma_M - \sigma_m}{M(\sigma_m)(1-D)}\right]^{\upsilon} \tag{9}$$

$$\frac{dD_c}{dt} = \left[\frac{\sigma}{A(1-D)\sigma_u}\right]^{r} [1 - D]^{r-k(\sigma)} \tag{10}$$

where σ_M and σ_m are the maximum and mean stresses in the cycle and A, r and υ are temperature-dependent constants. The rupture strength in a monotonic test is designated as σ_u. Framing the fatigue damage evolution equation in terms of stress is an advantage for application to nickel-base superalloys since the plastic strains are typically small and somewhat inaccurately determined in contrast to stress. Specific forms for α and M have been introduced [7-8] as

$$\alpha[\sigma_M,\sigma_m] = 1 - a\left\{\frac{\sigma_M - \sigma_\ell^*(\sigma_m)}{\sigma_u - \sigma_M}\right\} \tag{11}$$

$$\sigma_\ell^*(\sigma_m) = \sigma_\ell + \left[1 - b\frac{\sigma_\ell}{\sigma_u}\right]\sigma_m \tag{12}$$

$$M(\sigma_m) = M_o\left[1 - b\frac{\sigma_m}{\sigma_u}\right] \tag{13}$$

where M_o and a are temperature-dependent constants, σ_ℓ is the fatigue limit under completely reversed loading, σ_ℓ^* is the fatigue limit for non-zero mean stress and b is a temperature-independent coefficient. The exponent $k(\sigma)$ introduces nonlinear stress level dependence and nonlinear cumulative damage in creep. Likewise, $\alpha[\sigma_M, \sigma_m]$ does the same for fatigue. Hence, sequence effects in creep, fatigue or creep-fatigue are presumably accounted for. The continuum damage approach, of course, can be easily applied in incremental form to any complex history in contrast to other parametric

damage approaches. Note that in this formulation, no distinction is made between tensile and compressive hold periods [8].

The continuum damage approach as outlined here is often argued as thermodynamically consistent on the basis that D may be introduced into the Helmholtz free energy and dissipation potential which ensures satisfaction of a dissipation inequality which includes $\dot{D}$ and its associated conjugate thermodynamic force. Assuming the damage is isotropic as in the previous discussion, we may express the free energy density function as

$$\psi = \psi^{(e)}\left[\underline{\epsilon}^{e},\ D,\ T\right] + \psi^{(c)}\left[\underline{\alpha},\ p,\ D,\ T\right] \tag{14}$$

where $\psi^{(e)}$ and $\psi^{(c)}$ are the elastic and inelastic parts, and $\underline{\alpha}$ and p are internal variables which describe dislocation rearrangement associated with inelastic deformation. For the isothermal case, in accordance with the concept of effective stress (equivalence in an elastic strain sense), we may write

$$\psi^{(e)} = \frac{(1-D)}{\rho}\left[\frac{1}{2}\left[\lambda\epsilon^{e\ 2}_{kk} + 2\mu\epsilon^{e}_{ij}\epsilon^{e}_{ij}\right]\right] \tag{15}$$

for an isotropic linear elastic material where ρ is the mass density and λ and μ are the Lamé constants. It should be noted that (15) is a very specific assumption for the coupling of $\psi^{(e)}$ with D; it means that damage is defined by change of elastic stiffness rather than by some particular physical/microstructural measure. Damage may be defined without assuming the form of equation (15) (c.f. [14]); in this case, the focus is on the identification of damage with the physical damage distribution and character rather than stiffness, although elastic stiffness will always be affected when damage is introduced in $\psi^{(e)}$.

For application of this approach to thermomechanical fatigue, there are several reservations. First, the damage parameters are clearly interpreted as change of stiffness due to the presence of cavities and microcracks. Different distributions and aspect ratios

of defects can result, however, in the same stiffness reduction. Second, features such as oxides do not appreciably contribute to stiffness change until weakened grain boundaries or slip bands fail, yet the development of oxides is essentially temporally continuous. We could view environmental penetration as belonging either to the set of internal variables ς in equations (7)-(8) or to D_t; however, explicit consideration of environment is almost always neglected. The assumption that the primary source of time-dependent damage for nickel-base superalloys is creep cavitation is inaccurate. Moreover, creep-plasticity interactions (e.g. change of creep cavity growth rate due to prior plasticity) are not accounted for in the creep damage evolution equation.

We may scrutinize the assumption of additivity of damage as in equations (7)-(8) which is introduced for purposes of interaction between D_f and D_c. As pointed out by Chaboche [15], additivity is perfectly acceptable from the viewpoint of the effective stress concept; the effect of damage on mechanical response is being summed rather than the physical damage components. However, it is somewhat difficult to justify the coupling implied by additivity, even if based on damage effect, from a physical viewpoint. For example, creep cavities may interact strongly with a growing intergranular fatigue crack, but bulk creep cavitation is insignificantly affected by the presence of fatigue microcracks until a much later point in life. Likewise, transgranular fatigue microcracks may not interact with intergranular creep or oxidation damage. In general, the rate of a specific form of damage depends on its current value, but not necessarily on the current values of all forms of damage. Also, some of the interactions are one-way rather than two-way.

A fundamental problem is the treatment of fatigue damage in terms of a continuum bulk damage parameter approach. This problem has nothing to do with the assumption of bulk stress and strain as driving forces, but rather with the assumption of distributed damage. Fatigue is largely a surface phenomenon, yet the assumptions of additivity of different components of damage and the effective stress concept infer uniformity of D in uniaxial test specimens from which the damage evolution functions are determined. This is physically not the case. The change of stiffness associated with fatigue is clearly dependent on the volume fraction of fatigue-damaged material. Such an approach is admissible for creep or fracture when the damage is distributed uniformly

through a uniaxial test specimen. For creep-fatigue interaction, it can only be strictly applied to components of the same dimension as the test specimens from which constants were determined; in a sense, then, the uniaxial test becomes a "component" test rather than a "materials" test by virtue of the assumed damage analysis. This problem will persist even if there is no interaction between the damage components in the evolution laws so long as the effective stress concept is adopted. Possible solutions include recognition of the gradient of fatigue damage by introduction of "surface elements" or the volume fraction of fatigue-damaged material. Chaboche and Lesne [16] have discussed an alternate, equivalent form for evolution of the fatigue damage parameter, D_f, which does not depend on the effective stress concept and hence becomes philosophically consistent with microcrack propagation.

It is important to note that the general form of equations (4)-(6) may be adopted without the other aforementioned assumptions, i.e. interpretation of damage as stiffness change and additive coupling. In fact, by not assuming additivity of the damage components, we are free to assign specific physical damage definitions and any form of coupled interactions (e.g. one-way) desired. Such a framework then forms the basis for coupled or decoupled fatigue microcrack propagation and creep cavity growth, for example, for high temperature materials [1,17-19]. Moreover, it does not suffer from the influence of nonuniformity of the fatigue damage field on stiffness. Such a formulation may be viewed as a member of the fourth set of approaches listed in the introduction, the damage rate approaches.

Modified Stress- or Strain-Life Approaches

Perhaps the most straightforward approach to the TMF problem is to introduce frequency as a modifying influence on the strain-life behavior as proposed by Coffin [20-22] and others. Such an approach implicitly includes time-dependence. An early example of this approach due to Coffin [20] admits the influence of cyclic frequency ν in the form

$$\left[N_i \nu^{K-1}\right]^{\phi} \Delta\epsilon_n = M \tag{16}$$

where ϕ, K and M are material constants for a given temperature, $\Delta\epsilon_n$ is the inelastic mechanical strain range and N_i is the number of cycles to crack initiation. In such an approach, hold periods are treated as a change in frequency. Effects of unbalanced tensile and compressive going frequencies (and hysteresis loop shapes) were later incorporated by Coffin in the form

$$N_i = \left[\frac{A}{\Delta\epsilon_n}\right]^{1/\phi} \left[\frac{\nu_t}{2}\right]^{1-K} \left[\frac{\nu_c}{\nu_t}\right]^{d} \tag{17}$$

where ν_t and ν_c are tensile- and compressive-going frequencies, respectively. Constants A, ϕ and K are determined from balanced loop data (i.e. $\nu_t = \nu_c$) and d is obtained from unbalanced data. For many superalloys, compressive strain hold periods are more damaging than tensile strain hold periods, possibly due to a combination of mean stress effects [21,23] and tensile cracking of oxides during the tensile-going portion of the cycle. Such an observation would be unusual for materials which experience significant creep damage relative to oxidation damage.

Ostergrens' damage function [23] provides an influence of mean stress in a frequency modified approach, i.e.

$$\sigma_t \, \Delta\epsilon_n \, N_i^{\phi} \, \nu^{\phi(\kappa-1)} = C \tag{18}$$

where ϕ, κ and C are temperature-dependent constants and σ_t is the peak tensile stress in the hysteresis loop. This form was proposed for simple hysteresis loops to provide dependence on the tensile-going portion of the plastic work; for more general paths, Ostergren proposed an integral form. As for the Coffin approach, the frequency may be modified to account for waveshape dependence. For $\kappa = 1$, the fatigue response is time-independent; for $\kappa = 0$, the time to failure is a function of $\Delta\epsilon_n$ only. Ostergren [23]

suggested $\kappa \simeq 1$ for several nickel-base superalloys under isothermal conditions. Halford and Saltsman argued [24] that the Ostergren function did not result in as reasonable interpretation of TMF behavior as an inelastic strain range criterion. The physical interpretation of the Ostergren parameter, particularly for TMF loading paths, is not very clear although it appears to be related to ΔJ-integral approaches to be discussed later.

Clearly, the definition of frequency ν for complex loading paths is somewhat difficult; ν must be distinctly defined for each cyclic waveshape. Moreover, the link between frequency in such approaches and the time-dependent damage mechanism is unclear. Coffin [20] clearly considers the frequency modification to pertain to environment-creep-fatigue interaction wherein strain localization due to grain boundary sliding, oxidation of freshly exposed material and continual disruption of protective films are operant mechanisms. Also, creep-plasticity interactions associated with variable loading histories may invalidate the constants determined from simple tests since the model is not path history/sequence dependent. Although one may argue in favor of the simplicity of frequency-modified approaches, it seems unlikely that the level of mechanistic detail is sufficient for general TMF loading paths. There does not appear to be compelling evidence of the capability of these approaches to correlate TMF life accurately. Ostergren and Krempl [25] showed that the frequency modified approaches may be viewed as a particular form of a parametric damage approach, so we may view the latter as more general.

The method of strain range partitioning (SRP) introduced by Manson et al. [26-30] relates cyclic inelastic strain to fatigue life without explicit consideration of environmental effects. The time-dependence is embedded in the creep part of a decomposition between rate- and time-independent plastic and creep components of the inelastic strain range. No explicit consideration of damage mechanisms is made; rather, it is assumed that distinguishing between tensile- and compressive-going creep and plastic strains, plasticity reversed by creep and creep reversed by plasticity is sufficient for describing various mechanistic facets of creep-fatigue interaction. Moreover, mean stress and waveshape effects are considered to be implicitly embedded in the framework.

According to this approach, we define four types of inelastic strain range, i.e. $\Delta\epsilon_{cp}$, $\Delta\epsilon_{pc}$, $\Delta\epsilon_{pp}$ and $\Delta\epsilon_{cc}$ where the order of subscripts denote the tensile- and compressive-going balanced components. For example, $\Delta\epsilon_{pp}$ denotes completely reversed plasticity whereas $\Delta\epsilon_{pc}$ denotes tensile-going plasticity reversed by compressive-going creep. Then we introduce the relationships

$$\Delta\epsilon_{pp} = A_1 N_{pp}^{B_1} \quad , \quad \Delta\epsilon_{pc} = A_2 N_{pc}^{B_2} \quad , \quad \Delta\epsilon_{cp} = A_3 N_{cp}^{B_3} \quad , \quad \Delta\epsilon_{cc} = A_4 N_{cc}^{B_4} \qquad (19)$$

where the A_i and B_i experimentally determined constants, and perform the damage summation according to

$$\frac{1}{N_i} = \frac{F_{pp}}{N_{pp}} + \frac{F_{cp}}{N_{cp}} + \frac{F_{pc}}{N_{pc}} + \frac{F_{cc}}{N_{cc}} \qquad (20)$$

where the inelastic strain fractions are given by

$$F_{pp} = \frac{\Delta\epsilon_{pp}}{\Delta\epsilon_n} \quad , \quad F_{cp} = \frac{\Delta\epsilon_{cp}}{\Delta\epsilon_n} \quad , \quad F_{pc} = \frac{\Delta\epsilon_{pc}}{\Delta\epsilon_n} \quad , \quad F_{cc} = \frac{\Delta\epsilon_{cc}}{\Delta\epsilon_n} \qquad (21)$$

and $\Delta\epsilon_n$ is the combined inelastic mechanical strain range. A maximum of three types of inelastic strain ranges can exist for a given hysteresis loop, so not all four terms would appear in equation (20) for any particular case.

Even though tensile and compressive loading trajectories are treated differently by this approach, the lack of explicit relation of the strain fractions to physical quantities results in a parametric theory; the fact that four different strain-life expressions are available to fit data under different tensile and compressive hold times, unbalanced cycle shapes, etc. leads both to acceptable correlation and rather extensive testing required for determination of constants. The theory has been generalized to multiaxial loading conditions [31] and to take into account differences between transgranular and

intergranular creep-fatigue crack propagation [32]. A total strain-based version of SRP has also been formulated [33] which would seem desirable for superalloys.

The principal disadvantage of this approach is its lack of specificity with respect to damage mechanism. For example, the strain fractions involving forward or reverse creep strain may bear some relation to creep damage for materials which undergo matrix strain-controlled cavity growth [19] (valid only in certain temperature and stress regimes), but would not relate directly to diffusion-controlled cavity growth since it is not uniquely related to the matrix creep deformation. The presence of significant grain boundary sliding often plays a key role in observed differences between $\Delta\epsilon_{pc}$ and $\Delta\epsilon_{cp}$ life correlations [20], but sliding is very limited for nickel-base superalloys. Likewise, for nickel-base superalloys the important element of oxidation damage is not featured by this framework. Since creep-fatigue interaction is assumed, isothermal tensile strain hold periods will be more damaging than compressive hold periods unless some special modification is introduced. The method in its inelastic strain format requires definition of plastic and creep strains, a decomposition which is inconsistent with the so-called unified creep-plasticity models.

It is further noted that although the theory is presented as an interactive damage law, no interaction of the physical damage processes is introduced via the approach; in fact, the theory can be derived from a straightforward modification of Miner's Rule [34]. It has been demonstrated that the accuracy of life prediction using this method can be enhanced using a true interaction parameter and by determining the life curves in a more rigorous manner [34].

Nitta and Kuwabara [35-36] and Ohtani et al. [38] have introduced a framework based on the fracture mechanics concept of the ΔJ-integral [37] applied to fatigue microcrack propagation and the ΔJ_c parameter obtained by the time-integration of the J^*-integral for creep crack growth [36,38] over a cycle, reckoning that much of the so-called "initiation" stage is spent in microcrack growth. Moreover, use of ΔJ or similar "strain energy parameter" implicitly includes contributions of higher order terms of the crack tip stress-strain series expansions, unlike ΔK. These authors find that $\Delta\epsilon_n$-based approaches such as Manson's universal slope method with the 10% rule for high

temperature correction or strain range partitioning work well for ductile materials under isothermal and TMF conditions, but are significantly nonconservative for nickel-base superalloys [35]. Materials examined included cast and forged Cr-Mo-V, Ni-Mo-V, 1.25Cr-0.5Mo, 2.25Cr-1Mo, 0.15%C steel, 12Cr-Mo-W-V steel, 304 stainless steel, 321 stainless steel, A 286, IN 718, IN 738LC, cast IN 939, cast Mar-M247, cast Rene 80, Hastelloy X, cast FSX 414 and cast FSX 430. It was noted that both the universal slope and strain range partitioning approaches based on inelastic strain range generally provided nonconservative life predictions for superalloys, even for isothermal loading conditions. The following cycle- and time-dependent microcrack growth rate equations [35,38] were proposed:

$$da/dN = C_f \Delta J_f^{m_f} \tag{22}$$

$$da/dt = C_c J^{*m_c} \tag{23}$$

where a is the microcrack length and m_f, m_c, C_f and C_c are constants which are nearly temperature-independent. Integrating equations (22)-(23) from initial crack length a_o to final length a_f under predominantly cycle-dependent conditions gives

$$\Delta\tilde{W}_f^{m_f} N_i = D_f \tag{24}$$

$$\Delta\tilde{W}_f = \frac{\Delta\sigma\ \Delta\epsilon_e}{2} + \frac{1/n' + 1}{2\pi} f(1/n') \frac{\Delta\sigma\ \Delta\epsilon_p}{1/n' + 1} \tag{25}$$

$$\left.\begin{aligned} D_f &= \frac{\ln\left[a_f/a_o\right]}{C_f 2\pi\ M_J} && ;\ m_f = 1 \\ D_f &= \frac{a_o^{(1-m_f)} - a_f^{(1-m_f)}}{C_f\left[m_f - 1\right]\left[2\pi M_J\right]^{m_f}} && ;\ m_f \neq 1 \end{aligned}\right\} \tag{26}$$

where $\Delta\tilde{W}_f$ is the "strain energy parameter" which relates to the ΔJ-integral solution for uniaxial mode I loading (elastic plus plastic parts), n' is the cyclic strain hardening exponent and M_J is the boundary correction factor divided by the flaw shape correction factor for mode I. For predominantly time-dependent microcrack growth,

$$\Delta\tilde{W}_c^{m_c} N_i = D_c t_o^{(1-m_c)} \tag{27}$$

$$\Delta\tilde{W}_c = \left[\int_{-1}^{1} \left\{\frac{1}{2^{2/3}} \frac{\sigma_{max}}{\Delta\sigma} \frac{\sigma_{max}\Delta\epsilon_e}{2} + \frac{n + 2}{2^{(n+1)/2 + 5/3}} (1 + x)^{(n + 1)/2} * \right.\right.$$

$$\left.\left. * \frac{n + 1}{2\pi} f(n) \frac{\sigma_{max}\Delta\epsilon_c}{n + 1}\right\}^{3/2} dx\right]^{2/3} \qquad ;\ m_c \neq 1 \tag{28}$$

$$\Delta\tilde{W}_c = \frac{\sigma_{max}}{\Delta\sigma}\frac{\sigma_{max}\Delta\epsilon_e}{2} + \frac{n+2}{n+3}\frac{n+1}{2\pi} f(n) \frac{\sigma_{max}\Delta\epsilon_c}{n+1} \quad ; \quad m_c = 1, \quad \beta = 0.5 \qquad (29)$$

$$\left.\begin{aligned} D_c &= \frac{\ln\left(a_f/a_o\right)}{C_c 2\pi M_J} && ; \quad m_c = 1 \\ D_c &= \frac{a_o^{(1-m_c)} - a_f^{(1-m_c)}}{C_c\left(m_c - 1\right)\left(2\pi M_J\right)^{m_c}} && ; \quad m_c \neq 1 \end{aligned}\right\} \qquad (30)$$

where $\Delta\tilde{W}_c$ is a creep "strain energy parameter" which employs an integrated average of the J^*-integral (or C^*-integral of Landes and Begley [39]) over the tensile-going portion of the cyclic deformation, n is the power law creep exponent, σ_{max} is the maximum tensile stress in the cycle, t_o is the tensile-going time, β is the stress wave form exponent, $\sigma = \sigma_{max}(t/t_o)^{\beta}$, and $f(n) = 3.85n^{1/2}(1\text{-}1/n) + \pi/n$. Here, the total mechanical strain range is decomposed into elastic, plastic and creep parts, $\Delta\epsilon = \Delta\epsilon_e + \Delta\epsilon_p + \Delta\epsilon_c$, where power law plasticity and creep are assumed in order to arrive at the specific forms of $\Delta\tilde{W}_f$ and $\Delta\tilde{W}_c$ listed. The authors point out that for type 304 stainless steel at 600°C, cycle-dependent microcrack advance (transgranular) holds for PP and PC isothermal cycle-types, using the terminology of strain range partitioning, while the time-dependent crack growth rate dominates for CP and CC type cycles (intergranular); likewise, in-phase TMF for this material is dominated by time-dependent microcrack propagation whereas out-of-phase TMF is dominated by the cycle-dependent term. Good correlations are achieved for nickel-base superalloys and Cr-Mo steels as well [38].

The microcrack propagation approach of Nitta and Kuwabara perhaps has a firmer mechanics basis than plastic strain range-based approaches, although use of isotropic continuum solutions for the driving forces for short cracks embedded in a strain localized, anisotropic region may be debated. Moreover, microstructural roughness and closure effects may be somewhat difficult to quantify, but these are not explicitly

considered in other initiation approaches either. Since crack growth rate equations are introduced, very complex histo ries may be rationally treated. Furthermore, it introduces both an elastic and plastic component of the driving force(s) for cyclic microcrack extension which is desirable for superalloys. However, the important element of oxidation is not explicitly included in the formulation. To assume that it is implicitly embedded in equation (23) is tantamount to demanding that the same term model both oxidation and creep processes; the activation energies and associated stress level dependencies for these two processes are different. With explicit introduction of oxidation effects, this approach may indeed offer a very general, powerful tool for TMF analysis. It may be considered a damage rate approach as discussed in a later section.

Mechanistic Approaches With Explicit Oxidation Effects:

Of particular applicability to nickel-base superalloys are approaches which explicitly consider oxide formation, fracture and interaction of slip bands with oxides and carbides on grain boundaries. As pointed out by Remy [2], environmental effects are very important for superalloys and are neglected by most models. He presents a microcrack propagation model in which the total crack growth rate is given by the sum of fatigue and oxidation components, i.e. $da/dN = (da/dN)_{fat} + (da/dN)_{ox}$. The fatigue component is obtained from a modified form of the fatigue microcrack propagation model of Tomkins [40]. The model is similar in principle to the additive assumption of fatigue and creep damage increments in the continuum damage theory discussed earlier, although in this case the damage has the physical definition of microcrack length and time-dependent effects are considered to be environmental penetration rather than creep. This distinction is very important for thermal fatigue of superalloys.

Antolovich [41] has proposed several approaches to predict in-phase and out-of-phase TMF of nickel-base superalloys. It is assumed first that the precipitate structure is stable (low mismatch between matrix and precipitate), i.e. aging effects are negligible. This is often the case for TMF of nickel-base superalloys which are operated within temperature ranges which do not induce microstructural changes. Since jet engine applications employing these materials have fairly well-defined histories, we may

consider some simple in-phase and out-of-phase cycles of temperature and mechanical strain.

Consider first out-of-phase TMF cycling as shown in the temperature versus mechanical strain plot in Figure 1. In this case, diffusion of oxygen occurs along either slip bands formed at low temperatures or more likely along grain boundaries. The grain boundaries are then susceptible to brittle fracture at lower temperatures by virtue of the impingement of slip bands. After this initiation process has occurred, microcracks can then continue to propagate along the slip bands. One may define the initiation criterion as the point where the diffusion length or effective penetration distance of oxygen is equal to the slip band spacing.

Assuming parabolic diffusion kinetics, which is valid for nickel-base superalloys [42], the effective penetration distance X is given by

$$X = \sqrt{Dt} \tag{31}$$

where D is the effective diffusion coeficient and t denotes time. The relation between slip band spacing and inelastic strain range has been determined to be of the form

$$i = A\Delta\epsilon_n^{-\delta} \tag{32}$$

where i is the slip band spacing, A and δ are experimentally determined constants and $\Delta\epsilon_n$ is the mechanical inelastic strain range. By equating (31) and (32),

$$N_i = \frac{A^2\nu}{D_o} \exp\left(\frac{Q}{RT_{eff}}\right) \Delta\epsilon_n^{-2\delta} \tag{33}$$

where ν is cycle frequency, D_o is a diffusion coefficient, $D = D_o\exp(-Q/RT_{eff})$, Q is the activation energy, R is the universal gas constant and T_{eff} is the effective temperature defined by

$$\exp\left[-\frac{Q}{RT_{eff}}\right] = \frac{1}{\Delta T}\int_{T_\ell}^{T_h} \exp\left[-\frac{Q}{RT}\right] dT \qquad (34)$$

where $\Delta T = T_h - T_\ell$, T_h and T_ℓ are the upper and lower cycle temperatures, respectively. Although δ and A may be determined by slip band measurements, Antolovich suggests an engineering form of equation (33) as

$$N_i = C_1(\nu)\ \exp\left[\frac{B}{T_{eff}}\right] \Delta\epsilon_n^{-\kappa} \qquad (35)$$

in which C_1, B and κ would be experimentally determined. One would expect this approach to apply if the stress at the tip of the intersecting slip band at the low temperature in the cycle exceeds the cohesive strength of the oxygen-degraded grain boundary. Note also that this equation should apply independent of whether one considers the initial oxide rupture event as defining initiation or a sequence of intermittent oxide ruptures so long as oxygen penetration obeys the same diffusion kinetics. Periodic oxide rupture and surface oxide scaling, for example, may result in more rapid oxidation than the parabolic law would suggest.

For in-phase TMF of nickel-base superalloys with stable precipitate structure, as shown in Figure 1, Antolovich and Jayaraman [3] have derived the form

$$N_i = C_2\ \frac{\nu}{1+\nu t_h}\ \exp\left[\frac{Q}{RT_{eff}}\right] \Delta\epsilon_n^{-8n'} \qquad (36)$$

which is of the same general form as (33) but differs in terms of the exponent on inelastic strain range. Here, n' is the cyclic strain hardening exponent and t_h is the high temperature hold time, if any. This expression is derived by considering a rupture criterion for oxygen-degraded boundaries or slip bands at high temperature,

$$\sigma_{max} X^{\eta} = C_3 \tag{37}$$

where the constant η has been determined for several superalloys as approximately 1/4. Here it is assumed that damage occurs predominately at the high temperature so that the low temperature stress is less than the cohesive strength of the oxygen-degraded grain boundaries. No interaction is assumed between the high and low temperature damage modes, as substantiated experimentally.

Antolovich has also suggested forms for the case of metastable precipitate structure and for carbide formation and coarsening. If it is assumed that the precipitate arrangement of typical nickel-base superalloys remains in a cubic array during coarsening, then the interprecipitate spacing is related to the volume fraction of precipitates and the decay of Orowan dislocation looping stress with cycles may be estimated. This leads to a life relation which is dependent on coarsening of precipitates. The exponent on mechanical inelastic strain range in the N_i versus $\Delta\epsilon_n$ relationship depends on the mechanism of crack initiation and on the stability of the precipitate structure.

For some nickel-base superalloys, formation of $M_{23}C_6$ carbides on grain boundaries is significant. Vacancies formed via low temperature slip diffuse at high temperatures to carbide/matrix interfaces at grain boundaries which have been shown to be nucleation sites for voids. Then, for out-of-phase loading, failure occurs when the effective stress on the grain boundary due to slip band impingement exceeds the cohesive strength of the carbide/matrix interface. This condition may be expressed as

$$\sigma_c = \frac{\sigma_{max}}{1 - n_A \pi r_v^2} \tag{38}$$

where σ_c is the cohesive strength, σ_{max} is the maximum stress at the low temperature, n_A is the number of voids per unit area and r_v is the mean void radius at failure. Assuming

parabolic diffusion of vacancies to grain boundary carbides and constant per cycle void volume accumulation, we arrive at the out-of-phase TMF life expression

$$N_i = C_4\left(\frac{\nu}{n_A}\right)^{1/2}\left[\frac{\sigma_c-\sigma_{max}}{\sigma_c}\right]^{3/2}\exp\left(\frac{Q}{2RT_{eff}}\right) \tag{39}$$

This may also be a viable physical model for austenitic stainless steels and other ductile alloys prone to carbide formation and void growth under out-of-phase TMF cycles.

These micromechanical TMF approaches may conceptually be used to discern the dominant TMF mechanism since the exponent on mechanical plastic strain range in the life relations is mechanism-dependent.

As stated by Neu and Sehitoglu [43], damage occurring during in-phase TMF is typically creep-dominated whereas out-of-phase TMF damage is oxidation-dominated. In-phase and out-of-phase TMF loading correspond to intergranular and transgranular cracking, respectively. These observations are based primarily on steels, and would be expected to hold true for creep-sensitive alloys. For nickel-base superalloys, however, the in-phase TMF behavior is still often dependent on cracking of oxygen-degraded grain boundaries at the high temperature as pointed out by Antolovich.

According to Neu and Sehitoglu [43], it is necessary to consider the type of oxidation process, temperature, strain rate, mechanical strain range and strain-temperature phasing (i.e. in-phase, out-of-phase or other more general path) for accurate TMF life prediction. Assuming linear damage and unity damage at failure, they defined the total damage per cycle, D^{tot}, as

$$D^{tot} = D^{fat} + D^{ox} + D^{creep} \tag{40}$$

or

$$\frac{1}{N_i} = \frac{1}{N_i^{fat}} + \frac{1}{N_i^{ox}} + \frac{1}{N_i^{creep}} \tag{41}$$

where the N_i's represent the number of cycles to initiation of a crack under each mode independently. They propose use of the mechanical strain-life relation

$$\frac{\Delta\epsilon_m}{2} = \frac{\sigma_f'}{E}(2N_i^{fat})^b + \epsilon_f'(2N_i^{fat})^c \tag{42}$$

for the fatigue component of damage, where the constants pertain to room temperature fatigue response. Here, $\Delta\epsilon_m$ is the total mechanical strain range and σ_f', b, ϵ_f' and c are fatigue properties. For oxidation and creep damage, they propose

$$\frac{1}{N_i^{ox}} = \left[\frac{h_{cr}\delta_o}{B\,\Phi^{ox}K_p^{eff}}\right]^{-\frac{1}{\beta}} \frac{2(\Delta\epsilon_m)^{(2/\beta)+1}}{\dot{\epsilon}^{(1-\Omega/\beta)}} \tag{43}$$

where δ_o, B and Ω are material constants, h_{cr} is the critical oxide depth, β is the exponent of time in the oxide growth law, K_p^{eff} is the effective parabolic oxidation constant (in the sense of effective temperature in (34)), and Φ^{ox} is a "phasing factor" which takes into account phasing between mechanical and thermal strain, i.e.

$$\Phi^{ox} = \frac{1}{t_c}\int_0^{t_c} \exp\left[-\frac{1}{2}\left[\frac{\dot{\epsilon}_{th}/\dot{\epsilon}_m + 1}{\xi^{ox}}\right]^2\right] dt \tag{44}$$

Here, t_c is the continuous cycle time ($=2\Delta\epsilon_m/\dot{\epsilon}$), ξ^{ox} is a constant, and ϵ_{th} is the thermal strain; Φ^{ox} is unity for out-of-phase TMF ($\dot{\epsilon}_{th}/\dot{\epsilon}_m = -1$), zero for unconstrained expansion/contraction ($\dot{\epsilon}_{th}/\dot{\epsilon}_m = \pm\infty$), and between zero and unity for in-phase TMF ($\dot{\epsilon}_{th}/\dot{\epsilon}_m = 1$). A coupling is noted between the oxidation damage and the deformation history through the phasing factor.

The creep component of damage is given by

$$D^{creep} = \Phi^{creep} \int_0^{t_c} A \exp(-\Delta H/RT) \left(\frac{\alpha_1 \bar{\sigma} + \alpha_2 \sigma_H}{K} \right)^m dt \qquad (45)$$

where α_1, α_2 are scaling factors, A and m are constants and ΔH is the activation energy for creep. As per Hayhurst et al. [44], this is a power law expression in isochronous stress where $\bar{\sigma}$ and σ_H are the effective and hydrostatic stresses, respectively. Denominator K is the drag stress in a viscoplastic constitutive law which may be assumed constant for steady-state TMF cycling; however, creep cavity growth-plasticity interaction can be introduced with variable K. The phasing factor for creep is given by

$$\Phi^{creep} = \frac{1}{t_c} \int_0^{t_c} \exp\left(- \frac{1}{2} \left[\frac{\dot{\epsilon}_{th}/\dot{\epsilon}_m - 1}{\xi^{creep}} \right]^2 \right) dt \qquad (46)$$

where ξ^{creep} is a constant. Neu and Sehitoglu have obtained good correlation of numerous in-phase, out-of-phase and intermediate phase TMF tests on 1070 steel in air and in a helium atmosphere [43,45]. This approach permits consideration of distinct damage mechanisms and hence contains the necessary elements for application to TMF of nickel-base superalloys as well; in fact, Sehitoglu and co-workers have applied it recently to TMF of nickel-base alloy Mar-M247 [46]. Since all mechanisms and TMF loading histories are treated simultaneously by this method, it is quite promising for application to complex TMF histories of nickel-base superalloys.

Damage Rate Approaches

This type of approach is typified by explicit identification of damage variables with microcrack length, cavity size and spacing, oxygen penetration depth, etc. Such approaches have been successfully applied to creep-fatigue interaction and TMF of ductile high temperature alloys which experience significant creep cavitation [1,47-48]. Here, we refer to the approach in perhaps broader terms than its original form, which addressed creep-fatigue interaction of ductile alloys.

One approach is to write a fatigue microcrack propagation law and a cavity growth law, neglecting interaction effects, e.g.

$$\frac{da}{dN} = F(\Delta\sigma, \Delta\epsilon_n, a) \quad , \quad \frac{dr}{dN} = G(\dot{\epsilon}, t_c, D_{gb}, \sigma, \lambda, r) \tag{47}$$

where a and r are mean microcrack length and cavity size, t_c is the cycle time, D_{gb} is the grain boundary diffusivity and λ is the cavity spacing. Both F and G are temperature- and microstructure-dependent functions. Often, cycle and hold periods are treated separately and mean stress relaxation is accounted for in the calculation of dr/dN. Also, expressions have been derived for both constrained and unconstrained cavity growth in accordance with deformation mechanism maps for creep (c.f. [19]).

It should be noted that even though bulk stress and strain parameters are employed as driving forces as in the continuum damage approach, the damage variables may be measured rather than inferred.

The so-called "damage rate approach" which includes interaction of creep damage with microcrack propagation was proposed by Majumdar and Maiya [47]. According to this strain-based approach, fatigue microcrack propagation is coupled with cavity growth via the equation

$$\frac{1}{a}\frac{da}{dt} = \begin{Bmatrix} T \\ C \end{Bmatrix} (1 + \alpha \ln(r/r_o)) \; |\Delta\epsilon_n|^m \; |\dot{\epsilon}_n|^k \tag{48}$$

where T, C, m, k and α are temperature, environment and microstructural dependent material parameters; T and C apply to tensile and compressive stress, respectively. If the cavity size $r \leq r_o$, it is assumed that the crack growth rate is unaffected by the presence of cavities. For cavity growth, they introduced the decoupled law

$$\frac{1}{c}\frac{dc}{dt} = \begin{Bmatrix} G \\ -G \end{Bmatrix} |\Delta\epsilon_n|^m \; |\dot{\epsilon}_n|^{k_c} \tag{49}$$

where m and k_c are temperature-, environment- and microstructure-dependent material parameters and G is a coefficient with sign dependent on the sign of applied stress. Equation (49) infers cavity healing in compression. This damage rate approach has been successfully applied, for example, to creep-fatigue interaction of austenitic stainless steels [47-48] and Cr-Mo-V steels [1].

Clearly, the damage rate approach is amenable to incorporation of detailed damage mechanisms as discussed previously. Moreover, the equations are of rate-type so that complex loading paths in mechanical strain-temperature space may be readily treated.

For example, defining D_f as microcrack length, D_e as environmental penetration depth, and D_c as the area fraction of creep cavities, we may write

$$\delta D_f = \chi(\sigma, D_f) \left\{1 + \Lambda(D_c, D_e)\right\} |\dot{\epsilon}_n|^m |\Delta\epsilon_n|^k \delta N \tag{50}$$

$$\dot{D}_e = E K_p^{eff} t^{\beta} \tag{51}$$

$$\dot{D}_c = < \frac{\sigma}{A\sigma_u(1 - D_c)} >^r (1 - D_c)^{r-k(\sigma)} \tag{52}$$

where χ and Λ are temperature-dependent functions. Appropriate temperature dependence is assumed for all parameters. The environmental penetration rate and creep damage rate are based on diffusion kinetics and continuum damage concepts, respectively. One would expect Λ to contribute insignificantly to fatigue microcrack propagation in an inert atmosphere or vacuum for most nickel-base superalloys at high temperature. Coefficient χ introduces mean stress effects and microcrack length dependence. In practice, specification of the coupling of the fatigue microcrack propagation rate with the environmental penetration is difficult and requires perhaps more extensive experimental characterization than the aforementioned approaches. It should be clear from earlier discussion that use of the inelastic mechanical strain range

in the fatigue damage rate equation may be inadvisible for TMF of nickel-base superalloys.

Failure criteria for each mode of damage operating independently may be expressed as

$$\Delta\sigma^{max}\left(D_f\right)^{\eta_f} = Y_f \quad \text{or} \quad D_f = D_f(\text{critical}) \tag{53}$$

$$\sigma^{max}\left(D_e\right)^{\eta_e} = Y_e \tag{54}$$

$$\sigma^{max}\left(D_c\right)^{\eta_c} = Y_c \quad \text{or} \quad D_c = D_c(\text{critical}) \tag{55}$$

where Y_f, Y_e, Y_c, η_f, η_e and η_c are constants. Equation (53.1) is a pseudo-fracture criterion. Y_e in equation (54) relates to the cohesive strength of oxygen-degraded grain boundaries or grain boundary carbides. Equation (55.1) introduces the oft neglected stress level dependence of creep rupture [49]; equations (53.2) and (55.2) employ assumptions of a critical level of damage to failure. It is thought that the stress level-dependent forms for failure are more consistent with subsequent macrocrack propagation analysis for cases where the initiation (microcrack propagation stage) life is significantly less than the total life.

For practical applications, the damage rate equations are integrated over a complete TMF cycle to estimate the per cycle damage increment. Typically a set of anisothermal viscoplastic constitutive equations are necessary to accurately determine the stress and inelastic mechanical strain histories (c.f. [50-53]); coupling of damage with the viscoplastic deformation may typically be neglected for nickel-base superalloys until very late in life. Much of this incremental history information is neglected for the sake of simplicity in conventional approaches based on overall cycle stress and strain measures.

The "micromechanical" approaches of Antolovich et al. and Neu and Sehitoglu discussed earlier may be viewed as integrated or averaged forms of a damage rate

approach, although the Neu-Sehitoglu theory involves integration over a cycle to determine phasing and couples with a viscoplastic stress-strain model. Conceptually, one may frame their basic assumptions in the context of the damage rate approach coupled with an appropriate anisothermal viscoplastic model.

Implementation of a cycle- and time-dependent fatigue microcrack growth laws based on fracture mechanics as in equations (22)-(30) would fit into the general framework of damage rate approaches as outlined here. In this case, the focus is on crack extension by virtue of a combination of cycle- and time-dependent effects. If $(da/dt)_{ox}$ and $(da/dt)_{creep}$ are both introduced, the time-dependencies of oxidation and creep may be accounted for separately. It is perhaps this class of approaches, combining microcrack propagation concepts with micromechanical aspects of oxidation, that offer most promise for TMF life prediction of nickel-base superalloys from a fundamental viewpoint.

CONCLUSIONS

In this paper, we have briefly reviewed and critiqued some contemporary approaches for correlation of fatigue life at high temperature in the presence of several competing damage mechanisms. The emphasis has been on determining strengths and weaknesses of the approaches with respect to TMF life prediction of nickel-base superalloys which often exhibit copious oxidation effects in lieu of significant creep cavitation. It is recognized that methods for treating the anisothermal aspects of TMF are essentially in their infancy, yet it is also clear from first principles that approaches which explicitly treat fatigue, creep and environmental damage are most promising. Creep-fatigue interaction models which exclude environmental effects or include them only implicitly must be applied cautiously to TMF life prediction, since their mechanistic basis is suspect.

ACKNOWLEDGMENTS

Dr. McDowell is grateful for the support of the Allison Gas Turbine Engine Division of the General Motors Corporation and the U.S. National Science Foundation for related investigations.

REFERENCES

1. Priest, R.H. and Ellison, E.G., "An Assessment of Life Analysis Techniques for Fatigue-Creep Situations," Res Mechanica, Vol. 4, 1982, pp. 127-150.
2. Remy, L., "Recent Developments in Thermal Fatigue," Proc. Int. Seminar on the Inelastic Behaviour of Solids Models and Utilisation, MECAMAT, Vol. IV, 1988, pp. 1-19.
3. Antolovich, S.D. and Jayaraman, N., "The Effect of Microstructure on the Fatigue Behavior of Ni Base Superalloys," Fatigue: Environment and Temperature Effects, J.J. Burke and V. Weiss, Eds., Plenum Press, NY., 1983, pp. 119-144.
4. Kachanov, L., Fundamental of Fracture Mechanics, Nauka, Moscow, 1974.
5. Rabotnov, Y.N., Creep Problems in Structural Members, Amsterdam, North Holland Publishing Co., 1969.
6. Chaboche, J.L., "Continuous Damage Mechanics - A Tool to Describe Phenomena Before Crack Initiation," Nuclear Engr. and Design, Vol. 64, 1981, pp. 233-247.
7. Lemaitre, J. and Chaboche, J.L., "A Non-Linear Model of Creep-Fatigue Damage Cumulation and Interaction," Mechanics of Visco-Plastic Media and Bodies, Ed. Jan Hult, Springer, Berlin, 1975, pp. 297-301.
8. Chaboche, J.L., Policella, H., and Kaczmarek, H., "Applicability of the SRP Method and Creep-Fatigue Damage Approach to the LCHTF Life Prediction of IN 100 Alloy," AGARD SMP-243 Meeting on Strain Range Partitioning, April 11-12, 1978, Aalborg, Denmark, April 1978, 4.1-4.20.
9. Lemaitre, J., "Damage Modelling for Prediction of Plastic or Creep-Fatigue Failure in Structures," Paper L5-1, SMIRT-5 Conference, Berlin, 1979.
10. Guinemer, J.-Y. and Plumtree, A., "An Elevated Temperature Fatigue Crack Model for Stainless Steels," in Mechanical Testing for Deformation Model Development, ASTM STP 765, R.W. Rohde and J.C. Swearengen, Eds., Philadelphia, 1982, pp. 452-466.
11. Lemaitre, J. and Plumtree, A., "Application of Damage Concepts to Predict Creep-Fatigue Failures," ASME J. Engr. Materials and Technology, Vol. 101, 1979, pp. 284-292.
12. Bui-Quoc, T. and Biron, A., "A Phenomenological Approach for the Analysis of Combined Fatigue and Creep," Nucl. Engr. Des., Vol. 71, 1982, pp. 89-102.
13. Bui-Quoc, "Recent Developments of Damage Concepts Applied to Creep-Fatigue Combinations," Post-Conference Seminar on Inelastic Analysis and Life Prediction in High Temperature Environment, SMiRT-6, Paris, August 1981.

14. Leckie, F.A., "The Constitutive Equations for High Temperatures and Their Relationship to Design," Proc. Int. Conf. on Constitutive Laws for Engineering Materials, Eds. Desai and Gallagher, Univ. of Arizona, Tucson, Jan. 1983, p. 93.
15. Chaboche, J.L., "Continuum Damage Mechanics: Present State and Future Trends," Seminaire International sur l'Approche Locale de la Rupture, Moret-sur-Loing, June 3-5, 1986.
16. Chaboche, J.L. and Lesne, P.M., "A Non-Linear Continuous Fatigue Damage Model," Fatigue Fract. Engng. Mater. Struct., Vol. 11, No. 1, pp. 1-17, 1988.
17. Skelton, R.P., "The Prediction of Crack Growth Rates from Total Endurances in High Strain Fatigue," Fatigue of Engineering Materials and Structures, Vol. 2, 1979, pg. 305.
18. Wareing, J., "Creep-Fatigue Interaction in Austenitic Stainless Steels," Metallurgical Transactions, Vol. 8A, 1977, pg. 711.
19. Miller, D.A., Hamm, C.D., and Phillips, J.L., "A Mechanistic Approach to the Prediction of Creep-Dominated Failure During Simultaneous Creep-Fatigue," Materials Science and Engineering, Vol. 53, 1982, pp. 233-244.
20. Coffin, L.F., "Fatigue at High Temperatures - Prediction and Interpretation," Proc. Inst. Mech. Eng., Vol. 188, 1974.
21. Coffin, L.F., "Overview of Temperature and Environmental Effects on Fatigue of Structural Metals," Fatigue: Environment and Temperature Effects, J.J. Burke and V. Weiss, Eds., Plenum Press, N.Y., 1983, pp. 1-40.
22. Coffin, L.F., "A Review of Fatigue Predictive Methods in the Regime Where Inelastic Strains Dominate," Proc. Winter Annual Meeting of ASME, Dec. 2-7, 1979, pp. 1-24.
23. Ostergren, W.J., "A Damage Function and Associated Failure Equations for Predicting Hold Time and Frequency Effects in Elevated Temperature Low Cycle Fatigue," Journal of Testing and Evaluation, Vol. 4, 1976, pp. 327-339.
24. Halford, G.R. and Saltsman, J.F., "Calculation of Thermomechanical Fatigue Life Based on Isothermal Behavior," NASA TM 88864, 1987.
25. Ostergren, W.J. and Krempl, E., "A Uniaxial Damage Accumulation Law for Time-Varying Loading Including Creep-Fatigue Interaction," ASME Journal of Pressure Vessel Technology, Vol. 101, 1979, pp. 118-124.
26. Manson, S.S., Halford, G.R., and Hirschberg, M.H., "Creep-Fatigue Analysis by Strain Range Partitioning," NASA TM X-67838, 1971.
27. Manson, S.S., "The Challenge to Unify Treatment of High Temperature Fatigue - A Partisan Proposal Based on Strain Range Partitioning," Fatigue at Elevated Temperatures, ASTM STP 520, 1973, pp. 744-782.

28. Hirschberg, M.H., and Halford, G.R., "Strain Range Partitioning - A Tool for Characterizing High Temperature Low Cycle Fatigue," NASA TM X-71691, 1975.
29. Halford, G.R. and Nachtigall, A.J., "The Strainrange Partitioning Behavior of an Advanced Gas Turbine Disk Alloy, AF2-1DA," 15th Joint AIAA/SAE/ASME Propulsion Conf., Las Vegas, June 1979, pp. 1-9.
30. Manson, S.S., "The Development and Application of Strainrange Partitioning as a Tool in the Treatment of High Temperature Metal Fatigue," AGARD SMP-243 Meeting on Strain Range Partitioning, April 11-12, 1978, Aalborg, Denmark, April 1978, K.1-K.7.
31. Manson, S.S. and Halford, G.R., "Multiaxial Rules for Treatment of Creep-Fatigue Problems by Strainrange Partitioning," NASA TM X-73488, 1976.
32. Halford, G.R., Saltsman, J.F. and Hirschberg, M.H., "Ductility-Normalized Strainrange Partitioning Life Relations for Creep-Fatigue Life Prediction," Environmental Degradation of Engineering Materials, Virginia Polytechnic Institute and State Univ., Blacksburg, VA, 1977, pp. 599-612.
33. Halford, G.R. and Saltsman, J.F., "Strainrange Partitioning - A Total Strain Range Version," NASA TM 83023, 1983.
34. Bania, P.J., The High Temperature Low Cycle Fatigue Behavior of a Near-Alpha Titanium Alloy, Ph.D. Dissertation, University of Cincinnati, 1977.
35. Nitta, A. and Kuwabara, K., "Thermal-Mechanical Fatigue Failure and Life Prediction," Current Japanese Materials Research, Vol. 3, Elsevier, New York, 1988, pp. 203-222.
36. Kuwabara, K., Nitta, A., Kitamura, T. and Ogata, T., in Basic Questions in Fatigue: Volume II, ASTM STP 924, R.P. Wei and R.P. Gangloff, Eds., Philadelphia, 1988, pp. 41-59.
37. Dowling, N.E. and Begley, J.A., in Mechanics of Crack Growth, ASTM STP 590, Philadelphia, 1976, pp. 82-103.
38. Ohtani, R., Kitamura, T., Nitta, A. and Kuwabara, K., "High-Temperature Low Cycle Fatigue Crack Propagation and Life Laws of Smooth Specimens Derived from the Crack Propagation Laws," in Low Cycle Fatigue, ASTM STP 942, H.D. Solomon, G.R. Halford, L.R. Kaisand, and B.N. Leis, Eds., Philadelphia, 1988, pp. 1163-1180.
39. Landes, J.D. and Begley, J.A., in Mechanics of Crack Growth, ASTM STP 590, Philadelphia, 1976, pp. 128-148.
40. Tomkins, B., Creep and Fatigue in High Temperature Alloys, Ed. J. Bressers, Applied Science Publishers, London, 1981, p. 111.

41. Antolovich, S.D., in TMF Workshop Abstracts, NASA Lewis Research Center, Nov. 15-16, 1984.
42. Pedron, J.P. and Pineau, A., "Influence de L'Oxydation sur la Propagation des Fissures a Haute Temperature dans L"Alliage Inconel 718," Memoires et Etudes Scientifiques Revue de Metallurgie, December 1983, pp. 665-674.
43. Neu, R.W. and Sehitoglu, H., "Thermo-mechanical Fatigue, Oxidation and Creep," Parts I & II, accepted for publication in MET TRANS A, 1988.
44. Hayhurst, D.R., Leckie, F.A., and McDowell, D.L., "Damage Growth Under Nonproportional Loading," ASTM STP 853, 1985.
45. Karasek, M.L., Sehitoglu, H. and Slavik, D.C., "Deformation and Fatigue Damage in 1070 Steel under Thermal Loading," in Low Cycle Fatigue, ASTM STP 942, Philadelphia, 1988, pp. 184-205.
46. Boismier, D.A., "Thermo-mechanical Fatigue Mechanisms and Life Prediction for Mar-M247 Nickel-based Superalloy," M.S. Thesis, University of Illinois at Urbana-Champaign, 1988.
47. Majumdar, S. and Maiya, P.S., "A Mechanistic Model for Time-Dependent Fatigue," ASME Journal of Engineering Materials and Technology, Vol. 102, Jan. 1980, pp. 159-167.
48. Majumdar, S., "Thermomechanical Fatigue of Type 304 Stainless Steel," Proc. ASME Conf. on Thermal Stress, Material Deformation and Thermo-mechanical Fatigue, Eds. H. Sehitoglu and S.Y. Zamrik, PVP-Vol. 123, 1987, pp. 31-36.
49. Woodford, D.A., "Creep Damage and the Remaining Life Concept," ASME J. Engr. Materials and Technology, Vol. 101, Oct. 1979, pp. 311-316.
50. Slavik, D. and Sehitoglu, H., "A Unified Creep-Plasticity Model Suitable for Thermo-Mechanical Loading," NASA CP 10010, pp. 295-306.
51. Benallal, A. and Ben Cheikh, A., "Damage and Rupture of Viscoplastic Structures under Anisothermal Cyclic Loadings," Proc. Int. Seminar on the Inelastic Behaviour of Solids Models and Utilisation, MECAMAT, Vol. II, 1988, pp. 37-52.
52. Cailletaud, G., Culie, J.P., and Kaczmarek, H., "Mechanical Description of Viscoplastic and Damage Behaviour Under Variable Temperature in Presence of Microstructural Instabilities," Comm. Symposium IUTAM on Creep in Structures, Leicester, 1980, pp. 48-70.
53. Ohno, N., Takahashi, Y. and Kuwabara, K., "Constitutive Modeling of Anisothermal Cyclic Plasticity of 304 Stainless Steel," ASME J. Engr. Materials and Technology, Vol. 111, Jan. 1989, pp. 106-114.

LIST OF FIGURES

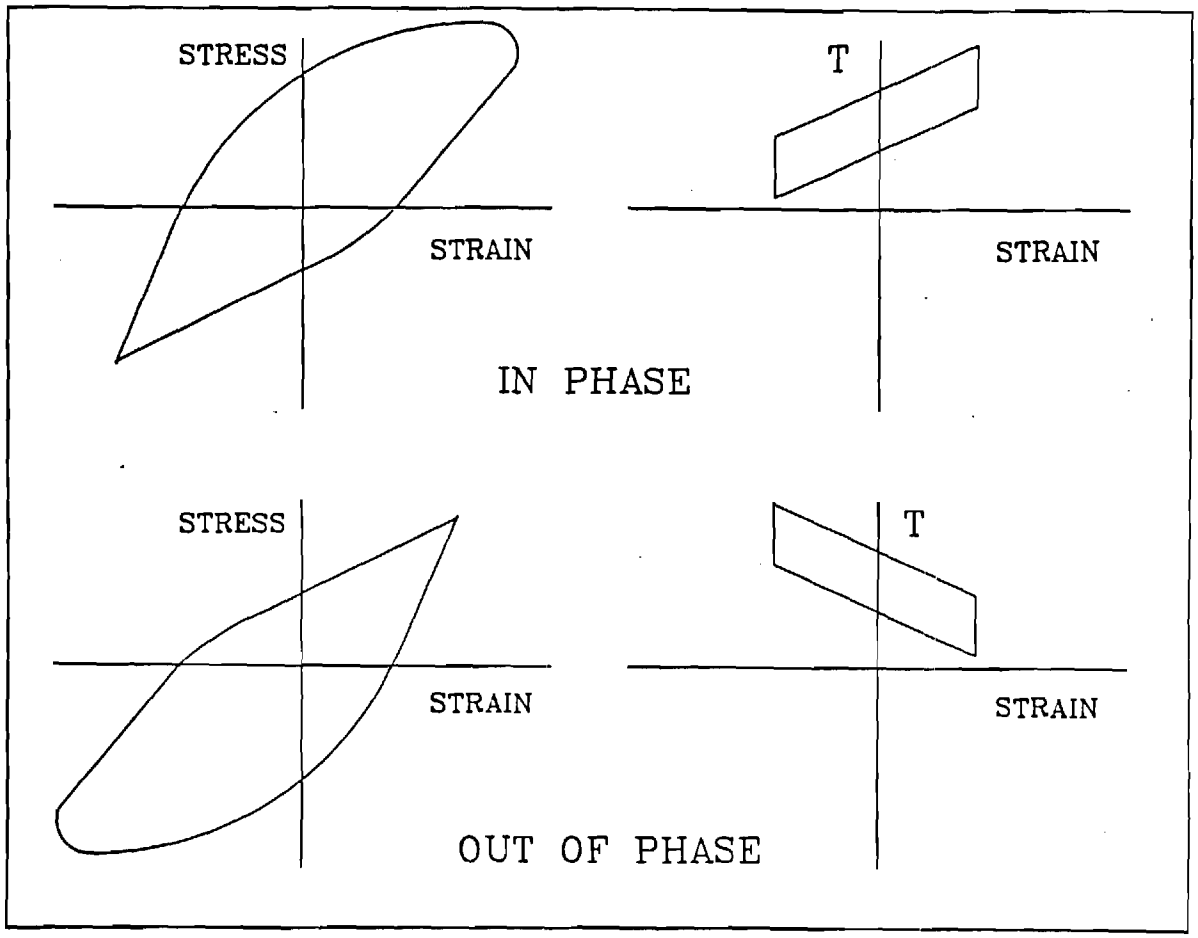

Figure 1. In-phase (top) and out-of-phase (bottom) temperature versus mechnical strain histories and associated typical stress strain responses.

DAMAGE RATE APPROACHES FOR THERMOMECHANICAL FATIGUE OF SUPERALLOYS

By David L. McDowell
Principal Investigator

R.L.T. Oehmke
Research Engineer

Matthew P. Miller
Graduate Student

Project # E-25-M77

November 1989

Submitted to Allison Gas Turbine Operations, General Motors Corporation

Sponsor Technical Contact:

Dr. Edwin Pope
Allison Gas Turbine Operations
General Motors Corporation
P.O. Box 420
Indianapolis, IN 46206-0420
(317) 230-2737

Sponsor Administration and Contractual Matters:

Roxanne Eley
Allison Gas Turbine Operations
General Motors Corporation
P.O. Box 420
Indianapolis, IN 46206-0420
(317) 230-3777

SUMMARY

A microcrack propagation model for creep-fatigue-environment interaction is presented with particular emphasis on Ni-base superalloys. The microcrack propagation consists of distinct contributions from cyclic strain, creep and oxidation components. The fatigue component is assumed to be controlled by the ΔJ parameter. The creep component is assumed to be controlled by a parameter analogous to the singularity strength of the time dependent HRR field. The oxidation component is ΔJ-controlled with an additional possible time-dependence associated with oxygen-degraded strength of material at the crack tip. Correlations of the data obtained to date for MAR M-246 are made on the basis of this model and discussed. Finally, goals for the fourth year of the program are outlined.

MICROCRACK PROPAGATION MODEL

The life prediction model builds on concepts introduced by Nitta and Kuwabara [1-2] and Ohtani et al. [3-4] (Appendix A) who introduced a framework based on the fracture mechanics concept of the ΔJ-integral [5] applied to fatigue microcrack propagation and the ΔJ_c parameter obtained by the time-integration of the J^*-integral for creep crack growth [1-4] over a cycle, reckoning that much of the so-called "initiation" stage is spent in microcrack growth. Moreover, use of ΔJ or similar "strain energy parameter" implicitly includes contributions of higher order terms of the crack tip stress-strain series expansions, unlike ΔK. These authors find that $\Delta\epsilon_p$-based approaches such as Manson's universal slope method with the 10% rule for high temperature correction or strain range partitioning work well for ductile materials under isothermal and TMF conditions, but are significantly nonconservative for nickel-base superalloys [1]. Materials examined included cast and forged Cr-Mo-V, Ni-Mo-V, 1.25Cr-0.5Mo, 2.25Cr-1Mo, 0.15%C steel, 12Cr-Mo-W-V steel, 304 stainless steel, 321 stainless steel, A 286, IN 718, IN 738LC, cast IN 939, cast MAR-

M247, cast Rene 80, Hastelloy X, cast FSX 414 and cast FSX 430. It was noted that both the universal slope and strain range partitioning approaches based on inelastic strain range generally provided nonconservative life predictions for superalloys, even for isothermal loading conditions.

The life prediction model presented here extends these concepts one step further by taking oxidation damage into account. Oxidation effects play a major role in the lives of nickel-base superalloys and are assumed to be implicitly embedded in the time-dependent component of crack growth rate in the formulation of Nitta et al. This assumption demands that the activation energies of both creep and oxidation processes as well as the stress level dependencies be the same. In general, this is not the case.

The oxidation effect is introduced as another component in the microcrack propagation rate equation da/dN, i.e.

$$\frac{da}{dN} = \frac{da}{dN}\bigg|_{fat} + \frac{da}{dN}\bigg|_{creep} + \frac{da}{dN}\bigg|_{ox} \tag{1}$$

where

$$\frac{da}{dN}\bigg|_{fat} = C_f(\Delta J)^{m_f} \tag{2}$$

$$\frac{da}{dN}\bigg|_{creep} = C_c\left[\frac{1}{t_c}\int_0^{t_c} C(t)\,dt\right]^{m_c} t_c \tag{3}$$

$$\frac{da}{dN}\bigg|_{ox} = C_o(\Delta J)^{m_o}(\Delta t)^{1/2-\xi} \tag{4}$$

where t_c corresponds to the tensile stress portion of a cycle, Δt is the cycle period, and

$$C_c = C_c' \exp(-Q_c/RT_{eff}) \tag{5}$$

$$C_o = C_o' \exp(-Q_{ox}/RT_{eff}) \tag{6}$$

where R is the universal gas constant and Q_c and Q_{ox} are activation energies for creep and oxidation, respectively. Note that T_{eff} is the effective temperature based on a the cycle-averaged integral of the exponential Arrhenius function. For the isothermal case, the Arrhenius temperature dependence terms may be absorbed in the constants. It is noted that the coefficient C_o' in equation (6) is also dependent on the partial pressure of oxygen, in general [6-7], such that there is no contribution of oxidation in a vacuum or a pure inert environment. It is noted that the exponent m_c in equation (3) is typically very close to unity. The form for the oxidation crack growth law in equation (4) is very important, as it infers that the crack growth rate is still ΔJ-controlled, but modified by the influence of cycle time by oxidation processes; this results in a frequency modified fatigue relation. Physically, it assumes that the cyclic crack growth rate is still controlled by the deformation in the vicinity of the crack tip, but that crack growth proceeds through oxygen-degraded material.

Simplified versions of the expressions for ΔJ and C(t) were employed. These are

$$\Delta J = \left[\frac{\Delta\sigma\Delta\epsilon_e}{2} + f(1/n')\Delta\sigma\Delta\epsilon_p \right] a \tag{7}$$

$$C(t) = \left[\frac{(1+2\eta n)}{(n+1)t} \frac{\sigma\epsilon_e}{2} + f(n)\sigma\dot{\epsilon}_c \right] a \tag{8}$$

In equations (7)-(8), $\Delta\sigma$ is the stress range, $\Delta\epsilon_p$ is the plastic strain range, $\Delta\epsilon_e$ is the elastic strain range ($= \Delta\sigma/E$), $\dot{\epsilon}_c$ is the creep strain rate, a is the crack length, n' is the cyclic strain hardening exponent, n is the creep exponent for power law secondary creep and η is a waveform exponent to be introduced shortly. The first term in equation (8) corresponds

to transient small scale creep, whereas the second term corresponds to the so-called steady state creep condition.

The material is assumed to behave in cyclic plasticity and creep according to

$$\frac{\Delta\sigma}{2} = K'(\Delta\epsilon_p/2)^{n'} \tag{9}$$

$$\dot{\epsilon}_c = D\sigma^n \tag{10}$$

A waveform function is introduced for the stress during the tensile-going portion of the cycle, i.e.

$$\sigma = \sigma_{max}(t/t_c)^{\eta} \tag{11}$$

In equations (7)-(8), the function f was introduced by Shih and Hutchinson [8] for short cracks as

$$f(1/n') = 3.85(1/n')^{1/2}(1 - n') + \pi n' \tag{12}$$

$$f(n) = 3.85(n)^{1/2}(1 - \frac{1}{n}) + \frac{\pi}{n} \tag{13}$$

Considering equations (2), (3) and (4) individually,

$$\left.\frac{da}{dN}\right|_{fat} = C_f(\alpha a)^{m_f} \tag{14}$$

$$\left.\frac{da}{dN}\right|_{ox} = C_o(\alpha a)^{m_o}(\Delta t)^{1/2-\xi} \tag{15}$$

since $\alpha = (\Delta\sigma^2/E + f(1/n')\Delta\sigma\Delta\epsilon_p)$ is constant throughout a constant amplitude history under the usual assumption of cyclic stability. Here Δt is the cycle period and ξ is a factor reflecting the influence of microstructure and local oxidation processes on departure from a parabolic oxidation law. Such processes include oxide buildup at the crack tip, passivation effects, etc.

For the creep crack growth rate, evaluation of the integral

$$\frac{1}{t_c}\int_0^{t_c}\left[\frac{(1+2\eta n)}{(n+1)t}\frac{\sigma\epsilon_e}{2} + f(n)\sigma\dot{\epsilon}_c\right]a\,dt \tag{16}$$

for a = constant over a cycle leads to

$$\left.\frac{da}{dN}\right|_{creep} = C_c t_c (\gamma a)^{m_c} \tag{17}$$

where γ is assumed constant for a constant amplitude, stable cycle for a given history, i.e.

$$\gamma = \frac{(1+2\eta n)}{(n+1)\eta t_c}\frac{\sigma_{max}^2}{4E} + f(n)\frac{D\sigma_{max}^{n+1}}{\eta(n+1)+1} \tag{18}$$

It is clear that the stress waveform function in equation (11) has been used to obtain equation (18). Combining (14), (15) and (17),

$$\frac{da}{dN} = C_f(\alpha a)^{m_f} + C_c t_c(\gamma a)^{m_c} + C_o(\alpha a)^{m_o}(\Delta t)^{1/2-\xi} \tag{19}$$

Equation (19) may be integrated between initial and final crack lengths a_o and a_f, respectively. If fatigue-dominated conditions exist (e.g. room temperature cycling or completely reversed cycling at relatively high frequencies at high temperatures), then we may write

$$Z_f = \alpha^{m_f} N_f \tag{20}$$

where

$$Z_f = \frac{a_f^{(1-m_f)} - a_o^{(1-m_f)}}{C_f(1-m_f)} \qquad \text{if } m_f \neq 1 \tag{21}$$

$$Z_f = \frac{\ln(a_f) - \ln(a_o)}{C_f} \qquad \text{if } m_f = 1 \tag{22}$$

With assumed initial and final crack sizes, C_f and m_f can be determined from a plot of N_f vs. α. Determination of the remaining coefficients and exponents is not quite so straightforward. Oxidation and creep do not operate independent of fatigue processes, in general. Monotonic creep tests are employed to determine D and n, but cyclic testing always introduces a fatigue component of damage. While creep rupture properties are of significance to bulk creep behavior, the influence of creep deformation on the propagation of fatigue microcracks is most pertinent from the viewpoint of calculation of fatigue life. Creep rupture behavior can be assessed in a separate, independent calculation based on the rupture curve.

The contribution of the oxidation term may be determined by consideration of frequency effects on completely reversed fatigue tests, provided the contribution of creep may be determined as negligible; to assess the latter, hold time tests are required.

Experimental Results and Correlations

A tabulation of experimental results obtained to date appears in Tables 1-2.

Room temperature tests were not conducted on MAR M-246 but completely

reversed, constant strain rate fatigue tests were conducted at 650°C and 900°C. Strain rates of $\dot{\epsilon} = 10^{-2}$ sec^{-1}, $\dot{\epsilon} = 10^{-3}$ sec^{-1} and $\dot{\epsilon} = 10^{-4}$ sec^{-1} were employed. In the absence of vacuum or inert environment data, we may initially plot all completely reversed fatigue data with the assumption that $C_o = 0$, i.e. neglect of oxidation or temperature effects.

Figure 1 shows the relationship between N_f (number of cycles to failure) and α (damage parameter described earlier) for the completely reversed fatigue tests. As noted in earlier reports, the specimen compliance changes significantly only over the last few cycles of any given test, indicating that the failure crack size is indeed small. Regressing this data, a value of $m_f = 2.2$ is determined. Initial and final crack lengths of 1.27 μm and 127 μm were used to determine C_f. It is noted that these values of a_o and a_f are selected arbitrarily as representative of flaw sizes on the order of 1/100th the minimum grain size dimension and the minimum grain size dimension, respectively; a_f is also on the order of a few interdendritic spacings. The analysis, in terms of N_f versus the driving force α, is insensitive to the actual values selected since they are absorbed in D_f. It is only necessary that these same initial and final values pertain to all mechanisms in the combined case of creep-fatigue-environment interaction. The value for C_f is $C_f = 333.5$ (MPa-m)$^{-2.2}$(m/cycle), assuming $C_o = 0$. For purposes of calculating α, n' = 0.147 at 650°C and n' = 0.151 at 900°C.

All the completely reversed fatigue data at 650°C and 900°C at strain rates of 10^{-2}, 10^{-3} and 10^{-4} sec^{-1} fall within a factor of two scatterband on life on a plot of α versus N_f; at first glance, the assumption of neglect of temperature and oxidation effects appears reasonable. Indeed, the use of ΔJ as a correlative parameter is clearly superior to either total or plastic strain range as presented in previous reports. However, close observation of the 900°C data reveals very little scatter at each of the three strain rates and a frequency separation of the data by approximately a factor of 1.5 to 2 on life for each decade of strain rate. Although this is not a particularly strong frequency effect, values of C_o and ξ will be determined in future work to describe this frequency separation. There is

also a temperature dependence of the data as exhibited by the difference in the 650°C and 900°C data at comparable strain rates. Frequency separation is a general characteristic in the so-called inititation regime (c.f. Coffin [9], Ostergren et al. [10-11], Cook et al. [12], etc.). There is precedence for weak frequency dependence for some Ni-base superalloys, e.g. IN-738 and Rene 80 [10].

It should be noted that it is possible that oxidation contributes significantly to microcrack propagation but the microcrack propagation process is not uniquely related to oxygen penetration rate; in this case, a parabolic oxidation law commonly applied to Ni-base superalloys is modified by ξ to reflect the actual time dependence of the crack growth law. This is analogous to the Coffin and Ostergren frequency-modified approaches [9-10]. At high temperatures, oxidation along grain boundaries and slip bands may proceed well in advance of the tip of the propagating fatigue microcrack such that process is essentially ΔJ-controlled, i.e. propagation proceeds through an already oxygen-degraded material. In this case, the completely reversed fatigue lives may be weakly time-dependent but the vacuum or inert environment results would differ since propagation would not proceed through oxygen degraded material. Vacuum or inert environment fatigue tests should help clarify the oxidation effect. This line of reasoning is consistent with the general observation of copious oxidation of Ni-base superalloys, with propagation of microcracks proceeding along already degraded paths in contrast to the often assumed mechanism of cycle-by-cycle crack tip rupture and rapid oxidation of the newly exposed crack tip material (c.f. [13-15]); in fact, this cycle-by-cycle oxidation assumption may be valid in certain lower temperature regimes in which the oxygen penetration rate (taking into account crack tip shielding and closure processes) is on the order of the rate of crack advance, leading to a time-dependent oxidation effect.

Several tensile strain hold time tests have been conducted at 900°C, including hold times of 10 sec, 600 sec and 1000 sec. Clearly, the 10 sec hold time test is essentially

equivalent to completely reversed cycling, whereas the 1000 sec hold time resulted in a significantly decreased life for the same $\Delta J/a$ or α value as for a completely reversed test. This additional time-dependent effect of the 1000 sec hold time can be attributed to creep. More hold time tests are necessary, however, to arrive at a statistically meaningful value of C_c.

Slow-fast and fast-slow cyclic tests without hold times have also been conducted to assess the effect of the stress waveform on life. No substantial difference was seen between the results of these two types of histories, indicating weak waveform- and frequency-dependence of the fatigue process, consistent with the completely reversed, constant strain rate tests. However, the lives were substantially lower for these experiments than for the majority of completely reversed tests; this appears to be a consistent trend for specimens machined from recent castings sent from GM which had significantly more curvature than previous batches. This curvature resulted in some machining difficulties and alteration of gage section dimensions as discussed with Dr. Schneider previously. It is also possible that there are significant structure/property asymmetries in these castings as-received from Allison. It is desirable to repeat theses slow-fast and fast-slow experiments with specimens machined according to original specifications to ensure uniformity of the specimens for comparative purposes.

Comparison with Selected Existing Approaches

It is worthwhile to compare this microcrack propagation approach with several contemporary models for TMF life prediction. In contrast to strainrange partitioning [16], this approach includes the influence of oxidation through dependence on cycle period Δt or, alternatively, frequency ν. Creep is included as an additional time dependent effect. This frequency dependence of fatigue microcrack propagation is absent in analogous Japanese models based on ΔJ for fatigue and ΔJ_c (time-averaged value of singularity

amplitude C(t)) for creep. Japanese researchers [1-4] distinguish between fatigue-dominated and creep-dominated conditions, applying only the single applicable da/dN equation rather than both. This procedure is entirely analogous to methods used by British researchers [17-18] who employ a cyclic plastic strain-based microcrack propagation law rather than a ΔJ-based law.

The present approach has some analogy with continuum damage concepts [19-20] although the damage in this case is specifically defined as microcrack length rather than change of stiffness. In damage mechanics models, however, there is no explicit introduction of the effect of oxidation, nor is there a coupling of the creep damage with the microcrack growth process in the same sense as in the present fracture mechanics-based approach.

The ΔJ approach obviously has something in common with plastic work approaches for low cycle fatigue since the plastic part of ΔJ is proportional to the plastic work over a cycle for power law plasticity. However, ΔJ also contains an elastic part related to the elastic strain energy density in a cycle; this contribution is particularly significant for Ni-base superalloys. It is interesting to note the similarity between the parameter α of the present ΔJ-based approach and Ostergren's damage parameter [10] which has shown promise as a correlating parameter for high temperature fatigue and TMF (c.f. [12]). For completely reversed cycling under isothermal conditions, Ostergren's damage parameter is given by

$$\sigma_t \Delta\epsilon_p N_f^{\beta} \nu^{\beta(k-1)} = C_1 \tag{23}$$

while the relation between α and N_f may be written as

$$\sigma_t \Delta\epsilon_p N_f^{\beta} (C_f + C_o \nu^{\xi - 1/2})^{\beta} = C_2 \tag{24}$$

where C_1 and C_2 are constants, it is assumed that $m_f = m_o$, $\beta = 1/m_f$ and the plastic part of ΔJ is assumed to dominate the elastic part. Here σ_t is the peak tensile stress in the cycle and is equal to the stress amplitude for completely reversed cycling. The similarity of the

two approaches is striking and quite encouraging given the success exhibited by the Ostergren parameter for correlation of high temperature, isothermal fatigue of ductile alloys and Ni-base superalloys. There are several fundamental differences, however, between the Ostergren and ΔJ approaches. First, the ΔJ parameter is composed of elastic and plastic parts, whereas the Ostergren parameter considers only the contribution associated with the cyclic plastic strain range. The former approach is desirable from the viewpoint of accuracy of the strains since the elastic strains are often at least comparable in magnitude to the plastic strains for typical fatigue applications of Ni-base superalloys. Second, there is no specific provision in the ΔJ approach to account for mean stress effects. In fact, mean stress effects must be viewed as affecting microcrack closure [21-22] such that the effective ΔJ, ΔJ_{eff}, is modified according to the mean stress (R ratio), i.e.

$$\Delta J_{eff} = G(\sigma_m, \sigma_t)\ \Delta J \tag{25}$$

where σ_m and σ_t are the mean and peak tensile stresses, respectively. An example of closure function G which is consistent with the Ostergren approach is

$$G(\sigma_m, \sigma_t) = \frac{\sigma_t}{2(\sigma_t - \sigma_m)} \tag{26}$$

According to this expression, tensile mean stresses are more damaging than compressive mean stresses. Hence, strain-controlled tests with compressive hold times may be more damaging than tensile hold time tests in Ni-base superalloys owing to the tensile mean stresses set up by the former history as is often experimentally observed. It should be noted that for Ni-base superalloys, the application of the same closure function to both the elastic and plastic parts of ΔJ may be acceptable since the transition fatigue life based

on equality of elastic and plastic strain amplitudes is quite short, often on the order of 10 cycles or so. On the other hand, more ductile alloys may require distinction between the closure function applied to the elastic and plastic parts of ΔJ [23] to emphasize the importance of mean stress in high cycle fatigue.

An area of much concern to engine companies is multiaxiality of the stress-strain state. Lives under combined loading may substantially differ from those obtained under uniaxial loading at the same plastic strain amplitude, for example. The ΔJ-based microcrack propagation model may be readily generalized and shown to provide quite reasonable representation of combined stress state effects as demonstrated recently [23] (Appendix B).

FURTHER ISSUES

Some issues which await clarification and/or further testing include:

(i) vacuum or inert environment fatigue behavior and determination of C_o and ξ,

(ii) in-phase and out-of-phase TMF behavior,

(iii) fatigue lives for fast-slow/slow-fast cycles,

(iv) compressive hold-time behavior and determination of C_c, and

(v) viscoplastic model for TMF behavior of MAR M-246.

Resolution of these issues will be the goal of the fourth year of research as presented in a proposal recently submitted to Allison (Appendix C). In addition, it will be useful for Allison to have benefit of some comparisons of this life prediction methodology with other very simple approaches such as linear time- and cycle-fraction summation for creep-fatigue interaction.

REFERENCES

1. Nitta, A. and Kuwabara, K., "Thermal-Mechanical Fatigue Failure and Life Prediction," Current Japanese Materials Research, Vol. 3, Elsevier, New York, 1988, pp. 203-222.
2. Kuwabara, K., Nitta, A., Kitamura, T. and Ogata, T., in Basic Questions in Fatigue: Volume II, ASTM STP 924, R.P. Wei and R.P. Gangloff, Eds., Philadelphia, 1988, pp. 41-59.
3. Ohtani, R., Kitamura, T., Nitta, A. and Kuwabara, K., "High-Temperature Low Cycle Fatigue Crack Propagation and Life Laws of Smooth Specimens Derived from the Crack Propagation Laws," in Low Cycle Fatigue, ASTM STP 942, H.D. Solomon, G.R. Halford, L.R. Kaisand, and B.N. Leis, Eds., Philadelphia, 1988, pp. 1163-1180.
4. Ohtani, R. and Kitamura, T., "Characterization of High Temperature Strength of Metals Based on the Mechanics of Crack Propagation," Current Japanese Materials Research, Vol. 3, Elsevier, New York, 1988, pp. 65-90.
5. Dowling, N.E. and Begley, J.A., in Mechanics of Crack Growth, ASTM STP 590, Philadelphia, 1976, pp. 82-103.
6. Wright, P.K., "Oxidation-Fatigue Interactions in a Single-Crystal Superalloy," in Low Cycle Fatigue, ASTM STP 942, H.D. Solomon, G.R. Halford, L.R. Kaisand, and B.N. Leis, Eds., Philadelphia, 1988, pp. 558-575.
7. Oshida, Y. and Liu, H.W., "Grain Boundary Oxidation and an Analysis of the Effects of Oxidation on Fatigue Crack Nucleation Life," in Low Cycle Fatigue, ASTM STP 942, H.D. Solomon, G.R. Halford, L.R. Kaisand, and B.N. Leis, Eds., Philadelphia, 1988, pp. 1199-1217.
8. Shih, C.F. and Hutchinson, J.W., "Fully Plastic Solution and Large Scale Yielding Estimates for Plane Stress Crack Problems," ASME Journal of Engr. Matls. Technol., Vol. 98, 1976, pp. 289-295.
9. Coffin, L.F., "Overview of Temperature and Environmental Effects on Fatigue of Structural Metals," Fatigue: Environment and Temperature Effects, J.J. Burke and V. Weiss, Eds., Plenum Press, N.Y., 1983, pp. 1-40.
10. Ostergren, W.J., "A Damage Function and Associated Failure Equations for Predicting Hold Time and Frequency Effects in Elevated Temperature Low Cycle Fatigue," Journal of Testing and Evaluation, Vol. 4, 1976, pp. 327-339.

11. Ostergren, W.J. and Krempl, E., "A Uniaxial Damage Accumulation Law for Time-Varying Loading Including Creep-Fatigue Interaction," ASME Journal of Pressure Vessel Technology, Vol. 101, 1979, pp. 118-124.
12. Cook, T.S., Kim, K.S and McKnight, R.L., "Thermal Mechanical Fatigue of Cast Rene 80," ASTM STP 942, H.D. Solomon, G.R. Halford, L.R. Kaisand, and B.N. Leis, Eds., Philadelphia, 1988, pp. 692-708.
13. Rezai-Aria, F., Dambrine, B. and Remy, L., "Thermal Fatigue of MAR-M509 Superalloy-II: Evaluation of Life Prediction Models," Fatigue Fract. Engng. Mater. Struct., Vol. 11, No. 4, 1988, pp. 291-302.
14. Remy, L., "Recent Developments in Thermal Fatigue," Proc. Int. Seminar on the Inelastic Behaviour of Solids Models and Utilisation, MECAMAT, Vol. IV, 1988, pp. 1-19.
15. Remy, L., Rezai-Aria, F., Danzer, R. and Hoffelner, W., "Evaluation of Life Prediction Methods in High Temperature Fatigue," ASTM STP 942, H.D. Solomon, G.R. Halford, L.R. Kaisand, and B.N. Leis, Eds., Philadelphia, 1988, pp. 1115-1132.
16. Halford, G.R. and Saltsman, J.F., "Calculation of Thermomechanical Fatigue Life Based on Isothermal Behavior," NASA TM 88864, 1987.
17. Skelton, R.P., "Application of Small Specimen Crack Growth Data to Engineering Components at High Temperature: A Review," ASTM STP 942, H.D. Solomon, G.R. Halford, L.R. Kaisand, and B.N. Leis, Eds., Philadelphia, 1988, pp. 209-235.
18. Tomkins, B., Creep and Fatigue in High Temperature Alloys, Ed. J. Bressers, Applied Science Publishers, London, 1981, p. 111.
19. Chaboche, J.L., "Continuum Damage Mechanics: Present State and Future Trends," Seminaire International sur l'Approche Locale de la Rupture, Moret-sur-Loing, June 3-5, 1986.
20. Chaboche, J.L. and Lesne, P.M., "A Non-Linear Continuous Fatigue Damage Model," Fatigue Fract. Engng. Mater. Struct., Vol. 11, No. 1, pp. 1-17, 1988.
21. T. Hoside and D. Socie, "Mechanics of Mixed Mode Small Fatigue Crack Growth", Engineering Fracture Mechanics, Vol. 26, No. 6, 1987, pp. 842-850.
22. McClung, R.C. and Sehitoglu, H., "Closure Behavior of Small Cracks Under High Strain Fatigue Histories," ASTM STP 982, 1988, pp. 279-299.
23. McDowell, D.L. and Berard, J.-Y., "A ΔJ-Based Approach to Biaxial Low Cycle Fatigue of Shear Damaging Materials," Third Int. Conf. on Biaxial/Multiaxial Fatigue, Stuttgart, FRG, April 3-6, 1989.

TABLE 1 MAR M 246 COMPLETED 900 C AIR TESTS

E(900)= 145.51 GPA

Specimen I.D.	STRAIN RATE /sec	STRESS AMP (MPA)	TOTAL STRAIN AMP	ELASTIC STRAIN AMP	INELASTIC STRAIN AMP	Nf (cycles)	DELTA t (secs)	ALPHAe (MPA)	ALPHAp (MPA)	ALPHA (MPA)
FULLY REVERSED										
G12	10E-2	1015.25	0.010143	0.006977	0.003166	24	4.06	14.16717	18.1535	32.3207
T010-2		725.06	0.009000	0.004983	0.004017	35	3.60	7.225785	16.4509	23.6767
T001-5		794.62	0.007000	0.005461	0.001539	78	2.80	8.678729	6.907476	15.5862
G5		775.52	0.006387	0.005330	0.001057	118	2.55	8.266528	4.631333	12.8979
T015-1		642.3	0.005000	0.004414	0.000586	374	2.00	5.670391	2.125402	7.7958
G22		529.48	0.003801	0.003639	0.000162	1288	1.52	3.853331	0.485104	4.3384
T010-1		424.12	0.003000	0.002915	0.000085	4000	1.20	2.472377	0.2043	2.6767
G16	10E-3	871.6	0.009824	0.005990	0.003834	18	39.30	10.44171	18.87447	29.3162
S999-1		797.16	0.009000	0.005478	0.003522	30	36.00	8.734301	15.85583	24.5901
T015-3		736.83	0.008000	0.005064	0.002936	38	32.00	7.462284	12.21963	19.6819
G18		717.51	0.007158	0.004931	0.002227	45	28.63	7.076085	9.025049	16.1011
G6		723.34	0.006058	0.004971	0.001087	96	24.23	7.191544	4.440653	11.6322
T015-5		649.44	0.005000	0.004463	0.000537	252	20.00	5.797159	1.96904	7.7662
G7		556.69	0.003968	0.003826	0.000142	583	15.87	4.259553	0.447157	4.7067
T001-4		275.4	0.003000	0.001893	0.001107	7421	12.00	1.042474	1.72246	2.7649
T132-4		619.92	0.007100	0.004260	0.002840	46	28.40	5.282122	9.942734	15.2249
T133-3		586.46	0.005100	0.004030	0.001070	198	20.40	4.727309	3.543001	8.2703
T138-1		536.42	0.004000	0.003686	0.000314	381	16.00	3.955005	0.949881	4.9049
G10	10E-4	746.94	0.009967	0.005133	0.004834	14	398.68	7.668468	20.39253	28.0610
T010-4		775.49	0.009000	0.005329	0.003671	28	360.00	8.265889	16.0771	24.3430
G8		763.79	0.008121	0.005249	0.002872	25	324.84	8.018352	12.38944	20.4078
T011-3		678.64	0.007000	0.004664	0.002336	32	280.00	6.33018	8.954426	15.2846
T016-1		594.14	0.005000	0.004083	0.000917	225	200.00	4.851932	3.076706	7.9286
G4		510.83	0.004024	0.003511	0.000513	374	160.96	3.586658	1.481218	5.0679
T011-2		356.97	0.003000	0.002453	0.000547	1504	120.00	1.751461	1.10239	2.8539
FAST-SLO										
132-2	-2/-4	503.43	0.006900	0.003460	0.003440	32	139.38	3.483496	9.782035	13.2655
T133-4		378.52	0.003000	0.002601	0.000399	274	60.60	1.969313	0.852316	2.8216
SLO-FAST										
T133-1		543.66	0.007000	0.003736	0.003264	24	141.40	4.062486	10.02184	14.0843
T133-5	-4/-2	341.72	0.002950	0.002348	0.000602	319	59.59	1.605011	1.16107	2.7661
TENSILE HOLD TIME TESTS										
10 second hold										
T132-3	10E-4	440	0.005	0.003024	0.001976	228	210	2.660985	4.911056	7.5720
1000 second hold										
T138-2	10E-4	346.25	0.005	0.002380	0.002620	29	1200	1.647846	5.124664	6.7725

TABLE 2 MAR M 246 COMPLETED 650 C AIR TESTS

E(650)= 171 GPA

Specimen I.D.	STRAIN RATE /sec	STRESS AMP (MPA)	TOTAL STRAIN AMP	ELASTIC STRAIN AMP	INELASTIC STRAIN AMP	Nf (cycles)	DELTA t (secs)	ALPHAe (MPA)	ALPHAp (MPA)	ALPHA (MPA)
FULLY REVERSED										
T138-4	10E-2	527.16	0.002950	0.003083	0.00000	5623	1.18	3.250265	0	3.2503
T138-3		854.37	0.006000	0.004996	0.001004	122	2.40	8.537405	4.933959	13.4714
T139-2		1048.21	0.009434	0.006130	0.003304	14	3.77	12.85081	19.92765	32.7785
T139-4		1053.94	0.010148	0.006163	0.003985	12	4.06	12.99169	24.16317	37.1549
T139-1	10E-4	535.28	0.003000	0.003130	0.00000	9167	120.00	3.351166	0	3.3512
T138-5		867.96	0.006000	0.005076	0.000924	162	240.00	8.811164	4.615546	13.4267
T139-5		1051.92	0.010000	0.006152	0.003848	35	400.00	12.94194	23.29259	36.2345
T580-1		1098	0.0071	0.006421	0.000679	37	280	14.10063	4.289344	18.3900
T563-2		843.7	0.004965	0.004934	0.000031	237	200	8.325493	0.150886	8.4764

FATIGUE LIFE

MAR M 246 900°C/650°C AIR

FULLY REVERSED

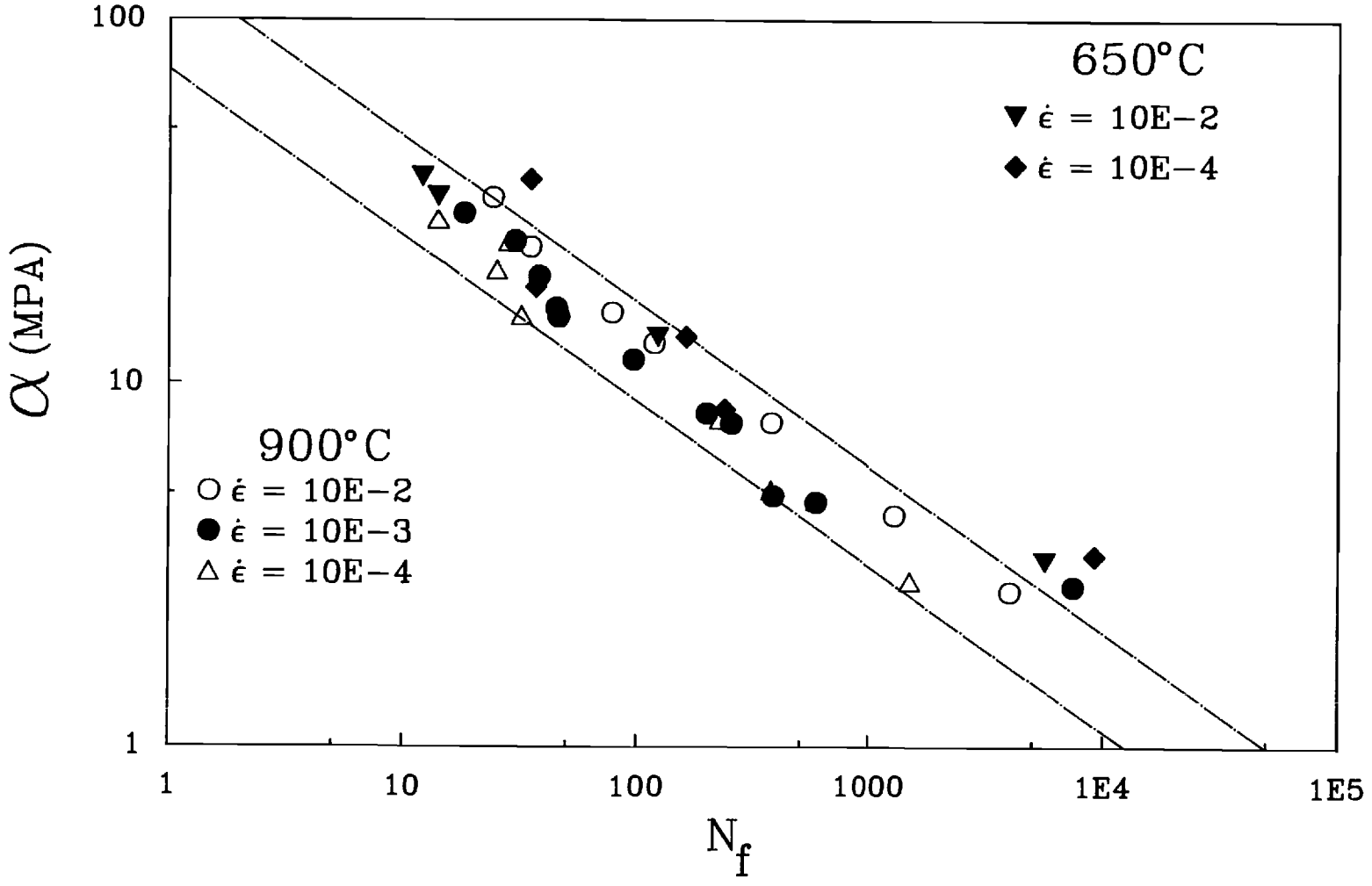

Figure 1

APPENDIX A

in HIGH TEMPERATURE CREEP-FATIGUE
Eds, Ryuichi Ohtani, Masateru Ohnami
and Tatsuo Inoue
Current Japanese Materials Research, Vol. 3
Elsevier Applied Science, 1988

Characterization of High Temperature Strength of Metals Based on the Mechanics of Crack Propagation

RYUICHI OHTANI and TAKAYUKI KITAMURA
Department of Engineering Science, Faculty of Engineering, Kyoto University, Yoshida, Sakyo-ku, Kyoto 606, Japan

ABSTRACT

Metallic materials show different types of strength behavior according to the operating conditions of stress, temperature and time, and certain typical types of behavior are usually distinguished and designated as different phenomena. The crack propagation behavior of such phenomena was investigated on the basis of fracture mechanics. The results are summarized and the characterization of high temperature strength is given in this paper. The crack propagation at high temperatures is clearly divided into two types: time dependent and cycle dependent. The crack propagation rate is correlated well with the creep J-integral range for the former and with the fatigue J-integral range for the latter. The boundary between the two types is given as a function of the J-integral ranges. Moreover, the fatigue life laws of a smooth specimen at high temperatures can be derived from the crack propagation laws, because the small cracks initiate at a very early stage of the life and the failure is subject to their propagation. A similar characterization to that for the crack propagation can be expected for the life laws of a smooth specimen.

INTRODUCTION

The strength of metallic materials at high temperatures has been phenomenally labeled as monotonic creep, dynamic creep, cyclic creep, tensile strength, low cycle fatigue, high cycle fatigue, thermal fatigue etc., according to the conditions of stress or strain cycle, temperature and time. Not only their characteristics but also the differences between them, however, are still vague. The complexity mainly originates from creep, which has a time effect on the other strengths. The effects of the environment and the microstructural change in materials, which have

other time dependences, are not referred to in this chapter. Figure 1 schematically illustrates the effects of stress cycle, cycle frequency, temperature and creep on the strength phenomena in three-dimensional coordinates of mean stress, stress amplitude and temperature. A brief outline of the phenomena is given as follows.

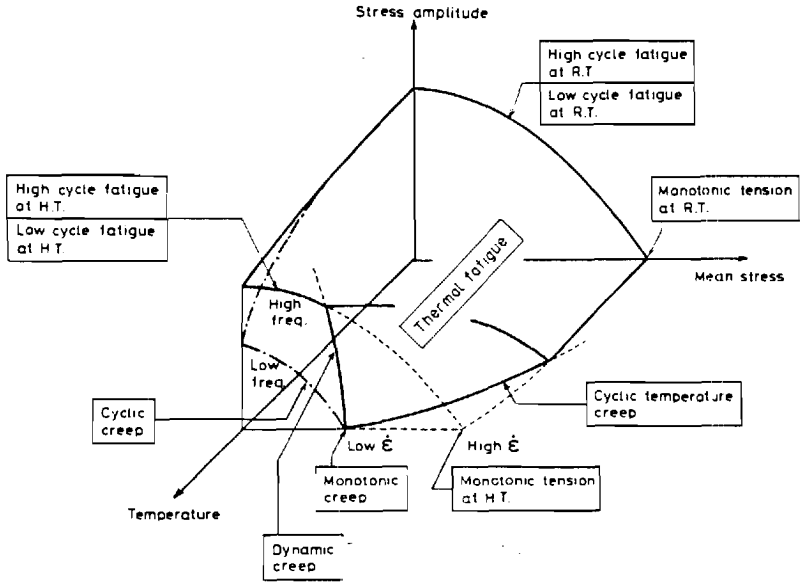

FIG. 1. Schematic diagram explaining the classification of high temperature strength on the basis of temperature, mean stress and stress amplitude.

The monotonic deformation is usually divided into two types, namely 'tensile deformation' and 'creep deformation', and the difference is their time dependence. Let us assume an ideal tensile deformation being purely time independent, which is expected to take place when the strain rate is fast enough to avoid the creep effect even at high temperatures. On the other hand, the creep deformation is defined as purely time dependent under a low strain rate. The usual tensile tests, however, are conducted at a medium strain rate and the test results are midway between ideal tension and creep.

Creep with a stress change is classified into 'dynamic creep' and 'cyclic creep' according to the stress waveform. The former means creep

under a high frequency vibration stress of a rather small amplitude superposed on a high mean stress. The latter is creep under a low frequency periodical change of stress. The typical stress waveforms are shown in Fig. 2. In some cases, the stress change drastically accelerates the creep rate and the crack propagation rate, leading to shortening of the creep life.

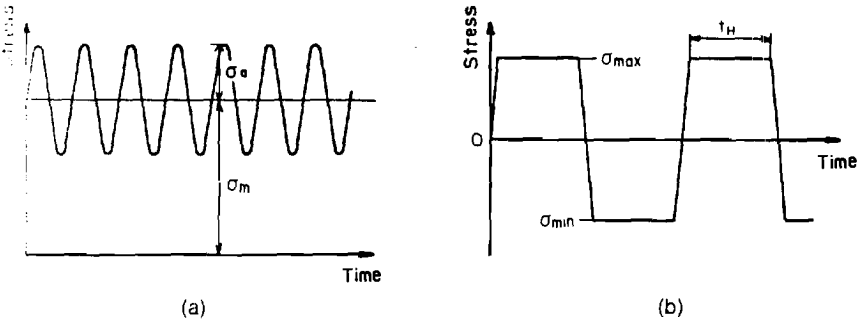

FIG. 2. Stress waveforms for dynamic creep and cyclic creep: (a) dynamic creep; (b) cyclic creep.

'Isothermal fatigue' is often divided into 'high cycle fatigue' and 'low cycle fatigue', for which the difference is originally defined on the basis of the number of cycles to fatigue failure. The definition, however, has no physical meaning. It is rather logical to separate them into elastic fatigue and elastic–plastic fatigue, or small-scale yielding fatigue and large-scale yielding fatigue, because linear fracture mechanics is applicable to the former but not to the latter. For high temperature fatigue, the creep effect is the most important problem, and will be discussed in detail in this chapter.

The temperature effect couples closely with the creep effect as the creep phenomenon is a thermally activated process. The fatigue strength at low temperatures (e.g. at room temperature), therefore, can be expressed by only one curve on the stress amplitude versus mean stress plane in Fig. 1, while that at high temperatures has to be given by many different curves for different stress frequencies and waveforms.

'Thermal fatigue' sometimes means the fatigue under a pure thermal stress cycle, and it is called 'thermal–mechanical fatigue' for fatigue under the combination of thermal stress and mechanical stress cycles. In a wide sense, however, 'thermal fatigue' includes all fatigue

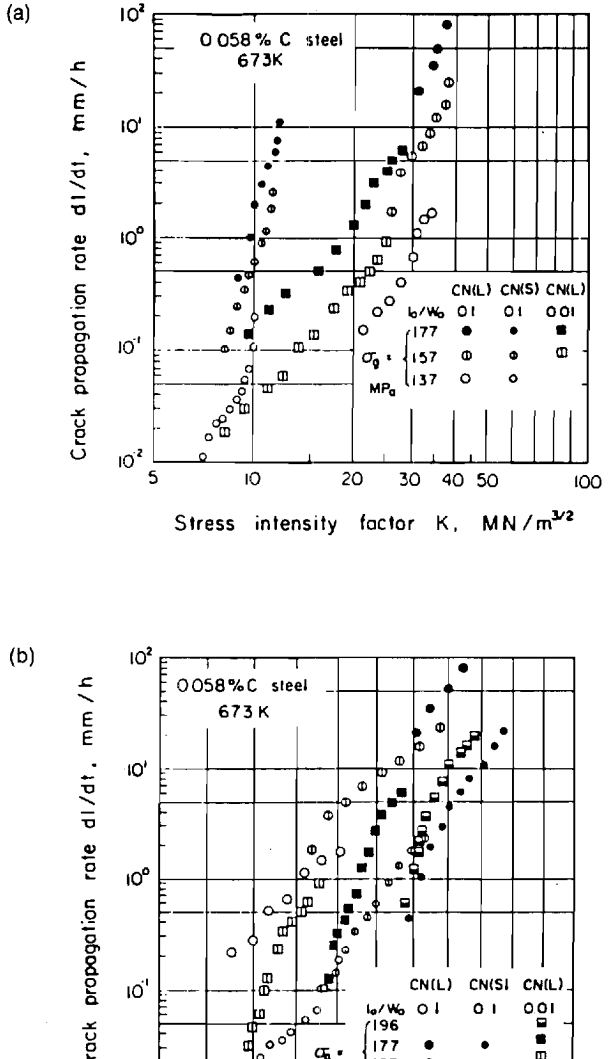

FIG. 3. Relationships between the crack propagation rate dl/dt and the fracture mechanics parameters in monotonic creep: (a) dl/dt versus K relationship; (b) dl/dt versus σ_{net} relationship.

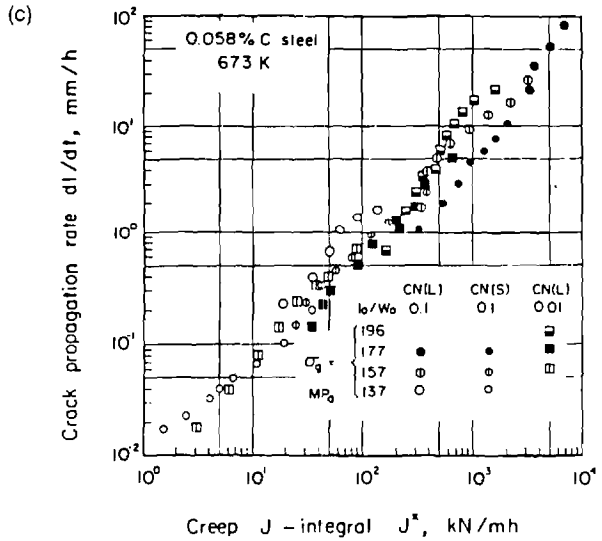

FIG. 3. — *contd.* (c) d*l*/d*t* versus J^* relationship.

phenomena under cyclic temperature conditions. Creep or fatigue subjected to both cyclic stress and cyclic temperature, therefore, can be placed in the category of thermal fatigue.

The crack propagation behavior under creep and fatigue conditions has been studied by the authors, and the crack propagation laws for each strength phenomenon have been clarified [1–22]. In this chapter the results are reviewed and summarized in order to characterize the phenomena and to give an overall view of high temperature strength, especially on creep and fatigue and their interaction.

CRACK PROPAGATION UNDER MONOTONIC CREEP

The fracture mechanics parameters usually used for crack propagation under monotonic creep are the elastic stress intensity factor K, the net section stress σ_{net} and the creep J-integral J^* (modified J-integral [23], C^*-parameter [24–26]). Figure 3 shows the relationships between the crack propagation d*l*/d*t* and these parameters in a thin plate specimen of 0·058% carbon steel tested at 673 K (400 °C) [4, 7]. Here, the initial plate widths $2W_0$ of the specimens of type CN(L) and CN(S) are 160 mm and 16 mm, respectively, and l_0 is the initial half

crack length. J^* is evaluated from the following equation proposed by Ohji *et al.* [27]:

$$J^* = \frac{n-1}{n+1}\sigma_{net}\dot{V}_c \tag{1}$$

where n is the stress exponent of the power law creep and $\dot{V}_c$ is the crack center opening displacement rate. The dl/dt–K and the dl/dt–σ_{net} relationships are strongly dependent on the specimen width, but the dl/dt–J^* relationship is independent of it. The results prove the validity of the creep J-integral as the controlling parameter of the creep crack propagation rate. The relationship is formulated as

$$dl/dt = C_c J^{*m_c} \tag{2}$$

where C_c and m_c are the material constants.

Figure 4 shows the dl/dt–J^* relationship in monotonic creep of metals, obtained up to now by the group of the authors [1, 14]. It reveals that the difference in the dl/dt–J^* relationship between the materials is small and that m_c is nearly equal to unity for all materials. The authors have already studied and reported elsewhere the effect of various factors on the creep crack propagation such as the environment [1], temperature [1], biaxial stress [6], fracture mode [1], pre-creep strain [1] and others [10].

CRACK PROPAGATION DURING STRESS RELAXATION

The creep J-integral J^* in a creeping body is analogous to the J-integral J in a linear or nonlinear elastic body. The creep J-integral is defined as the path-independent line integral converting the strain and the displacement in the J-integral equation into the strain rate and the displacement rate, respectively [23, 24]. Because the J-integral J can be defined even in an unloading condition for an elastic body (although it cannot for a plastic body), the creep J-integral J^* can be expected to be valid in a decreasing load condition, so long as the constitutive relationship of stress and strain rate can be expressed by the following type of equation at any moment:

$$\dot{\varepsilon} = f(t)g(\sigma) \tag{3}$$

where $f(t)$ and $g(\sigma)$ are functions of time and stress.

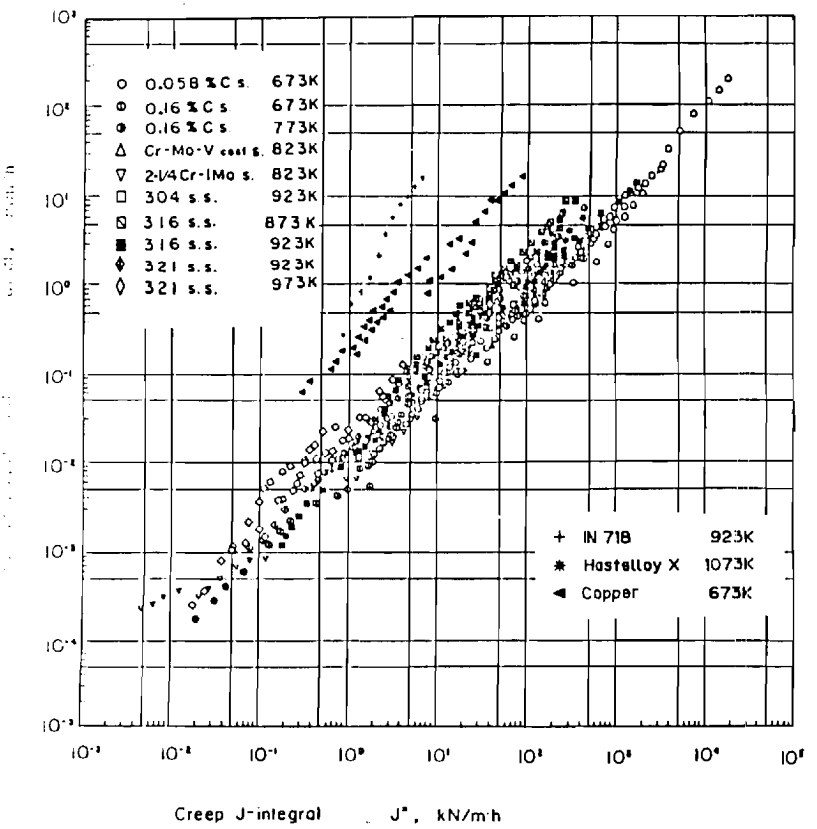

FIG. 4. Relationship between dl/dt and J^* in monotonic creep for several kinds of metallic materials.

The authors conducted creep crack propagation tests under stress relaxation conditions to verify the J^*-integral approach in the strain hold period of low cycle fatigue [21]. Figure 5 shows the typical results, indicating that the same straight-line relationship can be obtained even when the crack propagation rate decreases with the decrease in magnitude of J^* by the stress relaxation.

CRACK PROPAGATION UNDER DYNAMIC CREEP

Figure 6 shows the dependence of the crack propagation rate dl/dt on the stress frequency ν and the stress ratio R in the dynamic creep of a

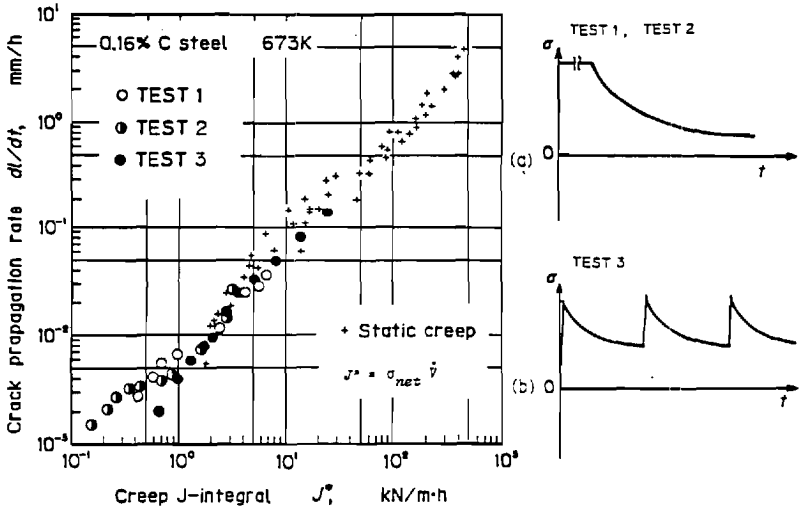

FIG. 5. Relationship between the crack propagation rate dl/dt and creep J-integral J^* in stress relaxation.

type 304 stainless steel tested at 923 K (650 °C) [9]. It becomes clear from the figure that dl/dt depends little on the frequency and increases as the equivalent stress σ_e increases. Here, σ_e is defined as the time-averaged stress in a cycle and is calculated by [28]

$$\sigma_e = \sigma_m \left[\int_0^1 \left\{ 1 + \frac{\sigma_a}{\sigma_m} \sin(2\pi\nu t) \right\}^n \mathrm{d}(\nu t) \right]^{1/n} \tag{4}$$

where ν is the frequency, σ_a is the stress amplitude and σ_m is the mean stress.

Figure 7 shows the relationship between dl/dt and J^* of the above tests except for $R = -0{\cdot}50$. dl/dt has a fairly good correlation with J^* and the relation corresponds to that of monotonic creep. Moreover, intergranular facets were observed on the fracture surface except for $R = -0{\cdot}50$. This result also indicates that the crack propagated by creep.

Striations, which suggest fatigue crack propagation, were observed on the fracture surface for $R = -0{\cdot}50$, so that the mutual relationship between dynamic creep and fatigue comes into this problem. This will be discussed later in detail.

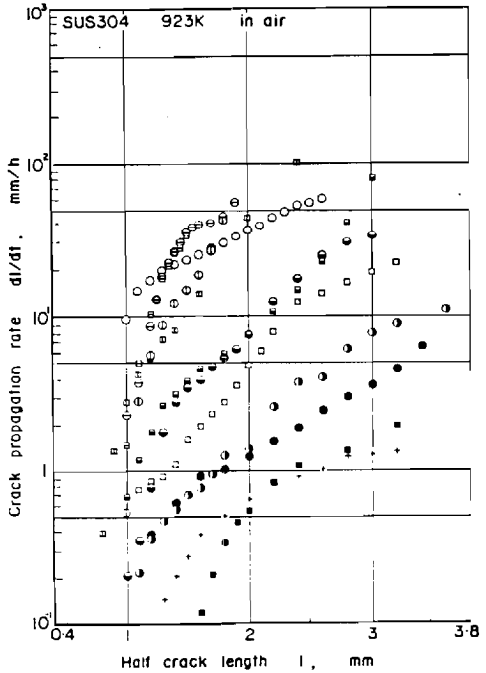

	Stress ratio $R = \sigma_{min}/\sigma_{max}$	*Mean stress* σ_m *(MPa)*	*Stress amplitude* a_a *(MPa)*	*Frequency* ν *(Hz)*	*Symbol in figures*
Static creep	1	137·2	0		+
Dynamic creep	0·87	137·2	9·8	5 0·5	● ■
	0·75	137·2	19·6	5	◑
	0·50	137·2	45·7	5 0·5	◒ ◧
	0·33	137·2	68·6	5 0·5	◍ ⊞
	0	102·9	120·9	5 0·5	⊖ ⊟
	−0·50	44·1	132·3	3 0·3	○ □

FIG. 6. Dependence of the crack propagation rate on the frequency and stress ratio in dynamic creep.

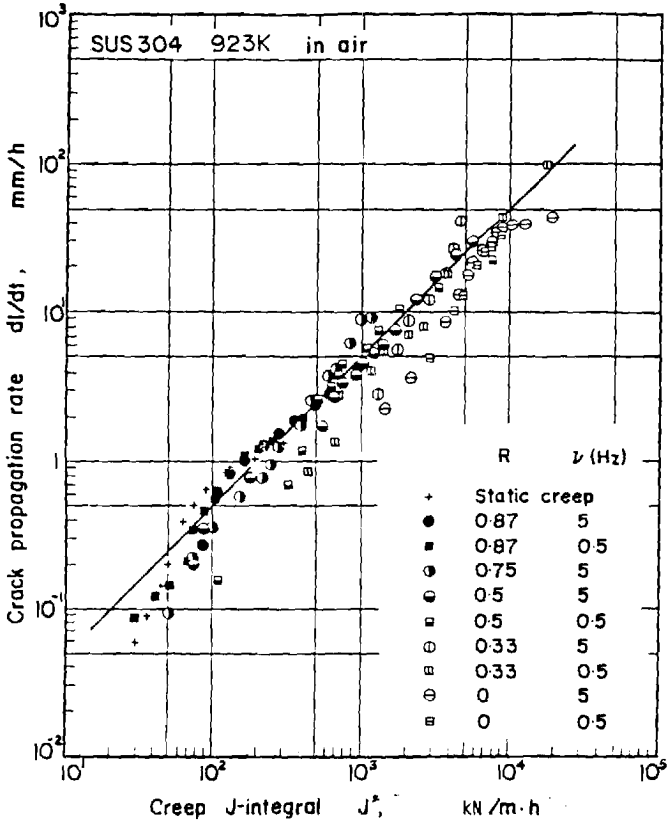

FIG. 7. Relationship between the crack propagation rate dl/dt and the creep J-integral J^*.

CRACK PROPAGATION UNDER CYCLIC CREEP

Figure 8 shows the crack propagation rate in cyclic creep of 0·16% carbon steel tested at 673 K (400 °C) using a trapezoidal stress waveform (Fig. 2(b)) with a 1 min stress hold time [5, 7]. As the stress ratio R decreases, the crack propagation rate increases markedly. The creep rate near the crack tip $\dot{\varepsilon}_{ct}$ during the tension period was measured simultaneously by the elongation of a nickel grid, whose pitch was 50 μm and was secured on the specimen surface by baking before the tests. The crack tip creep rate $\dot{\varepsilon}_{ct}$ was also accelerated in the lower stress ratio tests as shown in Fig. 9, this acceleration of creep rate being caused by dynamic recovery during the compression period†. J^* is the

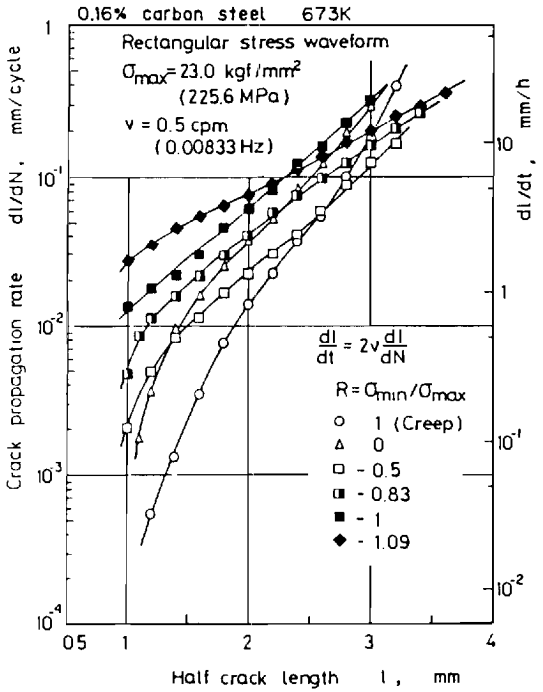

FIG. 8. Dependence of the crack propagation rate on the stress ratio in cyclic creep.

parameter which represents the intensity of creep rate in the vicinity of the crack tip and can describe the acceleration of $\dot{\varepsilon}_{ct}$ caused by the dynamic recovery and/or the small-scale creep. Therefore, dl/dt has a good correlation with J^* for cyclic creep as shown in Fig. 10.

Carrying through the time integral of Eqn. (2) during a cycle [3],

$$dl/dN = C_c \Delta J_c \tag{5}$$

$$\Delta J_c = \int J^* \, dt \tag{6}$$

are obtained for $m_c = 1$ in Eqn. (2). Here, dl/dN is the crack propagation

Another acceleration mechanism in cyclic creep is small-scale creep [29, 30], which is the phenomenon whereby the creep strain grows preferentially near the crack tip due to the constraint of the surrounding elastic strain field. This becomes a serious problem with high strength materials and under low stress conditions [12, 13]. The effect, however, is small enough in this case [17].

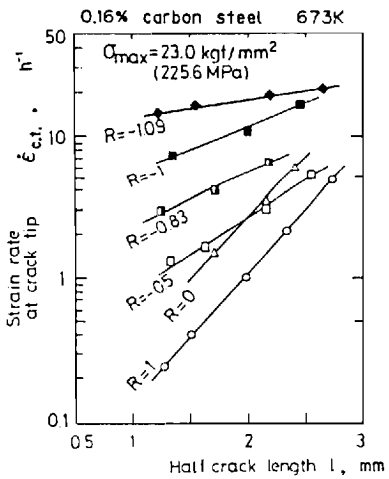

FIG. 9. Strain rate near the crack tip in cyclic creep.

rate (the crack propagation per unit cycle) and ΔJ_c is the time integral of J^* (named the creep J-integral range). The expression is sometimes more convenient for creep crack propagation under cyclic stress conditions. The value of ΔJ_c was simply evaluated by a load versus crack center opening displacement (P-V) loop as shown in Fig. 11(a), which was derived from the integral of Eqn. (1) [3, 8]. Supposing that the inelastic strain is composed of the creep (time-dependent) strain and the plastic (time-independent) strain, the method can be extended for the general stress (or strain) waveforms as illustrated in Fig. 11(b) [3, 8]. In this method, the inelastic strain can be partitioned in a similar way to the strain partitioning method (rapid straining method) [31, 32].

The authors conducted strain-controlled tests using a triangular strain waveform with low frequency and verified the validity of ΔJ_c. As a result, ΔJ_c was a reasonable parameter for dl/dN independently of the stress (or strain) waveform when the crack propagated by creep. Figure 12 shows the dl/dN–ΔJ_c relationships of several kinds of steels and alloys under various stress and temperature conditions [14].

CRACK PROPAGATION UNDER HIGH CYCLE FATIGUE

Figure 13 shows the relationship between dl/dN and the stress intensity factor range ΔK for 0·16% carbon steel tested at 673 K (400 °C) in high frequency (1–3 Hz) fatigue with a stress ratio of −1. The dotted

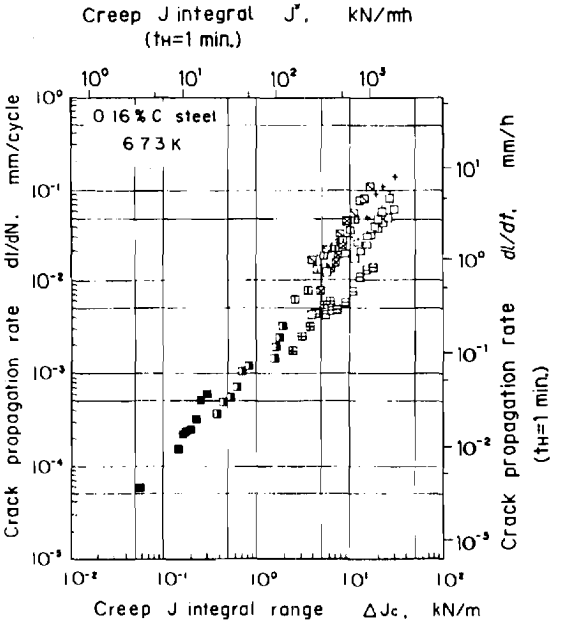

σ_{max} (*MPa*)	*R*	t_H (*min*)	*Symbol*
226	1	—	+
226	0	1	⊡
226	−1	1	□
206	−1	5	⊠
206	−1	1	⊟
206	−1	2/3	⊠
186	−1	1	⊟
167	−1	1	⊞
127	−1	1	◨
98	−1	1	■

FIG. 10. Relationship between d*l*/d*t* and *J** in cyclic creep.

line shows the relationship between d*l*/d*N* and the effective stress intensity factor range ΔK_{eff} which is defined as the difference between the maximum and the crack tip opening stress intensity factors. The figure reveals the existence of the crack propagation threshold in fatigue and good correlations under the lower stress conditions. The propagation curves have a strong resemblance to those for room temperature fatigue. Moreover, striations, which suggest that the crack propagated owing to

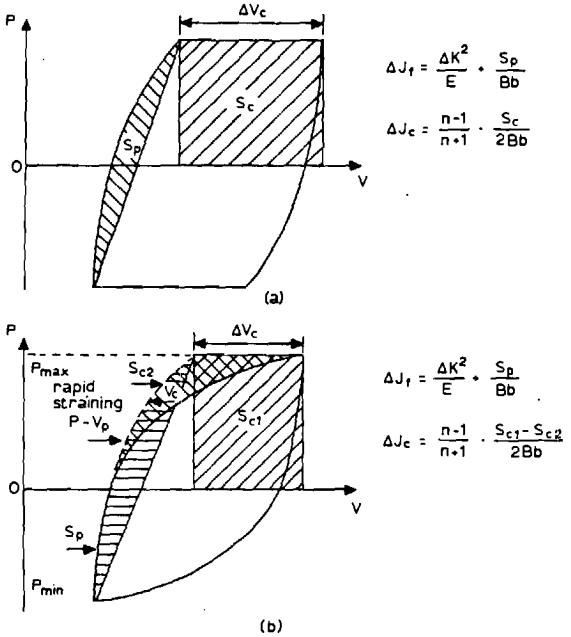

FIG. 11. Evaluation method for ΔJ_f and ΔJ_c on the basis of the load and crack center opening displacement: (a) trapezoidal stress waveform; (b) general stress waveform.

blunting and resharpening of the crack tip in each cycle, were observed on the fracture surface. It should be noted that the crack propagation was cycle-dependent and completely different from the creep (time-dependent) type. The confusion between these types has often created the misunderstandings of high temperature creep–fatigue strength. In this chapter, the cycle-dependent and the time-dependent phenomena are strictly distinguished from each other and are called fatigue and creep (in a wide sense), respectively. The fast crack propagation rate in the higher stress condition for an equal ΔK or ΔK_{eff} is due to the large-scale plasticity. Therefore, this should belong to the category of low cycle fatigue.

CRACK PROPAGATION UNDER LOW CYCLE FATIGUE

The fatigue J-integral range (cyclic J-integral) ΔJ_f was proposed by Dowling as a controlling parameter for dl/dN not only in high cycle

fatigue (elastic fatigue) but also in low cycle fatigue (elastic-plastic fatigue) at room temperature [33, 34]. Figure 14 shows the relationship between dl/dN and ΔJ_f of the tests shown in Fig. 13. The fatigue J-integral range is also valid in high temperature fatigue. The relationship is formulated as

$$dl/dN = C_f \Delta J_f^{m_f} \quad (7)$$

The validity of ΔJ_f, however, becomes questionable under the lower frequency and/or higher mean stress condition, because the creep effect is marked. The interaction between creep and fatigue becomes the most important problem under such conditions, and is discussed in the following section.

Figure 15 shows the dl/dN–ΔJ_f relationship for metals in the cycle-dependent fatigue condition obtained by the authors and their co-workers [14].

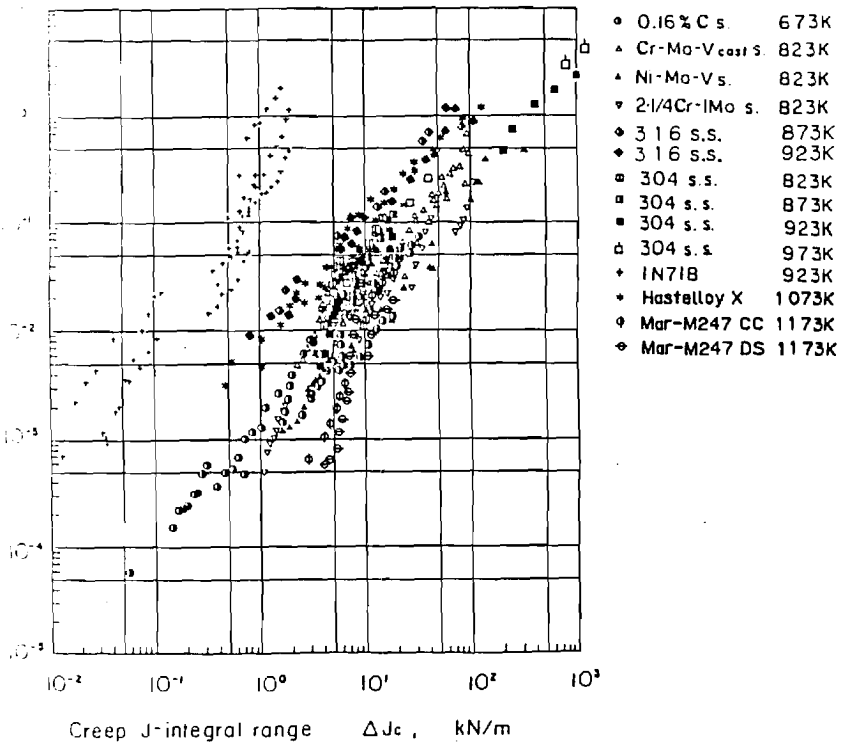

FIG. 12. Relationship between dl/dN and ΔJ_c in creep with a cyclic stress change.

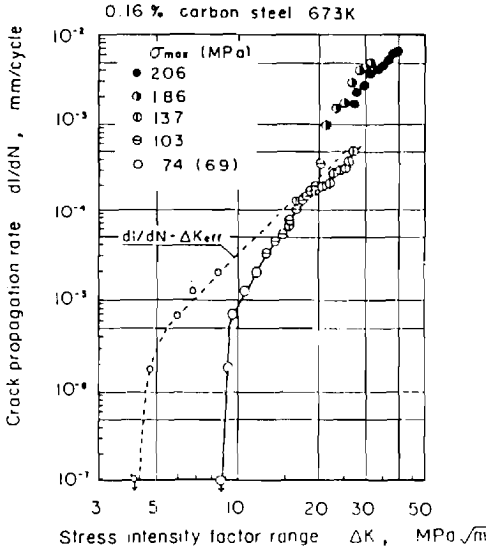

FIG. 13. Relationship between the crack propagation rate dl/dN and the stress intensity factor range ΔK in fatigue. The dashed line shows dl/dN as a function of the effective stress intensity factor range ΔK_{eff}.

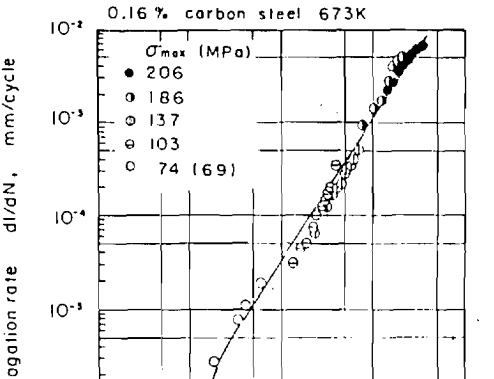

FIG. 14. Relationship between the crack propagation rate dl/dN and the fatigue J-integral range ΔJ_{f} in the fatigue of 0·16% carbon steel.

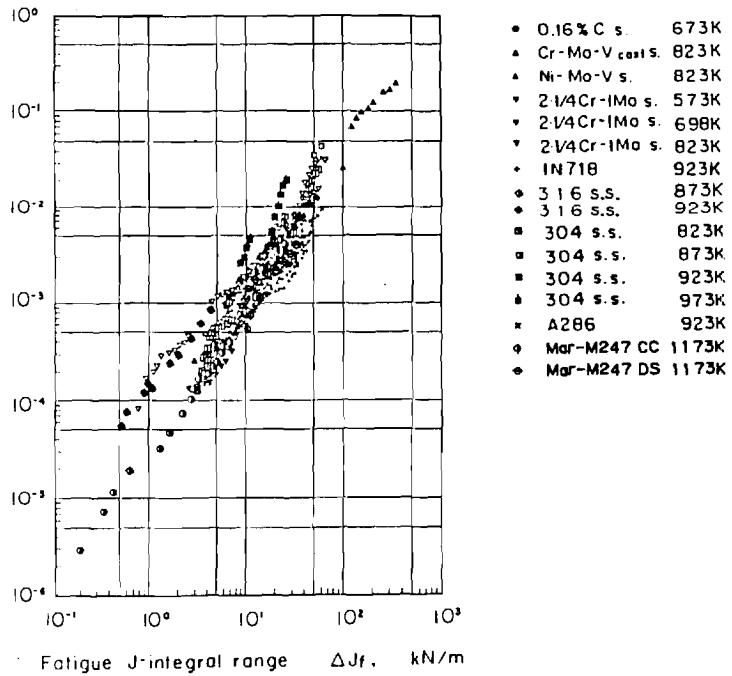

FIG. 15. Relationship between dl/dN and ΔJ_f in the fatigue of metallic materials.

CRACK PROPAGATION UNDER THERMAL FATIGUE

The crack propagation rate dl/dt of creep shows a strong dependence on the temperature, and its activation energy is almost equal to that of creep deformation [16]. The creep J-integral J^*, which is directly related to the crack tip creep rate, has also almost the same activation energy [16]. As a result, the dl/dt–J^* relationship hardly depends on temperature. In addition, dl/dN as well as ΔJ_f are almost independent of temperature in fatigue. The independence of the dl/dt–J^* and the dl/dN–ΔJ_f relationships from the temperature suggests the applicability of the crack propagation laws (Eqns. (5) and (7)) to thermal fatigue.

In order to simulate the crack propagation of thermal fatigue, crack propagation tests were carried out using a tubular specimen of 0·16% carbon steel under the specific stress–temperature conditions shown in Fig. 16 [22]. The creep effect was stronger than the fatigue effect in tests I1, I2, O3 and O4, and vice versa in tests O1 and O2, which can be judged

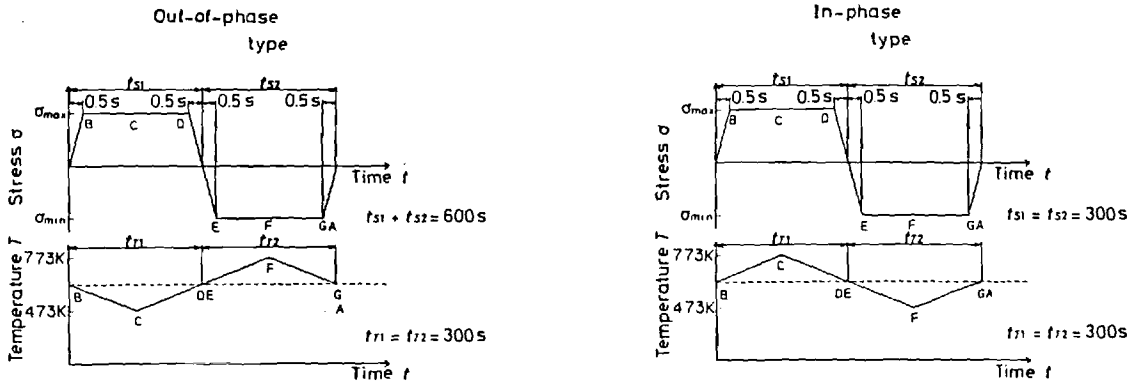

Test no.	*Type*	*Maximum stress (MPa)*	*Stress ratio*	t_{s1} *(s)*	t_{s2} *(s)*	$T_{up} = T_{down}$ *(K)*	*Symbol*
O1	Out of phase	211	−0·58	100	500	523	▲
O2	Out of phase	211	−0·58	200	400	573	◭
O3	Out of phase	206	−0·62	300	300	623	◬
O4	Out of phase	206	−0·62	500	100	723	△
I1	In phase	147	−1	300	300	623	▽
I2	In phase	176	−1	300	300	623	▼

$T_{max} = 773$ K; $T_{min} = 473$ K; $t_{T1} = t_{T2} = 300$ s.

FIG. 16. Stress and temperature waveforms for thermal fatigue simulation tests.

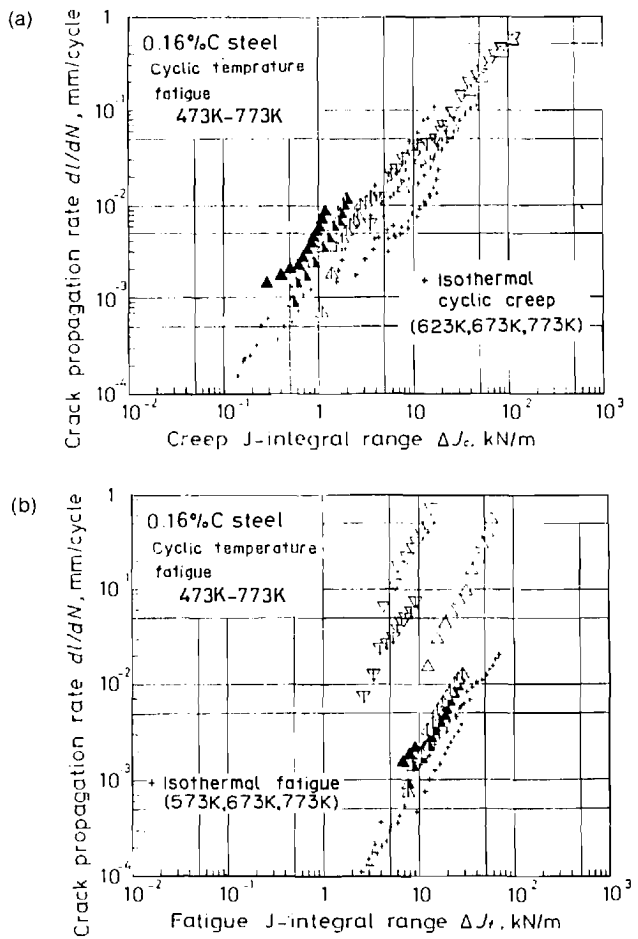

FIG. 17. Relationships between the crack propagation rate and J-integrals of 16% C steel cyclic temperature fatigue 473–773 K): (a) dl/dN versus ΔJ_c relationship; (b) dl/dN versus ΔJ_f relationship.

from the boundary equation between creep and fatigue (Eqn. (8)), described in the next section. Figure 17 shows the dl/dN–ΔJ_c relationship and the dl/dN–ΔJ_f relationship, the symbol + representing the results of isothermal cyclic creep and fatigue. dl/dN correlates with ΔJ_c in the former group and with ΔJ_f in the latter. Moreover, it signifies that the crack propagation of thermal fatigue obeys the same fracture mechanics laws as that of isothermal creep and fatigue.

FIG. 16. Stress and temperature waveforms for thermal fatigue simulation tests.

CRACK PROPAGATION LAWS AT HIGH TEMPERATURE

Crack propagation at high temperature is mainly classified into two types which are time dependent (creep) and cycle dependent (fatigue). The crack propagation laws are formulated as Eqns. (5) and (7). In order to clarify the interaction and the boundary between creep and fatigue, crack propagation tests on a 1Cr-1Mo-$\frac{1}{4}$V steel were carried out at 823 K (550 °C) using a trapezoidal stress waveform (Fig. 2(b)) with various stress hold times from 1 s to 1 h, and a sinusoidal stress waveform with a frequency of 1 Hz [19]. The crack propagation rate dl/dN was plotted against ΔJ_c under the constant ΔJ_f (= 10 kN m^{-1}) condition shown in Fig. 18. This expression gives dl/dN as constant for $\Delta J_c < 1$ kN m^{-1} in fatigue and as proportional to ΔJ_c for $\Delta J_c > 1$ kN m^{-1} in creep. It is obvious from Fig. 18 that the behavior is clearly divided into the two regions of creep and fatigue. The boundary is formulated from Eqns. (5) and (7) as [19]

$$\Delta J_c = \frac{C_f}{C_c} \Delta J_f^{m_f} \tag{8}$$

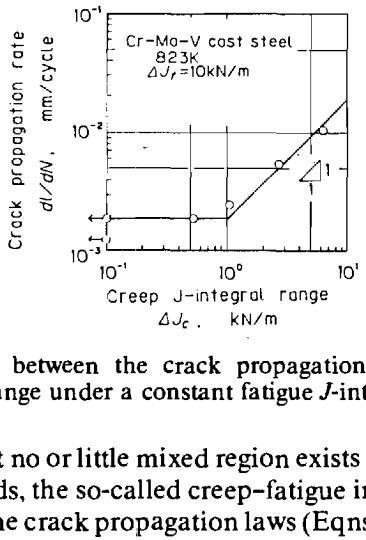

FIG. 18. Relationship between the crack propagation rate and the creep J-integral range under a constant fatigue J-integral range.

It is noteworthy that no or little mixed region exists between fatigue and creep. In other words, the so-called creep-fatigue interaction has no or little influence on the crack propagation laws (Eqns. (5) and (7)). It does not mean, however, that the dl/dN-$1/\nu$ (where ν is frequency) relationship for a given crack length is clearly divided into two regions where dl/dN is constant and proportional to $1/\nu$, because the values of ΔJ_f and ΔJ_c are strongly affected by the interaction between the creep deformation and elastic-plastic deformation. In fact, an intermediate

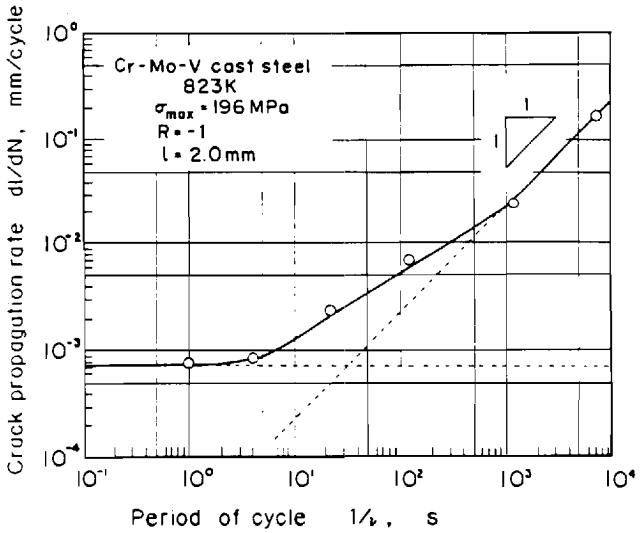

FIG. 19. Relationship between the crack propagation rate dl/dN and the cyclic period $1/\nu$.

region appears at the intermediate frequency of those tests as shown in Fig. 19 [19]. One of the typical interactions between them is the acceleration of creep rate caused by dynamic recovery during the previous compression period, the compression deformation markedly changing the creep constitutive equation of the following tension period. For example, the effect appears as the stress ratio effect of cyclic creep on dl/dt and $\dot{\varepsilon}_{ct}$ shown in Figs. 8 and 9. Again, attention should be paid to the fact that it has no effect on the dl/dt–J^* relationship shown in Fig. 10. The meaning of the difference between Figs. 18 and 19 can be similarly understood.

It is concluded that the deformation resistance (or the values of the two kinds of J-integrals) is strongly affected by creep–fatigue interaction, but the effect on the crack propagation resistance (or the fracture mechanics laws) is quite small. The characterization of high temperature strength is schematically summarized in Fig. 20.

LIFE LAWS FOR A SMOOTH SPECIMEN

At high temperatures, some small cracks often initiate on the surface of a smooth specimen at a very early stage of the fatigue life and bring

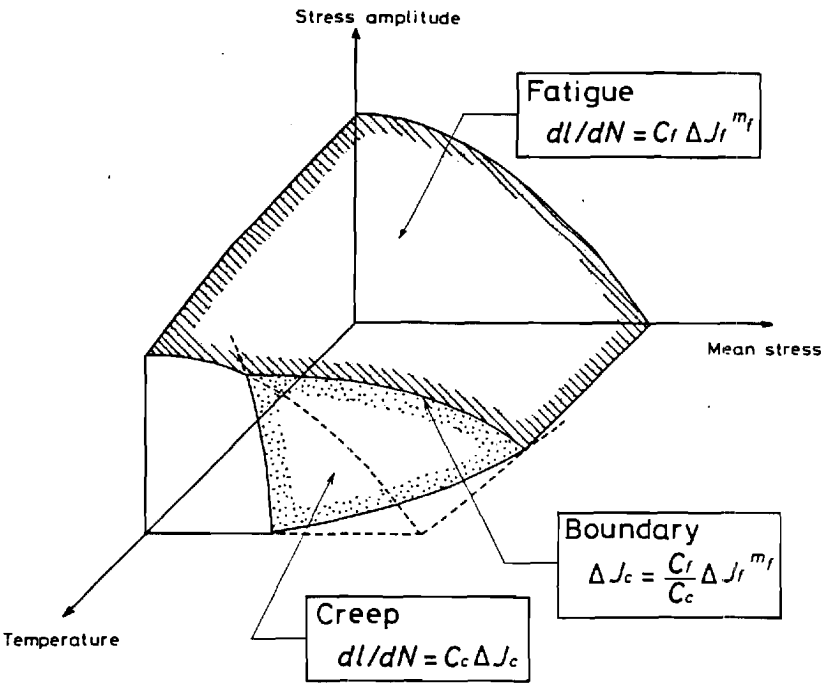

FIG. 20. Characterization of high temperature strength on the basis of the crack propagation laws.

about failure [35, 36]. In such a case, the life laws for the smooth specimen can be derived from the crack propagation laws described in the previous section. Carrying through the integral of Eqns. (5) and (7) from the initial crack length l_0 to the final crack length l_f the following laws are obtained [14, 15 20]:

$$\Delta \tilde{W}_c N_f = D_c \qquad \text{for creep} \tag{9}$$

$$\Delta \tilde{W}_f^{m_f} N_f = D_f \qquad \text{for fatigue} \tag{10}$$

where N_f is the failure and $\Delta \tilde{W}_c$ and $\Delta \tilde{W}_f$ are the strain energy parameters calculated by the following equations:

$$\Delta \tilde{W}_c = \frac{\sigma_{max}}{\Delta\sigma} \frac{\sigma_{max} \Delta\varepsilon_e}{2} + \frac{n+2}{n+3} \frac{n+1}{2\pi} f(n) \frac{\sigma_{max} \Delta\varepsilon_c}{n+1} \tag{11}$$

$$\Delta \tilde{W}_f = \frac{\Delta\sigma \Delta\varepsilon_e}{2} + \frac{n'+1}{2\pi} f(n') \frac{\Delta\sigma \Delta\varepsilon_p}{n'+1} \tag{12}$$

$$f(n) = 3{\cdot}85\sqrt{n}(1 - 1/n) + \pi/n \tag{13}$$

Here, σ_{max} is the maximum stress, $\Delta\sigma$ is the stress range, n and n' are the stress exponents of power law creep and power law plasticity, $\Delta\varepsilon_e$, $\Delta\varepsilon_p$ and $\Delta\varepsilon_c$ are the elastic, plastic and creep strain ranges, respectively, and

$$D_c = \frac{\ln(l_f/l_0)}{C_c \times 2\pi M_J} \tag{14}$$

$$D_f = \frac{l_0^{1-m_f} - l_f^{1-m_f}}{C_f(m_f - 1)(2M_J)^{m_f}} \qquad m_f \neq 1$$

$$D_f = \frac{\ln(l_f/l_0)}{C_f \times 2\pi M_J} \qquad m_f = 1 \tag{15}$$

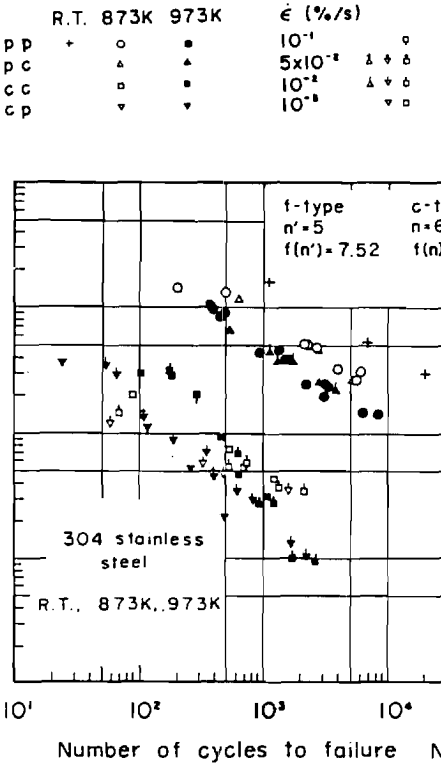

FIG. 21. Relationships between the strain energy parameters and the number of cycles to failure for a smooth specimen.

where M_J is the crack-shape and boundary correction factor. Details of the derivation and the general formulae (including the case of $m_c \neq 1$ in Eqn. (2)) have been reported in the previous paper [15]. The boundary between creep and fatigue is given as [18]

$$\Delta \tilde{W}_c = \frac{D_c}{D_f} \Delta \tilde{W}_f^{m_f} \tag{16}$$

Figure 21 shows the experimental results for a type 304 stainless steel at room temperature, 873 K (660 °C) and 973 K (700 °C) in creep–fatigue tests, using asymmetric and symmetric triangular strain waveforms with various strain rates. Two types of relationships, which are Eqns. (9) (the creep type) and (10) (the fatigue type), can obviously be obtained from Fig. 21. The authors and their co-workers have verified the life laws for 13 kinds of steels and alloys, including low alloy steels, stainless steels and superalloys [14]. Moreover, the life laws have been also confirmed in thermal fatigue for several steels and alloys [14]. This suggests the applicability of characterizing, on the basis of crack propagation laws, by the life laws of a smooth specimen at high temperatures.

CONCLUSION

High temperature strength has been divided into many specific regions according to the stress-cycle, temperature and time conditions. In this chapter they were synthetically characterized on the basis of the crack propagation behavior, with the results illustrated in Fig. 20. The crack propagation behavior at high temperature was mainly classified into the two types of creep and fatigue, which are time dependent and cycle dependent, respectively. It is noteworthy that creep–fatigue interaction had little effect on the crack propagation laws (Eqns. (5) and (7)), but strongly affected the values of the fatigue and creep J-integral ranges. In other words, the interaction in crack propagation is no more than the interaction of creep and elastic–plastic deformation. Therefore, characterization of the deformation behavior becomes one of the most important problems and has been actively studied [37]. Another interesting point for refining the characterization of high temperature strength is to study the mechanisms and mechanics of crack nucleation and small crack growth. Research on these is now under way and a systematic approach is expected in the near future.

REF

REFERENCES

[1] S. Taira, R. Ohtani and T. Kitamura, *Trans. Am. Soc. Mech. Eng., Ser. H,* **101**, 154 (1979).
[2] S. Taira, R. Ohtani and T. Komatsu, *Trans. Am. Soc. Mech. Eng., Ser. H,* **101**, 162 (1979).
[3] S. Taira, R. Ohtani, T. Kitamura and K. Yamada, *J. Mater. Sci., Jpn.,* **28**, 414 (1979).
[4] S. Taira, R. Ohtani, R. Shimizu, T. Kitamura and T. Kashiwagi, *Trans. Jpn. Soc. Mech. Eng.,* **46**, 468 (1980).
[5] S. Taira, R. Ohtani, T. Yonekura, M. Osada and T. Kitamura, *Trans. Jpn. Soc. Mech. Eng.,* **46**, 861 (1980).
[6] S. Taira, R. Ohtani and F. Wada, *Trans. Jpn. Soc. Mech. Eng.,* **46**, 1213 (1980).
[7] R. Ohtani, Creep in structures, *Proc. 3rd IUTAM Symp., Leicester, UK,* Springer, Berlin, 542 (1981).
[8] R. Ohtani, T. Kitamura and K. Yamada, *Proc. USA–Japan Joint Seminar, Hayama,* Nijhoff, 263 (1981).
[9] R. Ohtani, K. Yamada, T. Kashiwagi and H. Matsubara, *Trans. Jpn. Soc. Mech. Eng.,* **A48**, 1378 (1982).
[10] A. Nitta, T. Kitamura and K. Kuwabara, *J. Mater. Sci., Jpn.,* **33**, 185 (1984).
[11] K. Kuwabara, A. Nitta, and T. Kitamura *J. Mater. Sci., Jpn.,* **33**, 338 (1984).
[12] T. Kitamura, A. Nitta, and K. Kuwabara *J. Mater. Sci., Jpn.,* **33**, 585 (1984).
[13] K. Kuwabara, A. Nitta, T. Kitamura and T. Ogata, *ASTM STP 924,* presented at *Int. Symp. on Fundamental Questions and Critical Experiments on Fatigue, Dallas–Fort Worth, TX, 1984,* to be published.
[14] R. Ohtani, T. Kitamura, A. Nitta and K. Kuwabara, *ASTM STP 942,* presented at *Int. Symp. on Low Cycle Fatigue, Sagamore, New York, 1985,* to be published.
[15] R. Ohtani and T. Kitamura, *J. Mater. Sci., Jpn.,* **34**, 843 (1985).
[16] T. Kitamura, *Doctoral thesis,* Kyoto University, (1986).
[17] T. Kitamura, H. Sugihara and R. Ohtani, *J. Mater. Sci., Jpn.,* **35**, 259 (1986).
[18] R. Ohtani and T. Kitamura, *Proc. Int. Conf. on Role of Fracture Mechanics in Modern Technology, Fukuoka, Japan, 1986,* North-Holland, Amsterdam, 353 (1987).
[19] T. Kitamura and R. Ohtani, *Trans. Jpn. Soc. Mech. Eng.,* **52A**, 1816 (1986).
[20] R. Ohtani, T. Kitamura and T. Kinami, *J. Iron Steel Inst. Jpn.,* **72**, 711 (1986).
[21] R. Ohtani, T. Kitamura and S. Enomoto, *Proc. 24th Symp. on High Temperature Strength, Japan,* Society of Materials Science, Kyoto, Japan, 56 (1986).
[22] R. Ohtani, T. Kitamura and N. Tada, *ICM5, Beijing, China,* preprints, **2**, 1101 (1987).
[23] K. Ohji, K. Ogura and S. Kubo, *Trans. Jpn. Soc. Mech. Eng.,* **42**, 350 (1976).
[24] J. D. Landes and J. A. Begley, *ASTM STP 590,* 128 (1976).
[25] K. M. Nikbin, G. A. Webster and C. E. Turner, *ASTM STP 601,* 47 (1976).
[26] M. P. Harper and E. G. Ellison, *J. Strain Analysis,* **12**, 167 (1977).
[27] K. Ohji, K. Ogura and S. Kubo, *Trans. Jpn. Soc. Mech. Eng.,* **44**, 1831, (1978).
[28] R. Koterazawa, *J. Mater. Sci., Jpn.,* **8**, 209 (1959).

[29] K. Ohji, K. Ogura and S. Kubo, *J. Mater. Sci., Jpn.,* **29**, 456 (1980).
[30] H. Riedel and J. R. Rice, *ASTM STP 700,* 112 (1980).
[31] G. R. Halford, M. H. Hirschberg and S. S. Manson, *ASTM STP 520,* 658 (1973).
[32] S. S. Manson, *ASTM STP 520,* 744 (1973).
[33] N. E. Dowling and J. A. Begley, *ASTM STP 590,* 82 (1976).
[34] N. E. Dowling, *ASTM STP 601,* 19 (1976).
[35] S. Usami, Y. Fukuda and S. Shida, *J. Mater. Sci., Jpn.,* **33**, 685 (1984).
[36] R. Ohtani, T. Kinami and H. Sakamoto, *Trans. Jpn. Soc. Mech. Eng.,* **52A**, 1824, (1986).
[37] T. Inoue, *J. Mater. Sci., Jpn.,* **32**, 594 (1983).

APPENDIX B

A ΔJ-BASED APPROACH TO BIAXIAL LOW CYCLE FATIGUE OF SHEAR DAMAGING MATERIALS

David L. McDowell and Jean-Yves Berard*

Georgia Institute of Technology
Atlanta, GA 30332-0405

Third International Conference on Biaxial/Multiaxial Fatigue
April 3-6, 1989 Stuttgart, FRG

INTRODUCTION

A number of approaches have been forwarded over the years regarding correlation of fatigue life under combined stress state conditions. Among these approaches recent studies have focused on so-called critical plane theories which associate the most critically damaged plane with the maximum shear strain amplitude plane which experiences the maximum normal strain [1] and/or normal stress [2-4]. These critical plane theories can evidently be traced back to the high cycle fatigue theories of Gough [5], Findley [6], and others. A review of the historical development may be found in Ref. [7].

In this paper, we focus on microcrack nucleation and Stage I propagation in persistent slip bands aligned with maximum shear strain amplitude planes. This type of cracking is observed in many ductile metals.

In the late 1970s, Brown and Miller postulated the so-called Γ plane approach [1,8-9] wherein the orientation of the maximum shear strain amplitude planes with respect to the specimen surface distinguished two very different types of fatigue regimes. They defined a general relationship between the maximum shear strain amplitude and the normal strain amplitude to the maximum shear strain amplitude plane for a given life as

$$\left[\frac{\Delta\gamma_{max}}{2g}\right]^j + \left[\frac{\Delta\epsilon_n}{2h}\right]^j = f(N_i) \qquad (1)$$

for the case in which the outward normal vectors of the maximum shear strain

---

* In contract with UNIREC, FRANCE

amplitude planes are perpendicular to the specimen surface. Here, $f(N_i)$ denotes a function of number of cycles to crack initiation, N_i. On the other hand, they note that experimental evidence implies that the maximum shear strain is constant for a given life if the maximum shear strain planes intersect the surface at 45° as is the case with tension-tension loading. In this case,

$$\frac{\Delta\gamma_{max}}{2} = f_g(N_i) \tag{2}$$

Hence, a constant $\Delta\gamma_{max}$ is associated with a given life. These two cases are referred to as A and B, respectively. This approach demonstrated the capability of correlating tension-torsion and tension-tension experiments for completely reversed loading. It has been exercised primarily for cases of proportional loading, although it has met with some success in prediction of preferred crack orientation and life for nonproportional loading conditions.

Other proposals have been set forth. Lohr and Ellison [10] proposed that the critical plane is always the plane which intersects the free surface, causing relative extrusions and intrusions which relate to classical low cycle fatigue initiation. In very recent work, Socie and colleagues [2-4,11] have developed several approaches for low cycle fatigue of metals which damage in shear governed fashion. They are careful to distinguish between these materials and others that exhibit predominantly normal stress dependent cracking even under low cycle fatigue conditions.

Socie and Bannantine [3] concluded that a correlation of the form

$$\frac{\Delta\gamma_{max}}{2} + C_1\frac{\Delta\epsilon_n}{2} + C_2\frac{\sigma_{no}}{E} = f_s(N_i) \tag{3}$$

where C_1 and C_2 are constants, E is Young's modulus, $\Delta\epsilon_n/2$ is the normal strain amplitude to the plane of maximum shear strain amplitude $\Delta\gamma_{max}/2$, and σ_{no} is the mean normal stress to this plane. In yet later work, a form which also includes a normal stress effect was proposed by Fatemi and Socie [12] and Fatemi and Kurath [13]. This form may be stated as

$$\frac{\Delta\gamma_{max}}{2}\left[1 + k\frac{\sigma_n^{max}}{\sigma_y}\right] = f_f(N_f) \tag{4}$$

where k is a constant, σ_n^{max} is the maximum normal stress to the plane of maximum shear strain range and σ_y is the yield stress. It is difficult to attribute specific physical meaning to these approaches due to the additive nature of shear and normal strains; however, they appear to enjoy some measure of success by virtue of introducing necessary first-order dependencies into the correlation. Critical plane approaches are specific with regard to the directional character of the normal stress influence, rather than the somewhat vague precedential theories which modify an effective strain or maximum shear strain criteria by the hydrostatic stress [14-15].

Another class of theories which has received significant attention are energy based approaches. Although early forms of these approaches were based on the plastic work in a cycle, more recent forms have included the influence of mean stress [16-18].

In the following section, we will establish a form of correlation for materials in which microcracks propagate in shear-dominated fashion based on the ΔJ-integral. We will proceed to show how such an approach compares with some of those listed above for completely reversed histories on the basis of the convenient Γ plane representation [1].

AN APPROACH MOTIVATED BY ΔJ-INTEGRAL

The ΔJ-integral was first introduced by Dowling and Begley in 1976 [19] as an alternative to ΔK for cases of elastic-plastic fatigue crack growth. It is an extremely useful concept for cases of cracks embedded in a plastic deformation field. Correlation with fatigue crack growth rate under elastic-plastic conditions has been obtained for both short cracks [20-21] and longer cracks based on ΔJ-integral. A closure modification may be applied to ΔJ to enhance accuracy. The ΔJ-integral may be written in form [21]

$$\Delta J = \int_\Gamma \Delta W\, dy - \Delta t_i \frac{\partial \Delta u_i}{\partial x}\, ds \tag{5}$$

where $\Delta W = \int \Delta\sigma_{ij} d\Delta\epsilon_{ij}$ and $\Delta t_i = \Delta\sigma_{ij} n_j$.

In Equation (5), Γ is a contour taken counterclockwise from the lower crack surface to the upper surface and $\Delta\sigma_{ij}$, $\Delta\epsilon_{ij}$ and Δu_i are the stress, strain and displacement ranges for cyclic loading. The traction range Δt_i is determined by the outward unit normal vector n_j to contour Γ. Path-independence of ΔJ requires a unique relationship between $\Delta\sigma_{ij}$ and $\Delta\epsilon_{ij}$, i.e. $\Delta\sigma_{ij} = \partial\Delta W/\partial\Delta\epsilon_{ij}$. Path-independence thus depends on equivalent nonlinear elastic behavior [22] and relies on the assumption of proportional loading as embodied by the deformation theory of plasticity.

For materials which exhibit shear dominated crack initiation, cracks initiate along persistent slip bands aligned with maximum shear strain amplitude orientations. Hence, as seen in Figure 1, the microcracks are embedded in a plastically deformed region which experiences concentrated cyclic plastic shear strains; in addition, there is a normal stress influence on the crack opening. This is obviously a mixed mode crack growth problem. Owing to the nature of persistent slip bands and associated inhomogeneity of plastic deformation, it may be anticipated that continuum plasticity solutions pertaining to the character of Mode I and Mode II contributions to the ΔJ-integrals would be of approximate character.

For short cracks in pure Mode I, Shih and Hutchinson [23] have proposed a J-integral form which exhibits dependence on strain hardening exponent n. Following their work, Hoshide and Socie [24] have proposed the following J-integral form for combined Mode I and Mode II loading:

$$J = \frac{\pi\left(\sigma^2 + \tau^2\right)}{E} a_{eff} + \tilde{J}\left(n, \lambda_\sigma, \eta_\sigma\right) \bar{\sigma}\, \bar{\epsilon}^p a = J_e + J_p \qquad (6)$$

where a and a_{eff} are actual and effective crack lengths and λ_σ and η_σ are stress biaxiality ratios, i.e. $\lambda_\sigma = \tau/\sigma_{yy}$ and $\eta_\sigma = \sigma_{xx}/\sigma_{yy}$ where τ and σ_{yy} are the far field shear and normal stresses, respectively; σ_{xx} is the normal stress parallel to the crack. J_e and J_p are the elastic and plastic components of J, respectively. In general, $\tilde{J}$ is a function derived from numerical calculations which depends on the biaxiality ratios λ_σ and η_σ and strain hardening exponent n. Following the developments in Hoshide et al. [24], one may assume that the crack increment during a cycle can be expressed as a power-law function

of ΔJ (or crack tip opening displacement range) for each mode so we may express the crack increment per cycle in terms of ΔJ and biaxiality factors λ_σ and η_σ for mixed mode loading as

$$\frac{da}{dN} = \phi_I(\lambda_\sigma, \eta_\sigma)\ \Delta J^{M_I} + \phi_{II}(\lambda_\sigma, \eta_\sigma)\Delta J^{M_{II}} \tag{7}$$

Exponents M_I and M_{II} are not, in general, equal. Hoshide and Socie used an analogous formulation with $M_I = M_{II}$ to correlate growth of fatigue cracks of length less than 10^{-3} m in Inconel-718. They correlated the data with a growth law of the form

$$\frac{da}{dN} = C_J\ (\Delta J)^{M_J} \tag{8}$$

where C_j and M_j depend on the biaxiality ratios. However, the variation of M_j was only between 1.31 and 1.45.

In the spirit of Equation (8), after some rearrangement,

$$\frac{da}{dN} = C_p \left[\beta_p(\lambda_\sigma,\ \eta_\sigma)\ \frac{\Delta\sigma_n/2}{\Delta\tau_n/2} + 1\right]^m \left[\frac{\Delta\tau_n}{2}\ \frac{\Delta\gamma_{max}^p}{2}\right]^m a^m \tag{9}$$

where it is assumed that the coefficients C_p and β_p have absorbed the transformation of plastic strain components to the maximum plastic strain amplitude $\Delta\gamma_{max}^p/2$. In Equation (9), $\Delta\sigma_n$ and $\Delta\tau_n$ denote the normal stress range to the maximum shear strain range plane and the maximum shear stress range in this plane, respectively. Note that Equation (9) applies in the limit as the plastic strains dominate the elastic strains, i.e. fully plastic solution.

It should be noted that β_p introduces dependence on biaxiality. Although C_p is actually dependent on the biaxiality ratio as well, we neglect this dependence here. This may be viewed as a microcrack propagation rule when the plastic component of ΔJ dominates the elastic component in magnitude, i.e. low cycle fatigue conditions. Obviously, specification of β_p is not a trivial matter; it may be determined by finite element calculations or by comparison with fatigue data at various biaxiality ratios. The

latter option is selected in this work in view of the uncertainty of numerical continuum solutions for this case. In analogous fashion, for the elastic high cycle fatigue case, we may write the microcrack propagation law as

$$\frac{da}{dN} = C_e \left[\beta_e(\lambda_\sigma, \eta_\sigma) \frac{\Delta\sigma_n/2}{\Delta\tau_n/2} + 1 \right]^M \left[\frac{\Delta\tau_n}{2} \frac{\Delta\gamma^e_{max}}{2} \right]^M a^M \qquad (10)$$

where β_e and C_e are factors analogous to β_p and C_p and M is an exponent different than m. In Equation (10), it is assumed that the plastic component of ΔJ is negligibly small.

The reader should note that ΔJ_{eff} should, in general, be used for correlation of crack growth rate, c.f. [25]. However, available models and experimental data indicate that ΔJ_{eff} may be based on the entire stress range for small cracks under very high cyclic tensile strain conditions normal to the microcrack. The torsional mean strain case is not so straightforward. On the other hand, for completely reversed loading under elastic high cycle fatigue conditions, one would base ΔJ_{eff} on the stress amplitude in the elastic limiting case in Equation (10). Hence, if one were attempting to determine crack growth rate for intermediate conditions, an assessment of closure as a function of strain amplitude would be necessary, as in [25].

The forms in Equations (9)-(10) should be regarded as being motivated by the ΔJ approach rather than being strictly equivalent.

STRAIN LIFE FORMS FOR COMPLETELY REVERSED LOADING

For completely reversed, constant amplitude loading where the plastic component of ΔJ dominates the elastic component we may integrate the crack growth rate in Equation (9). Likewise, we may integrate Equation (10) for predominantly elastic conditions. We assume uniaxial and pure torsional strain life and cyclic stress-strain relations of the form

$$\frac{\Delta\gamma}{2} = \frac{\tau'_f}{G} \left(2N_i\right)^{b_o} + \gamma'_f \left(2N_i\right)^{c_o} \quad , \quad \frac{\Delta\epsilon}{2} = \frac{\sigma'_f}{E} \left(2N_i\right)^{b} + \epsilon'_f \left(2N_i\right)^{c} \qquad (11)$$

$$\frac{\Delta\tau}{2} = K_o' \left[\frac{\Delta\gamma^p}{2}\right]^{n_o'} \quad , \quad \frac{\Delta\sigma}{2} = K' \left[\frac{\Delta\epsilon^p}{2}\right]^{n'} \tag{12}$$

We next integrate Equations (9)-(10) assuming predominantly plastic and elastic conditions, respectively, further assuming constant initiation and final microcrack lengths, to get the strain life expression

$$\frac{\Delta\gamma_{max}}{2} = C_e' \left\{\left[\beta_e \left[\frac{\Delta\sigma_n/2}{\Delta\tau_n/2}\right]+1\right]\frac{\Delta\tau_n}{2}\right\}^{-1} (2N_i)^{-\frac{1}{M}} + C_p' \left\{\left[\beta_p \left[\frac{\Delta\sigma_n/2}{\Delta\tau_n/2}\right]+1\right]\frac{\Delta\tau_n}{2}\right\}^{-1} (2N_i)^{-\frac{1}{m}} \tag{13}$$

where the elastic and plastic components of $\Delta\gamma_{max}$ have simply been summed. Insisting that the uniaxial and torsional strain life expressions be obeyed under those respective conditions leads to

$$\beta_e = \left[4\left[\frac{\tau_f'}{\sigma_f'}\right]^2 - 1\right] \hat{\beta}_e \left[\frac{\Delta\sigma_n/2}{\Delta\tau_n/2}\right] \tag{14}$$

$$\beta_p = \left[\frac{4}{3}\frac{K_o'\left(\gamma_f'\right)^{1+n_o'}}{K'\left(\epsilon_f'\right)^{1+n'}} - 1\right] \hat{\beta}_p \left[\frac{\Delta\sigma_n/2}{\Delta\tau_n/2}\right] \tag{15}$$

where dependence of $\hat{\beta}_e$ and $\hat{\beta}_p$ on biaxiality ratios λ_σ and η_σ is replaced by dependence on the ratio of normal stress to shear stress amplitude on the plane of maximum shear strain. It is noted that this ratio is equal to unity for uniaxial loading and zero for pure torsional loading so that if $\hat{\beta}_e$ and $\hat{\beta}_p$ are homogeneous functions of the ratio $(\Delta\sigma_n/2)/(\Delta\tau_n/2)$, we will recover the strain life forms given in Equation (11). The precise character of this dependence on biaxiality ratio has not been worked out for mixed mode conditions either analytically or computationally in complete fashion; however, it may be assessed by tension-torsion tests at several biaxiality ratios. Coefficients C_e' and C_p' are

given by

$$C_e' = \frac{\left(\tau_f'\right)^2}{G} \quad , \quad C_p' = K_o' \left(\gamma_f'\right)^{\left(1 + n_o'\right)} \tag{16}$$

It should be noted that there are no assumptions regarding equivalent relationships between uniaxial and pure torsional behavior. It is generally observed for ductile metals that the life exponents b_o and b and c_o and c are approximately equal; we may therefore express exponents m and M in the following approximate manner

$$m = \frac{-1}{\bar{c}\left(1 + \bar{n}'\right)} \quad , \quad M = \frac{-1}{2\bar{b}} \tag{17}$$

where barred quantities denote averages of axial and torsional cases. Obviously, treatment of anisotropic materials would negate this approximation.

It is noted that the shear stress amplitude on the maximum shear strain plane is explicitly retained on the right hand side of Equation (13) in order to model the increased damage associated with additional hardening under nonproportional loading as suggested by Fatemi et al. [13]. Some important conclusions may be drawn from the form of Equation (13). It appears very much like an energy approach, which is not surprising since it motivated by ΔJ. The normal stress effect is manifested by dependence on the amplitude of normal stress rather than the maximum normal stress [13]. All pertinent constants except for the biaxiality functions $\hat{\beta}_c$ and $\hat{\beta}_p$ are determined by uniaxial and torsional tests.

Γ_p PLANE REPRESENTATION FOR COMPLETELY REVERSED LOADING

It is instructive to plot the plastic component of Equation (13) on the Γ plane corresponding to plastic strain amplitudes for purposes of comparing with experimental evidence under axial-torsional and tension-tension loading. We choose to work illustratively with the plastic component of $\Delta\gamma_{max}/2$ because the gamma plane representation in this case is simple and, of course, pertains to low cycle fatigue conditions. We refer herein to this plane as the Γ_p plane. The Γ_p plane plots

corresponding to Equations (1)-(2) appear in Figure 2 for two different lives and j values; the assumption is made that the elastic strain amplitudes are negligible compared to the plastic strain amplitudes. Note that $\epsilon_n^{p^*}$ is the value of the plastic strain normal to the maximum $\Delta\gamma_{max}^p/2$ plane at the occurrence of peak tensile stress; $\epsilon_n^{p^*}$ is related to $\Delta\gamma_{max}^p/2$ in each case in the Appendix. Since the Brown and Miller approach may be viewed as an empirical fit to a rather extensive database, it forms a sort of baseline contour in the Γ_p by which other theoretical forms may be judged for completely reversed, constant amplitude, proportional loading.

In regard to the present ΔJ-motivated approach, we select homogeneous functions for β_e and β_p of degree of order j_e and j_p, respectively, in $(\Delta\sigma_n/2/\Delta\tau_n/2)$, i.e.

$$\hat{\beta}_e = \left[\frac{\Delta\sigma_n/2}{\Delta\tau_n/2}\right]^{j_e} \quad , \quad \hat{\beta}_p = \left[\frac{\Delta\sigma_n/2}{\Delta\tau_n/2}\right]^{j_p}$$

where j_e and j_p are exponents which, in general, may differ. Note that these forms for the β functions range from zero for pure shear to unity for uniaxial loading.

Referring to the Appendix, one may write for the axial-torsional Case A,

$$\left[\xi\left(\frac{1}{1+\frac{4}{9}\lambda_\gamma^2}\right)^{(1+j_p)/2}+1\right]\left[1+\frac{3}{4}\left(\frac{1}{\frac{9}{4}+\lambda_\gamma^2}\right)\right]^{\frac{n'-1}{2}}\left[\frac{\Delta\gamma_{max}^p}{2}\right]^{1+n'} = G(N_i) \tag{18}$$

This quantity is equal to a constant for a given life. Here,

$$\xi = \frac{4}{3}\frac{K_o'}{K'}\frac{\left[\gamma_f'\right]^{1+n_o'}}{\left[\epsilon_f'\right]^{1+n'}} - 1 \tag{19}$$

and λ_γ is the strain ratio as defined in the Appendix. For Case B, where the maximum

plastic shear strain range planes intersect the free surface at 45°, the simple expression

$$\left[1 - \lambda_s + \lambda_s^2\right]^{\frac{(n'-1)}{2}} \left[\frac{\Delta\gamma_{max}^p}{2}\right]^{1+n'} = G'(N_i) \qquad (20)$$

holds where $\lambda_s = (\Delta\sigma_2/\Delta\sigma_1)$ and $\Delta\sigma_1 \geq \Delta\sigma_2$ are the ordered principal stress ranges. It is noted that for Case B the maximum plastic shear strain amplitude is the same for uniaxial ($\lambda_s=0$) and equibiaxial ($\lambda_s=1$) loading conditions, analogous to the Brown and Miller Case B assumption given in Equation (2); however, there is a stress ratio dependence in Equation (20), resulting in a variation in the plastic shear strain range for intermediate λ_s values for a given life.

In Figures 3-1 and 3-2, Case A and B constant life contours are plotted in the Γ_p plane for several values of $\Delta\gamma_{max}^p/2$ in torsion and multiple values of j_p for n'=0.15, a typical value. It is observed that the Case B contour is independent of all material properties except for n'. The endpoint of the Case A contour along the uniaxial loading line corresponds to the Coffin-Manson law under uniaxial loading. For intermediate strain ratios under axial-torsional loading, however, it is clear that the Case A contour trajectory depends on j_p; hence, the dependence on biaxiality ratio may be assessed by consideration of intermediate biaxiality ratio experiments. This is entirely analogous to the exponent j in the Brown and Miller Equation (2) which is adjusted to fit the Case A contour trajectory. From Figure 3, it is evident that for the case $j_p=0$ the contour is nearly linear for Case A. On the other hand, for j_p = 1 or 2 it is nonlinear, exhibiting a trajectory very similar to that of many experimental results.

It is concluded that this approach yields a Γ_p plane contour in accordance with the general observations of Brown and Miller which led them to formulate their theory in Equations (1)-(2) for completely reversed loading. Even though the Γ_p plane representation has been plotted, the elastic representation is analogous, and leads to the same conclusions.

COMPARISON WITH SOME RECENT CRITICAL PLANE APPROACHES FOR LOW CYCLE FATIGUE

It is convenient to compare the formulation given by Equation (13) with recent critical plane theories for low cycle fatigue of shear damaging materials under constant amplitude, completely reversed proportional loading conditions. Such comparison is necessarily inexhaustive but we may start with Equations (1)-(4). It is really unnecessary to compare with the Brown and Miller formulation since this form was prescribed by observation of experimental Γ plane contours and is not amenable to inclusion of normal stress or mean stress effects. The formulations in Equations (3)-(4) by Socie and co-workers expressly include normal and mean stress effects and have been shown in their publications to correlate a wide variety of Case A and Case B data. Without loss of generality we may re-write Equation (3) as

$$\frac{\Delta\gamma_{max}^{p}}{2} + C_1 \frac{\Delta\epsilon_n^{p}}{2} + C_2 \frac{\sigma_{no}}{E} = f_s(N_i) \tag{21}$$

Equation (21) may be written for completely reversed loading as

$$\text{CASE A: } \frac{\Delta\gamma_{max}^{p}}{2}\left[1 + \frac{C_1}{4}\frac{1}{\sqrt{\frac{9}{4} + \lambda_\gamma^2}}\right] = f_s(N_i) \tag{22}$$

$$\text{CASE B: } \frac{\Delta\gamma_{max}^{p}}{2}\left[1 + \frac{C_1}{6}\left|1 - 2\lambda_s\right|\right] = f_s(N_i) \tag{23}$$

In Figure 4, these contours for Case A and B are plotted for several values of the constant C_1 in the Γ_p plane. As in the ΔJ-based theory, the value of maximum plastic shear strain amplitude is the same for uniaxial and equal-biaxial loading for Case B. However, an important difference is that Case A and B contours superimpose for positive mean normal strains. This behavior is quite unlike material responses which have been recorded experimentally for Case B. Also, owing to the linearity of the parameter, the Case A contour is linear which also departs from many experimentally observed Γ_p plots in the Case A regime. It should be noted that if C_1 is optimized to fit a

nonlinear trajectory of data points for Case A for various λ_γ values, both the uniaxial values of maximum plastic shear strain amplitude and the Case B values will be overestimated, perhaps significantly. Although in their previous work, Socie et al. have allowed C_1 to be an adjustable parameter, it may be fixed for low cycle fatigue by the condition that the Case A Γ_p contour must meet the uniaxial asymptote in correspondence with the uniaxial Coffin-Manson law. The value of C_1 which pertains to this constraint is $C_1=4(\gamma_f'/\epsilon_f')-6$. If this condition is imposed it is doubtful that intermediate biaxiality ratios can be properly correlated; if not imposed, uniaxial behavior cannot be accurately correlated on the basis of pure shear tests. A separate but important issue is that the criterion is quite nonconservative for Case B tension-tension loading for intermediate λ_s values, compared to the Case B Brown and Miller observation that $\Delta\gamma_{max}^p/2 \approx$ constant for a given life.

We turn next to Equation (4), the approach of Socie, Fatemi et al. [12-13], which appears more closely related to ΔJ in that the product of stress and strain appears in correlation parameter. However, one should note that it is an additive combination of a plastic shear strain and a product of plastic shear strain and normal stress instead of an energy product. Furthermore, the accommodation of mean stress influence is not analogous to a ΔJ_{eff} approach. We may write this equation for the dominant plastic strain case as

$$\frac{\Delta\gamma_{max}^p}{2}\left[1 + k\frac{\sigma_n^{max}}{\sigma_y}\right] = F_f(N_i) \tag{24}$$

Using the proportionality flow rule (see Appendix), one may arrive at Case A and Case B contours for this theory of the following forms:

$$\text{CASE A: } \frac{\Delta\gamma_{max}^p}{2}\left\{1 + \frac{1}{2}\frac{k}{\sigma_y}K'\left[\frac{1}{3} + \frac{1}{4}\left(\frac{1}{\frac{9}{4} + \lambda_\gamma^2}\right)\right]^{\frac{n'-1}{2}}\left(\frac{\Delta\gamma_{max}^p}{2}\right)^{n'}\frac{1}{\sqrt{\frac{9}{4} + \lambda_\gamma^2}}\right\} = F_f(N_i) \tag{25}$$

$$\text{CASE B: } \frac{\Delta\gamma_{max}^{p}}{2}\left[1 + \frac{k}{\sigma_y}\frac{K'}{3}\left(\frac{2}{3}\sqrt{1 - \lambda_s + \lambda_s^2}\right)^{n'-1}\left(\frac{\Delta\gamma_{max}^{p}}{2}\right)^{n'}\right] = F_f'(N_i) \qquad (26)$$

Equations (25)-(26) are relatively complex, exhibiting dependence on n', K', σ_y and material constant k. As pointed out by Fatemi and Kurath [13], k is actually life-dependent in order to appropriately model uniaxial test results over a wide range of lives. However, for practical purposes they settle on a constant value of k. Due to this, if the approach is normalized to the uniaxial case, it cannot properly capture the torsional case and vice versa. Hence, but perhaps to a lesser extent, it suffers the same problem in this regard as the theory in Equation (21). The Γ_p plane representation for Equations (25)-(26) is shown in Figures 5-1 and 5-2 for several K'/σ_y ratios and several values of k. It is again noted that the Case A Γ_p plane contour is nearly linear which could, of course, be corrected by admitting an exponent on normal stress as mentioned by Fatemi and Kurath [13]. The Case B tension-tension contour is quite similar to that given by the ΔJ-based approach with less variation of maximum plastic shear strain. This approach gives a Γ_p contour much more in agreement with general experimental results than Equation (21).

CONCLUSIONS

This study has focused on a multiaxial fatigue microcrack initiation formulation motivated by ΔJ concepts. These ΔJ concepts have been used to guide the formulation, with departures at points where rigorous solutions have yet to be established for influence of biaxiality and mean stress. Nonetheless, restrictions on admissible forms of correlating parameters have been established and the general shape of experimentally observed Γ_p plane contours are essentially reproduced. Correlation with axial-torsional and tension-tension experimental results reveal that the ΔJ based approach is physically appealing and quite promising. It is argued that such an approach contains the most desirable features of plastic work type approaches and critical plane approaches. In addition, microcrack propagation may be written cycle by cycle for integration, if desired, in the event of varying mean stresses, etc. Such an approach may be desirable from the

viewpoint of rectifying anomalies between short crack and long crack behavior. It is recommended that more attention be devoted to satisfaction of both uniaxial and torsional baseline behaviors, as this influences the accuracy of correlation of Case B type loading histories.

Care is taken in this work to distinguish between materials for which microcrack propagation occurs along maximum shear strain amplitude planes and those for which propagation is normal to the maximum principal stress amplitude. The former class of materials is treated in this paper. The ΔJ-integral approach may also be applied to the latter class of materials, recognizing that Mode I dominates but with an influence of biaxiality.

An important result of the present work is that theories which are capable of correlating Case A axial-torsional experiments are not necessarily capable of doing so for Case B. The theory of Equation (3) is an example. The characteristic Γ_p plane contours of each theory provide a means to compare each model with the empirical form suggested by Brown and Miller for constant amplitude, completely reversed proportional loading. This rather simple evaluation is often overlooked in proposing new correlative parameters but is quite fundamental to any theory. It may be anticipated that more physically abstract correlative parameters will exhibit anomalous behavior in the Γ_p plane. The use of consistent microcrack propagation models is a good starting point for realistic Γ_p plane behavior.

ACKNOWLEDGMENTS

The authors would like to express gratitude for the support of UNIREC in this work. D.L. McDowell is also grateful for the support of the U.S. National Science Foundation.

REFERENCES

1. Brown, M. and Miller, K., "A Theory for Fatigue Failure Under Multiaxial Stress-Strain Conditions", Proceedings of the Institution of Mechanical Engineering, Vol. 187, No. 65, 1973, pp.745-755.

2. Socie, D., Waill, L. and Dittmer, D., "Biaxial Fatigue of IN718 Including Mean Stress Effects", Multiaxial Fatigue ASTM STP 853, Eds. K. Miller and M. Brown, American Society Testing and Materials, Philadelphia 1985, pp.463-481.

3. Bannantine, J. and Socie, D., "Observations of Cracking Behavior in Tension and Torsion Low Cycle Fatigue", ASTM Symposium "Low Cycle Fatigue" STP 942, American Society for Testing and Materials.

4. Socie, D., "Multiaxial Fatigue Damage Models", Journal of Engineering Materials and Technology, Vol. 109, October 1987, pp. 293-298.

5. Gough, H. and Pollard, H., "The Strength of Metals Under Combined Alternating Stresses", Proceedings of the Institution of Mechanical Engineering, Vol. 131, No. 3, November 1935, pp. 3-54.

6. Findley, W. in Transactions ASME, Vol. 79, 1957, pp. 1337-1347.

7. Krempl, E., "The Influence of State of Stress on Low Cycle Fatigue of Structural Materials: A Literature Survey and Interpretive Report", STP 549, ASTM, Philadelphia 1974.

8. Brown, M. and Miller, K., "Two Decades of Progress in the Assessment of Multiaxial Low-Cycle Fatigue Life", Low Cycle Fatigue and Life Prediction, ASTM 770, Eds. C. Amzallag, B. Leis, and P. Rabbe, American Society of Testing and Materials, 1982, pp. 482-499.

9. Brown, M. and Miller, K., Fatigue of Engineering Materials and Structures, 1979, Vol. 2, pp. 93-106.

10. Lohr, R. and Ellison, E., "A Simple Theory for Low Cycle Multiaxial Fatigue", Fatigue of Engineering Materials and Structures, Vol. 3, 1980, pp. 1-17.

11. Socie, D. and Shield, T., "Mean Stress Effects in Biaxial Fatigue of IN718", Journal of Engineering Materials and Technology, Vol. 106, July 1984, pp. 227-232.

12. Fatemi, A. and Socie, D., "A Critical Plane Approach to Multiaxial Fatigue Damage Including Out of Phase Loading", Fatigue Fracture of Engineering Materials and Structures, Vol. 11, No. 3, pp. 145-165, 1988.

13. Fatemi, A. and Kurath, P., "Multiaxial Fatigue Life Predictions Under the Influence of Mean Stress", Journal of Engineering Materials and Technology, Vol. 110, October 1988, pp. 380-388.

14. Libertiny, G., "Short Life Fatigue Under Combined Stresses", Journal of Strain Analysis, Vol. 2, No. 1, 1967, pp. 91-95.

15. Mowbray, D.F., "A Hydrostatic Stress-Sensitive Relationship for Fatigue under Biaxial Stress Conditions," ASTM JTEVA, Vol. 8, No. 1, 1980, pp. 3-8.

16. Garud, Y., "A New Approach to the Evaluation of Fatigue Under Multiaxial Loading", Proceedings of the Symposium on Methods for Predicting Materials Life in Fatigue, J. Osfergren and J. Whitehead, Eds., The American Society of Mechanical Engineers, New York 1979, pp. 247.

17. Leis, B., "An Energy-Based Fatigue and Creep-Fatigue Damage Parameter", Journal Pressure Vessel Technology, Trans. ASME, Vol. 99, No. 4, November 1977, pp. 524-533.

18. Ellyin, F., "Effect of Tensile Mean Strain on Plastic Strain Energy and Cyclic Response," ASME Journal of Engr. Matls. Technol., Vol. 107, 1985, pp. 119-125.

19. Dowling, N. and Begley, J., "Fatigue Crack Growth During Gross Plasticity and the J Integral", ASTM STP 590, American Society for Testing and Materials, 1976, pp. 82-103.

20. Lankford, J., "The Growth of Small Fatigue Cracks in 7075-TG Aluminum", Fatigue of Engineering Materials and Structures, No. 5, 1982, p. 223.

21. Chan, K., Lankford, J. and Davidson, D., "A Comparison of Crack-Tip Field Parameters for Large and Small Fatigue Cracks," ASME Journal of Engr. Matls. Technol., Vol. 108, 1986, pp. 206-213.

22. Tanaka, K., "The Cyclic J-Integral as a Criterion for Fatigue Crack Growth," International Journal of Fracture, Vol. 22, 1983, pp. 91-104.

23. Shih, C.F. and Hutchinson, J.W., "Fully Plastic Solution and Large Scale Yielding Estimates for Plane Stress Crack Problems," ASME Journal of Engr. Matls. Technol., Vol. 98, 1976, pp. 289-295.

24. T. Hoside and D. Socie, "Mechanics of Mixed Mode Small Fatigue Crack Growth", Engineering Fracture Mechanics, Vol. 26, No. 6, 1987, pp. 842-850.

25. McClung, R.C. and Sehitoglu, H., "Closure Behavior of Small Cracks Under High Strain Fatigue Histories," ASTM STP 982, 1988, pp. 279-299.

APPENDIX

Γ_p Plane Quantities for Completely Reversed, Proportional Loading

For proportional loading, we may express the flow rule as

$$\Delta\epsilon_{ij}^{p} = \Lambda\ \Delta\sigma'_{ij} \tag{A.1}$$

for a von Mises plastic potential, where $\sigma'_{ij} = \sigma_{ij} - \sigma_{kk}\delta_{ij}/3$.

Case A : Axial-Torsional Loading

In this case, since we assume no stress normal to the free surface,

$$\Delta\epsilon^{p} = \frac{2}{3}\,\Lambda\,\Delta\sigma \quad , \quad \Delta\gamma^{p} = 2\,\Lambda\,\Delta\tau \tag{A.2}$$

and

$$\lambda_{\gamma} = \frac{\Delta\gamma^{p}}{\Delta\epsilon^{p}} = 3\,\frac{\Delta\tau}{\Delta\sigma} = 3\,\lambda_{\tau} \tag{A.3}$$

where $\Delta\epsilon^{p}$, $\Delta\gamma^{p}$ and $\Delta\sigma$, $\Delta\tau$ are the axial and shear engineering plastic strain and stress ranges, respectively, in the longitudinal-circumferential tube coordinate system. From Mohr's circle of stress and the relation

$$\frac{\Delta\sigma_n}{2} = \frac{1}{2}\,\frac{\Delta\sigma}{2} \tag{A.4}$$

we arrive at

$$\frac{\Delta\sigma_n/2}{\Delta\tau_n/2} = \frac{1}{\sqrt{1 + 4\lambda_{\tau}^{2}}} = \frac{1}{\sqrt{1 + \frac{4}{9}\lambda_{\gamma}^{2}}} \tag{A.5}$$

From Mohr's circle of plastic strain,

$$\frac{\Delta\gamma_{max}^{p}}{2} = \sqrt{\left[\frac{3}{2}\,\frac{\Delta\epsilon^{p}}{2}\right]^{2} + \left[\frac{\Delta\gamma^{p}}{2}\right]^{2}} \tag{A.6}$$

From (A.2) and the "universal" relationship

$$\frac{\Delta\bar{\sigma}}{2} = K'\left[\frac{\Delta\bar{\epsilon}^p}{2}\right]^{n'} \tag{A.7}$$

for the cyclic stress-strain curve where we implicitly assume $n' = n_o'$,

$$\Lambda = \frac{3}{2}\frac{1}{K'}\left[\frac{\Delta\bar{\epsilon}^p}{2}\right]^{1-n'} \tag{A.8}$$

where $\Delta\bar{\epsilon}^p$ is the effective plastic strain range based on on $\Delta\epsilon_{ij}^p$. For the case at hand, the amplitude of plastic strain normal to the $\Delta\gamma_{max}^p$ plane is given by

$$\frac{\Delta\epsilon_n^p}{2} = \frac{1}{4}\frac{\Delta\epsilon^p}{2} \tag{A.9}$$

and

$$\frac{\Delta\gamma_{max}^p}{2} = 4\sqrt{\frac{9}{4} + \lambda_\gamma^2}\left[\frac{\Delta\epsilon_n^p}{2}\right] \tag{A.10}$$

which gives the relation between the maximum plastic shear strain range and the plastic strain amplitude normal to its plane.

Combining results,

$$\frac{\Delta\tau_n}{2} = \frac{K'}{3}\left[\frac{1}{3} + \frac{1}{4}\left[\frac{1}{\frac{9}{4} + \lambda_\gamma^2}\right]\right]^{\frac{n'-1}{2}}\left[\frac{\Delta\gamma_{max}^p}{2}\right]^{n'} \tag{A.11}$$

The value ϵ_n^{p*} in Figures 2-5 is the value of ϵ_n^p at the instant of peak tensile loading. For Case A axial-torsional loading,

$$\epsilon_n^{p*} = \frac{\Delta\epsilon_n^p}{2} \tag{A.12}$$

Case B: Biaxial Tension

Here, we define the biaxiality ratio as the ratio of the ordered in-plane principal stress ranges

$$\lambda_s = \frac{\Delta\sigma_2}{\Delta\sigma_1} \tag{A.13}$$

where $\Delta\sigma_1 \geq \Delta\sigma_2$. Plane stress is assumed, i.e. $\sigma_3=0$. Using (A.1),

$$\Delta\epsilon_1^p = \Lambda\, \Delta\sigma_1 \left[2 - \lambda_s\right]/3 \tag{A.14}$$

$$\Delta\epsilon_2^p = \Lambda\, \Delta\sigma_1 \left|2\lambda_s - 1\right|/3 \tag{A.15}$$

$$\Delta\epsilon_3^p = \left| - \Delta\epsilon_1^p - \Delta\epsilon_2^p \mathrm{sgn}(2\lambda_s - 1) \right| = \frac{\left[1 + \lambda_s\right]}{\left[2 - \lambda_s\right]} \Delta\epsilon_1^p \tag{A.16}$$

where $\Delta\epsilon_3^p$ is the plastic strain range normal to the surface plane.

From Mohr's circle of plastic strain,

$$\frac{\Delta\gamma_{max}^p}{2} = \frac{\Delta\epsilon_1^p}{2}\left[\frac{3}{2 - \lambda_s}\right] \tag{A.17}$$

In this case,

$$\frac{\Delta\sigma_n}{2} = \frac{\Delta\tau_n}{2} = \frac{1}{2}\frac{\Delta\sigma_1}{2} \tag{A.18}$$

since $\Delta\sigma_1 \geq \Delta\sigma_2$. Λ is given by

$$\Lambda = \frac{3}{2}\frac{1}{K'}\left[\frac{2}{3}\sqrt{1 - \lambda_s + \lambda_s^2}\right]^{1-n'}\left[\frac{\Delta\gamma_{max}^p}{2}\right]^{1-n'} \tag{A.19}$$

and

$$\frac{\Delta\tau_n}{2} = \frac{K'}{3}\left[\frac{2}{3}\sqrt{1 - \lambda_s + \lambda_s^2}\right]^{n'-1}\left[\frac{\Delta\gamma_{max}^p}{2}\right]^{n'} \qquad (A.20)$$

The plastic strain amplitude normal to the plane of $\Delta\gamma_{max}^p/2$ is given by

$$\frac{\Delta\epsilon_n^p}{2} = \frac{1}{2}\frac{\Delta\epsilon_1^p}{2}\left|\frac{1 - 2\lambda_s}{2 - \lambda_s}\right| = \frac{1}{6}\frac{\Delta\gamma_{max}^p}{2}\left|1 - 2\lambda_s\right| \qquad (A.21)$$

and the normal strain corresponding to peak tensile stress σ_1 is given by

$$\epsilon_n^{p*} = \frac{1}{6}\frac{\Delta\gamma_{max}^p}{2}\left[1 - 2\lambda_s\right] \qquad (A.22)$$

Note that the uniaxial ($\lambda_s=0$) and equibiaxial ($\lambda_s=1$) asymptotes in the Γp plane are given by (A.22).

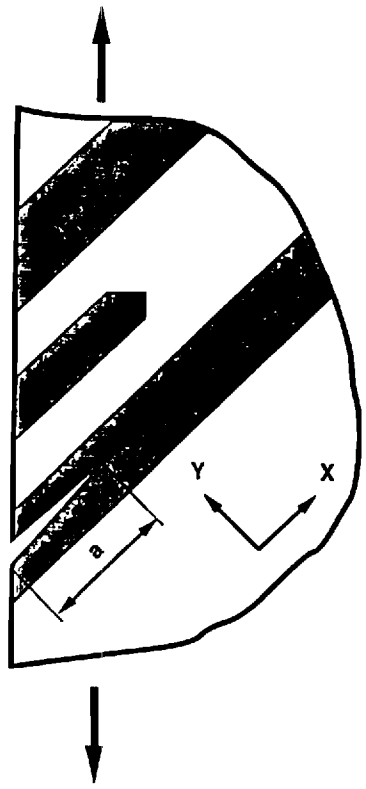

Figure 1 Crack Initiation and Propagation Process in Persistent Slip Bands.

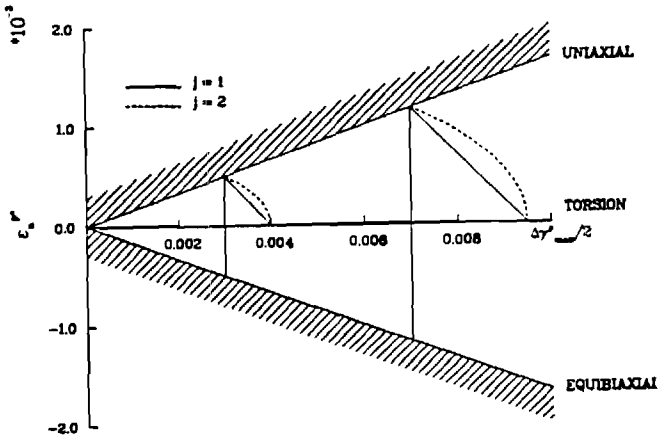

Figure 2 Brown & Miller Model Contour in the Γ_p Plane for $\gamma_f' = 1.75\ \epsilon_f'$

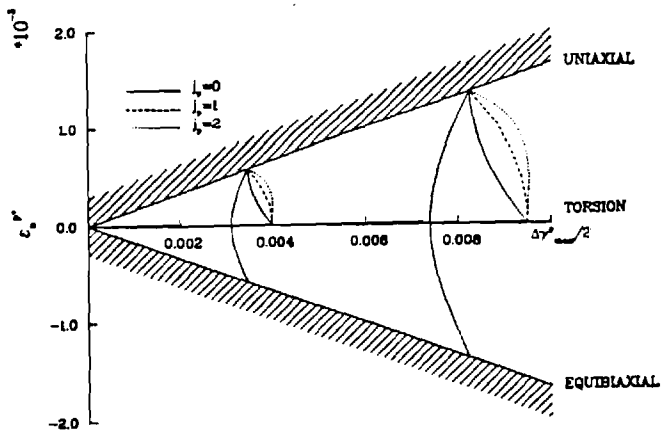

Figure 3-1 McDowell & Berard Model Contour in the Γ_p Plane for $n' = 0.15$ and $\tau_f'\gamma_f' = \sigma_f'\epsilon_f'$

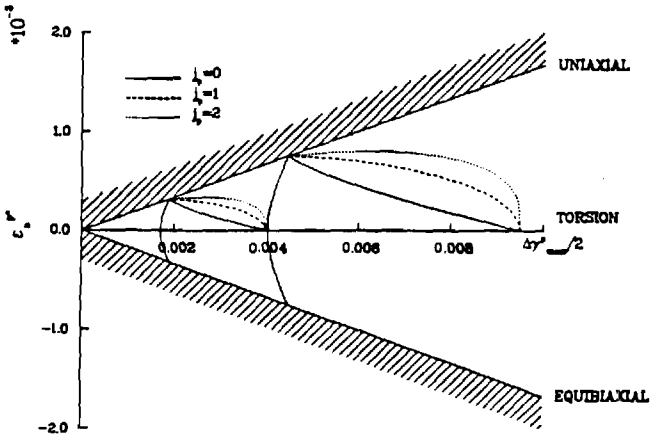

Figure 3-2 McDowell & Berard Model Contour in the Γ_p Plane for $n' = 0.15$ and $\tau_f'\gamma_f' = 2\sigma_f'\epsilon_f'$

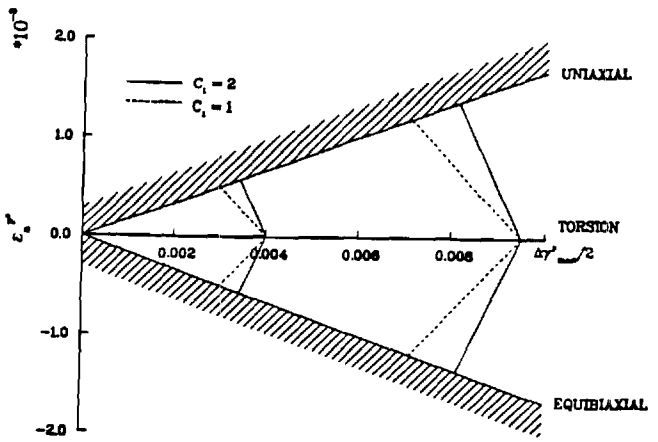

Figure 4 Socie Model Contour in the Γ_p Plane for $\gamma_f' = 1.75\ \epsilon_f'$ ($C_1 = 1$) and $\gamma_f' = 2\ \epsilon_f'$ ($C_1 = 2$)

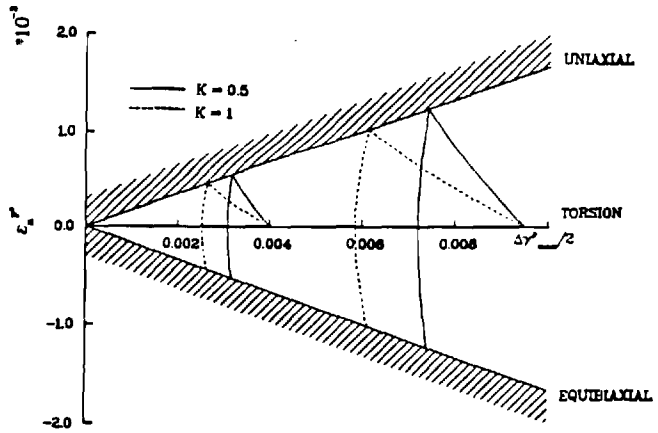

Figure 5-1 Fatemi, Kurath, Socie Model Contour in the Γ_p Plane for $n' = 0.1$ and $K'/\sigma_y = 1.9$

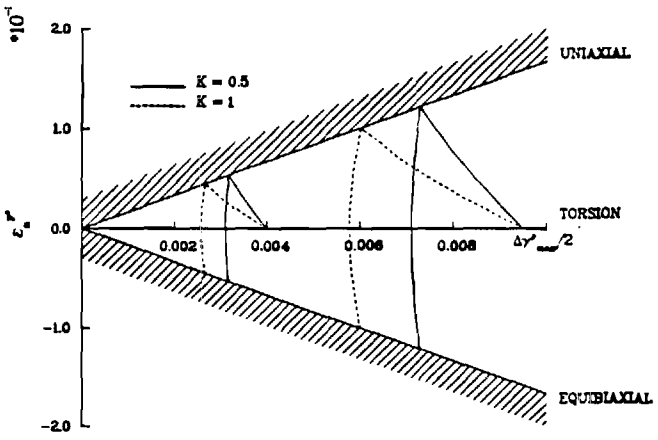

Figure 5-2 Fatemi, Kurath, Socie Model Contour in the Γ_p Plane for $n' = 0.2$ and $K'/\sigma_y = 3.5$

APPENDIX C

DAMAGE RATE APPROACHES FOR THERMOMECHANICAL FATIGUE OF SUPERALLOYS

A Proposal for Fourth Year Funding

To

Dr. Bill Schneider, T-10
Allison Gas Turbine Operations
P.O. Box 420
Indianapolis, IN 46206-0420

From

David L. McDowell
Associate Professor
George W. Woodruff School of Mechanical Engineering
Georgia Institute of Technology
Atlanta, GA 30332

October, 1989

ABSTRACT

In the first three years of this four-year program, experimental results have been obtained on MAR-M 246 at 650°C and 900°C, including monotonic and cyclic stress-strain behavior at three strain rates, ultimate strength characterization, creep response, and stress- and strain-life fatigue characterization, influence of tensile and compressive hold times. In the third year, we have conducted 650°C tests, have run hold time tests and are in the process of conducting vacuum tests. One M.S. thesis (Gary Reynolds) was completed last year and another M.S. student (Matthew Miller) is focusing his research on life prediction models capable of modeling nonisothermal, thermomechanical fatigue (TMF) for this material. This aspect will be the thrust of the fourth year of the program.

The fourth year of the program, to begin January 1, 1990, will involve development of a methodology for life prediction under combined thermal and mechanical cycling for Nickel-base superalloys in general, and MAR-M 246 in particular. We have fully characterized this material at temperatures near the lower and upper ends of typical TMF hot section operating cycle. As the next logical step to conclude the program, we propose to perform nonisothermal fatigue experiments to verify the life prediction methodology under development.

PROPOSED EXPERIMENTAL PROGRAM FOR FOURTH YEAR

The full set of experimental results obtained through the end of the third year will be presented in a forthcoming report for the third year of the project to be issued in November, 1989. These results comprise a thorough isothermal characterization of the fatigue behavior of MAR-M 246 at 650°C and 900°C at strain rates of 10^{-2}, 10^{-3} and 10^{-4} sec^{-1}.

We are in the process of conducting six tests in a vacuum environment, but have experienced significant mechanical difficulties with our vacuum system pump(s) and the induction heating interface for the vacuum system; we are still pursuing these experiments. As an alternative, in the event these problems can't be worked out in the

near term, we will consider testing in a chamber with flowing argon. However, we are pressing forward to try to complete six vacuum experiments. These tests will provide important information regarding the role of oxidation in the laboratory air experiments. We aim to complete these tests early in the fourth year of the program.

This past year, we have been developing a set of microcrack propagation equations, based on short crack fracture mechanics, to described the creep-fatigue-environment interactions of high temperature fatigue of MAR-M 246. We are in the process of examining all data gathered to date at 650°C and 900°C within the context of the theory. Such theories have great promise for thermomechanical fatigue of Ni-base superalloys as indicated by recent Japanese research. Creep crack growth is based on the C(t)-integral averaged over the tensile rise time and/or hold time of the cycle, which represents the average crack tip singularity strength. Fatigue crack growth is governed by the ΔJ parameter, which is an extension of the J-integral concept to cyclic loading. Crack growth rate associated with oxidation is assumed to be governed by ΔJ as well but modified by an Arrhenius temperature dependence with activation energy associated with diffusion of oxygen. A very attractive aspect of the model is that it is applicable to growth of long cracks as well since it is based on a fracture mechanics methodology; of course, some of the forms for coefficents differ for short and long cracks.

In addition to the creep-fatigue-environment characterization, we will fit the cyclic deformation and creep data of MAR-M 246 obtained in this program to a cyclic viscoplasticity theory with nonisothermal capability. This model may actually be used in some of the life prediction strategies employed but will certainly serve as a useful potential tool for Allison.

The next step in the program is to test this life prediction methodology under conditions of nonisothermal cycling. In particular, we propose to conduct tests in which the temperature is periodically varied between the limits previously characterized along with mechanical straining at strain rates within the range previously considered. We also propose to conduct a modest number of isothermal fatigue and creep experiments at an intermediate temperature (e.g. 800°C) as outlined in Table I to facilitate determination

of appropriate temperature dependencies of deformation and damage for the nonisothermal case.

The first set of proposed nonisothermal experiments consist of cycling at a mechanical strain amplitude of either 0.004 (or 0.008) at the minimum (maximum) temperature for 50% of the fatigue life at that temperature, and then switching to the maximum (minimum) temperature for the remainder of life. The temperature change will be conducted at zero load under load control to ensure the presence of only thermal strain increments; then the extensometer will be re-zeroed and the test will be resumed at the desired total strain amplitude. See Table II for the test matrix.

The second set of proposed nonisothermal experiments consist of so-called bi-thermal tests in which the mechanical strain is ramped isothermally until the stress returns to zero, the servocontroller is switched to load control, the temperature is increased (decreased) to the upper (lower) limit, the strain cycle is resumed. The tests may be either in-phase or out-of-phase. Although these experiments do not involve concurrent mechanical and thermal straining, they reproduce most of the temperature history dependent aspects of TMF including mean stress associated with out-of-phase cycling, detrimental high temperature effects in in-phase cycles, etc. See Table III and Figure 1 for details.

The uniaxial specimen design drawing is again included for reference in Figure 2. Note that some of the specimens which will undergo relatively rapid thermal excursions will be hollow to ensure a more uniform temperature field in the process. A solid specimen is permissible for very slow excursions as in the two-temperature experiments. We will require another 30 specimens from Allison to complete the proposed program.

DELIVERABLES

Following the conclusion of the project, we will deliver the following to Allison:

(a) A microcrack propagation damage rate model characterizing the creep-fatigue-oxidation interaction behavior of MAR-M 246 at high temperature which includes isothermal and nonisothermal capability;

(b) Evaluation of performance for nonisothermal histories; and

(c) A nonisothermal cyclic viscoplasticity model (state variable model) which characterizes the high temperature deformation behavior of MAR-M 246, including strain rate dependence, temperature dependence and cyclic hardening/softening behavior.

SUMMARY

The estimated cost of the proposed fourth year of the program is $51,677 with an intended starting date of January 1, 1990. A cost breakdown is supplied in the budget. One Research Engineer (R.L.T. Oehmke) will be supported 25% time by this contract; one graduate student (Matthew Miller) will also be supported.

The Principal Investigator is a recipient of the National Science Foundation Presidential Young Investigator Award. This award carries with it matching funds up to $37,500 for industrial grants which can be used as discretionary funds by the Principal Investigator in his interest area. Dr. McDowell intends to use his NSF matching funds for support of development of multiaxial high temperature constitutive equations for cyclic deformation and damage of both austentic stainless steels and superalloys. Though at a relatively modest funding level, such research is certainly complementary to that in this program and is considered a strong incentive for Allison to support his work.

It is assumed that the MAR-M 246 material will be supplied by Allison to Georgia Tech (or an agency specified by Georgia Tech) in the form of slightly oversize cast bars. Georgia Tech will contract with an external agency for specimen machining as per

specifications made in the enclosed drawing, Figure 2. A total of 30 additional specimens should be sufficient to complete the program.

TABLE I: Baseline Isothermal Tests at 800°C

$\dot{\epsilon} = 10^{-3}\ sec^{-1}$

Fatigue

# Tests	$\Delta\epsilon/2$
2	0.004
2	0.006
2	0.009

Creep

# Tests	σ (MPa)
1	300
1	413

TABLE II: Two-Level Temperature Tests

$\dot{\epsilon} = 10^{-3}\,sec^{-1}$

# Tests	$\Delta\epsilon/2$	T_1	T_2	Switch at *
2	0.004	T_{min}	T_{max}	$1/2\ N_i$
2	0.008	T_{min}	T_{max}	$1/2\ N_i$
2	0.004	T_{max}	T_{min}	$1/2\ N_i$
2	0.008	T_{max}	T_{min}	$1/2\ N_i$

$T_{min} = 650^{\circ}C$; $T_{max} = 900^{\circ}C$; N_i = cycles to initiation

* Corresponds to specified fraction of life at $T = T_1$

TABLE III: Bi-Thermal Tests

$\dot{\epsilon}_m = 10^{-3}\ sec^{-1}$, $\Delta\epsilon_m/2 = 0.007$

(ϵ_m = mechanical strain)

T min	T max	In-Phase	Out-of-Phase
650°C	900°C	X	
650°C	900°C	X	
650°C	900°C		X
650°C	900°C		X

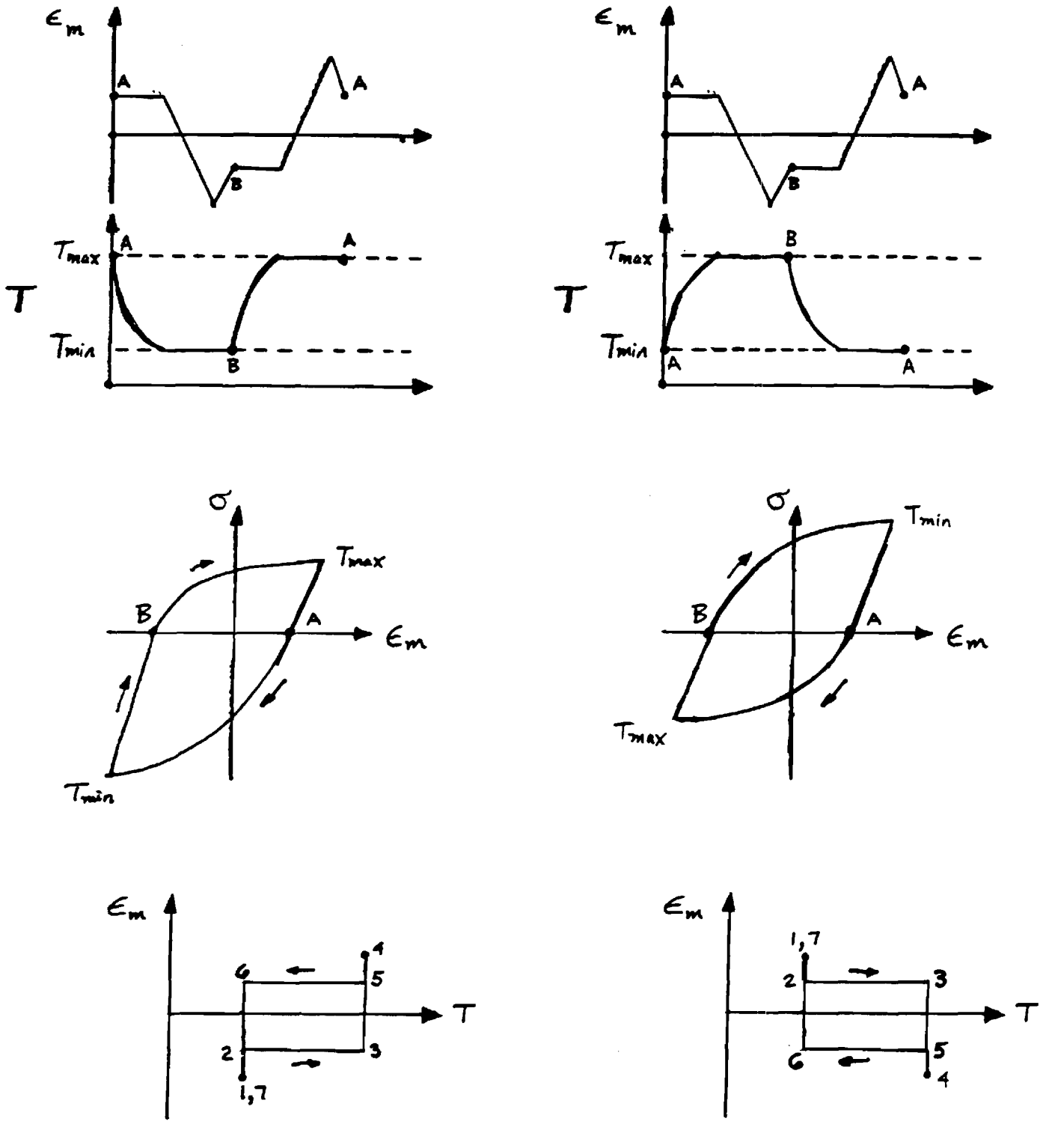

Figure 1. Bi-thermal cycles for (left column) in-phase and (right column) out-of-phase TMF.

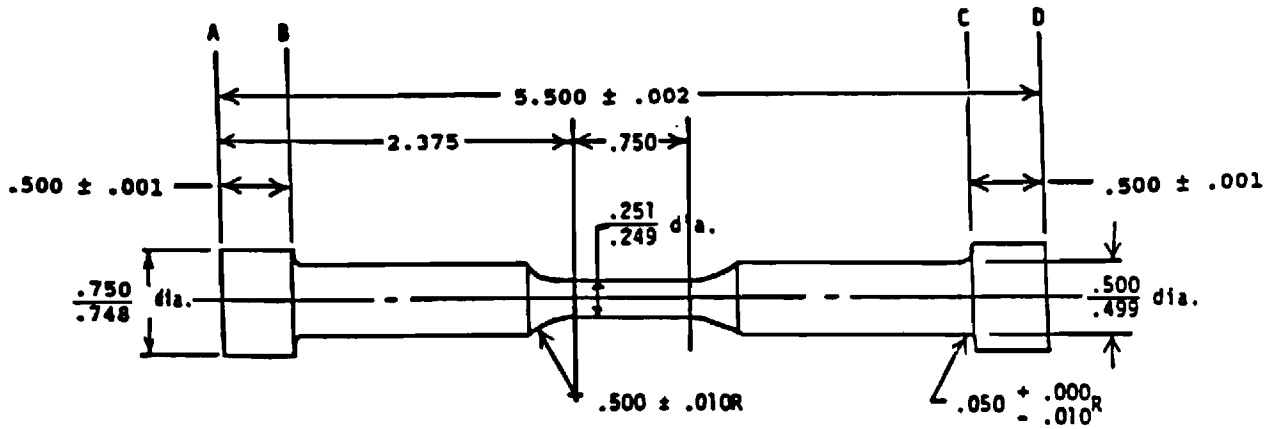

All dimensions are in inches.

Figure 2. Tensile and low cycle fatigue specimen dimensions.

(Note: Cast oversize by 0.120" on all diameters.)

YEAR FOUR BUDGET

Salaries

A.	Principal Investigator: D.L. McDowell (10% AY)	5,677
B.	Other personnel: Research Engineer (R. Oehmke, 25%) Graduate Research Assistant (M. Miller,50%)	 11,000 5,000
C.	**TOTAL SALARIES AND WAGES**	21,677
D.	Fringe Benefits (@26.3% of C)	4,386
E.	Subtotal for Personnel	26,063
F.	Travel	500
G.	Equipment (i) PID Temperature Controller with digital input/output	 1,200
H.	Supplies and Machining (a) laboratory supplies (b) specimen machining costs	 1,500 3,000
I.	**TOTAL DIRECT COSTS**	32,263
J.	Overhead (@62.5% of I less G)	19,414
K.	**TOTAL ESTIMATED COST**	51,677

BIOGRAPHICAL SKETCH

DAVID L. MCDOWELL
Associate Professor
School of Mechanical Engineering
Associate Director
Mechanical Properties Research Laboratory
Georgia Institute of Technology
Atlanta, GA 30332

Education

B.S.M.E.	1979	University of Nebraska-Lincoln
M.S.M.E.	1981	University of Illinois at Urbana-Champaign
Ph.D.	1983	University of Illinois at Urbana-Champaign

Current Research Interests

Nonlinear stress analysis, cyclic plasticity, viscoplasticity, nonlinear time-dependent fracture mechanics, fatigue and creep-fatigue interaction.

Academic and Professional Honors

1988 ASME Henry Hess Award by outstanding ASME journal article by an author less than 31 years of age at submission
1987 ASME/Pi Tau Sigma Gold Medal Award for most outstanding contributions by a Mechanical engineer less than 10 years beyond the baccalaureate degree
1986 Alfred Noble Prize, Jointly awarded by ASCE, ASME, IEEE, and others for most outstanding technical paper in any of these organization's respective journals by an author under 31 years of age
NSF Presidential Young Investigator Award, 1986
SAE Ralph R. Teetor Award, 1986
Atlanta Metro-Area Young-Engineer-of-the-Year, 1986
Georgia Tech Junior Faculty Award, Sigma Xi, 1986
Nominated for ASME Melville Award, 1985
One of six winners nationwide of International Harvestor Fellowship for Dissertation Research, 1981
MTS Corporation Fellow, 1979-1981
University Fellow, Mechanical and Industrial Engineering, UIUC, 1979-1981

External Professional

Reviewer for ASTM and ASME journals
Reviewer for NSF proposals
Reviewer for AIAA Journal
Reviewer for Fatigue of Engineering Materials and Structures

Academic and Professional Societies

Sigma Xi
American Society of Mechanical Engineers
Tau Beta Pi
Pi Tau Sigma
Society of Experimental Mechanics
American Society for Testing and Materials
ASEE
SAE

Publications

1. McDowell, D.L., Socie, D.F. and Lamba, H.S., "Multiaxial Nonproportional Cyclic Deformation," Low-cycle Fatigue and Life Prediction, ASTM STP 770, 1982, pp. 500-518.

2. McDowell, D.L., "On the Path Dependence of Transient Hardening and Softening to Stable States under Complex Biaxial Cyclic Loading," Proceedings of International Conference on Constitutive Laws for Engineering Materials: Theory and Application, University of Arizona, Tucson, Ariz., January 1983, pp. 125-132.

3. McDowell, D.L., "Transient and Stable Deformation Behavior under Cyclic Nonproportional Loading," ASTM STP 853, 1985, pp. 64-87.

4. Fash, J.W., Socie, D.F., and McDowell D.L., "Fatigue Life Estimates for a Simple Notched Component Under Biaxial Loading," ASTM STP 853, 1985, pp. 497-513.

5. Hayhurst, D.R., Leckie, F.A., and McDowell, D.L., "Damage Growth Under Nonproportional Loading," ASTM STP 853, 1985, pp. 688-699.

6. McDowell, D.L., Payne, R.K., Stahl, D., Antolovich, S.D., "Effects of Nonproportional Cyclic Loading Historics on Type 304 Stainless Steel, " Proc. of the International Spring Meeting of Societe Francaise de Metallurgie, Paris, May 1984.

7. McDowell, D.L., "A Two Surface Model for Transient Nonproportional Cyclic Plasticity: Part I - Development of Appropriate Equations," ASME Journal of Applied Mechanics, Volume 52, June 1985, pp. 298-302.

8. McDowell D.L., "A Two Surface Model for Transient Nonproportional Cyclic Plasticity: Part II - Comparison of Theory with Experiments," ASME Journal of Applied Mechanics, Volume 52, June 1985, pp. 303-308.

9. McDowell, D.L., "An Experimental Study of the Structure of Constitutive Equations for Nonproportional Cyclic Plasticity," ASME Journal of Engineering Materials and Technology, Oct. 1985, pp. 307-315.

10. McDowell, D.L., "The Significance of Nonproportional Loading Tests for Characterization of Cyclic Response of Metals," Proc. 1985 SEM Spring Conference on Experimental Mechanics, Las Vegas, June 1985, pp. 229-236.

11. Sotolongo, W., and McDowell, D.L., "An Evaluation of Several Constitutive Model Structures for Transient Nonproportional Cyclic Plasticity," ASME Journal of Pressure Vessel Technology, Vol. 108, Aug. 1986, pp. 273-279.

12. Sotolongo, W., and McDowell, D.L., "On the Numerical Integration of Elasto-Plastic Constitutive Model Structures for Nonproportional Cyclic Loading," Computers and Structures, Vol. 24, No. 4, 1986, pp. 595-606.

13. McDowell, D.L., "An Evaluation of Recent Developments in Hardening and Flow Rules for Rate-Independent, Nonproportional Cyclic Plasticity," ASME Journal of Applied Mechanics, Vol. 54, No. 2, 1987, pp. 323-334.

14. McDowell, D.L., "Simple Experimentally Motivated Cyclic Plasticity Model," ASCE Journal of Engineering Mechanics, Vol. 113, No. 3, March 1987, pp. 378-397.

15. McDowell, D.L., Moosbrugger, J., Doumi, M., and Jordan, E.H., "Some Implications for Cyclic Plastic and Viscoplastic Equations Based on Nonproportional Loading Experiments," Proc. 3rd Symposium on Nonlinear Constitutive Relations for High-Temperature Applications, NASA Lewis RC, University of Akron, Ohio, June 11-13, 1986.

16. McDowell, D.L. and Moyar, G.J., "A More Realistic Model of Nonlinear Material Response: Application to Elastic-Plastic Rolling Contact," Proc. 2nd Int. Symp. on Contact Mechanics and Wear of Rail/Wheel Systems, University of Rhode Island, Kingston, RI, July 8-11, 1986.

17. DeMane, M.F, Beals, N.B., McDowell, D.L., Greenwood, K.M., and Spector, M., "Porous Polysulfone-Coated Femoral Stems," ASTM STP F4, 1988.

18. Leung, Chun-Pok, McDowell, D.L., and Saxena, A., "A Numerical Study of Nonsteady State Creep at Stationary Crack Tips," ASTM STP 995, Vol. I, A. Saxena, J.D. Landes, and J.L. Bassani, Eds., 1989, pp. 55-67.

19. McDowell, D.L. and Moosbrugger, J.C., "A Generalized Rate-Dependent Bounding Surface Model," ASME PVP-Vol. 129, Eds. Chang, Gwaltney and McCawley, 1987, pp. 1-11.

20. McDowell, D.L., Stahl, D., Stock, S.R. and Antolovich, S.D., "Biaxial Path Dependence of Deformation Substructure of Type 304 Stainless Steel," Metallurgical Transactions A, Vol. 19A, May 1988, pp. 1277-1293.

21. McDowell, D.L., Ho, Kwang-Il, and Stalley, J., "An Anisotropic, Damage-Coupled Viscoplastic Model for Creep-Dominated Cyclic Loading," ASTM STP 995, Vol. I, A. Saxena, J.D. Landes, and J.L. Bassani, Eds., 1989, pp. 173-194.

22. Yoder, P.Y., and McDowell, D.L., "Bounding-Surface Plasticity: Stress Space versus Strain Space," Acta Mechanica, Vol. 77, 1989, pp. 13-45.

23. Beals, N., McDowell, D., and Spector, M., "Fatigue Behavior of Porous Polysulfone Surface Coatings for Orthopaedic Applications," International Journal of Fatigue, Vol. 9, No. 4, October 1987, pp. 211-216.

24. Leung, Chun-Pok, McDowell, D.L., and Saxena, A., "Consideration of Primary Creep at a Stationary Crack Tip: Implications for the C_t Parameter," International Journal of Fracture, Vol. 36, 1988, pp. 275-289.

25. McDowell, D.L., "Evaluation of Intersection Conditions for Two Surface Plasticity Theory," International Journal of Plasticity, Vol. 5, No. 1, 1989, pp. 29-50.

26. McDowell, D.L., Ho, K. and Moosbrugger, J.C., "Continuum Damage Representation of Creep-Dominated, Nonproportional Cyclic Loading," Proc. Int. Seminar on High Temperature Fracture Mechanisms and Mechanics, Dourdan, France, Oct. 13-15, 1987.

27. McDowell, D.L. and Moosbrugger, J.C., "Bounding Surface Interpretation of Rate-Dependent Metallic Behavior under Nonproportional Loading," Proc. Int. Seminar on the Inelastic Behaviour of Solids Models and Utilisation, Besancon, France, Aug. 30 - Sept. 1, 1988.

28. McDowell, D.L. and Berard, J., "A ΔJ-Based Approach to Biaxial Low Cycle Fatigue of Shear Damaging Materials," Third International Conference on Biaxial/Multiaxial Fatigue, Stuttgart, FRG, April 3-6, 1989.

29. McDowell, D.L. and Moosbrugger, J.C., "Application of Continuum Slip Approaches to Viscoplasticity," presented at the 19th Canadian Fracture Conference, Ottawa, Ontario, Canada, May 1989.

30. Moosbrugger, J.C. and McDowell, D.L., "On a Class of Kinematic Hardening Rules for Nonproportional Cyclic Plasticity," ASME Journal of Engineering Materials and Technology, Vol. 111, 1989, pp. 87-98.